Journal of the
OPTICAL SOCIETY
of AMERICA

VOLUME 32 APRIL, 1942 NUMBER 4

Interference Spectroscopy. Part II*

KARL WILH. MEISSNER†
Worcester Polytechnic Institute, Worcester, Massachusetts
(Received October 17, 1941)

II. COMPOUND INTERFEROMETER AND MULTIPLEX INTERFERENCE SPECTROSCOPE

§13. Principle of the Instruments

ALTHOUGH the Fabry-Perot interferometer has many advantages over other instruments of high resolving power, there is one disadvantage, which sometimes becomes very troublesome in the investigation of the structure of close complex lines. When the interferometer gap is increased in order to gain the necessary resolving power, the spectral range is decreased and the orders overlap.

W. V. Houston, E. Gehrcke, and E. Lau have shown the way to overcome this difficulty and to increase the spectral range of an interferometer without loss of its resolving power. Houston employed two Fabry-Perot interferometers in series ("compound interferometer"), while Gehrcke and Lau used two plane parallel silver-coated glass or quartz plates in series ("multiplex interference spectroscope"). In both cases, the thickness of one etalon or plate was a small multiple of the thinner one.

One can get a rather clear idea of the action of these instruments by interpreting the single etalons or plates as special light filters, transparent to light of a given wave-length λ in certain restricted directions φ only. In the case of the compound interferometer, which we will treat in the following, these directions are determined by the fundamental equations (2.3), $p_1\lambda=2t_1\cos\varphi_1$ and $p_2\lambda=2t_2\cos\varphi_2$, where t_1 and t_2 are the thicknesses of both instruments ($t_2>t_1$). If the light has to go through both etalons, adjusted so that the four reflecting surfaces are parallel, we observe appreciable intensity only for such angles where the "directions of transparency" of both etalons are equal.

Let us suppose φ_0 to be the innermost direction of this kind; then we have:

$$p_1\lambda=2t_1\cos\varphi_0, \tag{13.1}$$

$$p_2\lambda=2t_2\cos\varphi_0. \tag{13.2}$$

Therefore:

$$p_1t_2=p_2t_1. \tag{13.3}$$

The next angle, φ_1, of coinciding transparency will correspond to the next order (p_1-1) of the thinner etalon and to the order (p_2-k) of the thicker one. The orders between p_2 and p_2-k will correspond to angles φ smaller than φ_1 so that the intensity in these directions will be very weak. If the order p_2-k corresponds exactly to the angle φ_1, this order will appear with maximum intensity. The fundamental equations for the direction φ_1, therefore, will be

$$(p_1-1)\lambda=2t_1\cos\varphi_1, \tag{13.4}$$

$$(p_2-k)\lambda=2t_2\cos\varphi_1. \tag{13.5}$$

* Part I appeared in J. Opt. Soc. Am. **31**, 405 (1941).
† At present on leave of absence as visiting professor at Purdue University, Lafayette, Indiana.

BOSTON UNIVERSITY
COLLEGE OF LIBERAL ARTS
LIBRARY

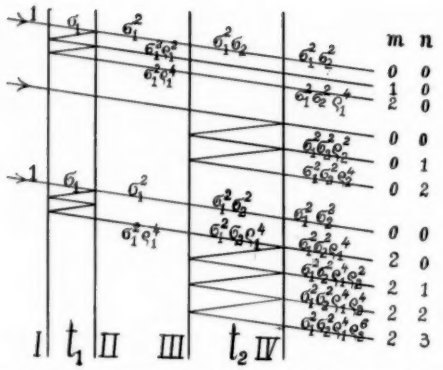

FIG. 10. Resultant amplitudes of multiply reflected waves.

Therefore

$$p_1 t_2 - t_2 = p_2 t_1 - k t_1. \tag{13.6}$$

The combination of Eqs. (13.3) and (13.6) yields the condition for the transmission of every kth order of the thicker etalon:

$$t_2 = k t_1. \tag{13.7}$$

This means that the gap of the thicker etalon has to be a multiple of the thinner separation. In this way, indeed, the range of dispersion of the thicker etalon is increased k times.

If there is a group of close lines, λ, $\lambda+\delta\lambda$, $\lambda+\delta'\lambda$, $\cdots$, all belonging to the same order, the whole complex of lines will be transmitted only in every kth order of the thicker etalon. This is a consequence of the fact that the dispersion of the Fabry-Perot interferometer is independent of the thickness (see formula (5.4)).

§14. Intensity Distribution in the Patterns

The conclusions we have reached in §13 by means of general discussions are to be confirmed by the more exact theory of the instrument which may be briefly outlined, with reference to §4. In Fig. 10 the four silver-coated surfaces of the interferometer plates may be represented by I, II, III, and IV. The thicknesses of the air plates are t_1 and t_2. Let us further suppose that the surfaces II and III are so far apart that the interference patterns produced by them are so close that they cannot be resolved. The same is then true for interference patterns produced by path differences between I and III, and between II and IV.

In order to find the intensity distribution, we have to consider the splitting of an incident wave into partial waves and their subsequent superposition, taking into account amplitudes and phase differences.

The incident wave is split into different partial waves in a more complex manner than in the single interferometer. In Fig. 10 a few cases are illustrated. The amplitudes of the emerging rays can easily be calculated if the reflection and transmission coefficients are given (ρ_1, ρ_2, and σ_1, σ_2, respectively). In Table VI, the amplitudes of a few waves are compiled which have undergone $2m$ reflections in the first etalon and $2n$ reflections in the second. These values are given in units of the amplitude of the transmitted direct ray which is $\sigma_1^2\sigma_2^2$, assuming that the incident wave has unit amplitude.

The general form of these amplitude expressions is obvious, and we can state that a wave which has been reflected $2m$ times in the first etalon and $2n$ times in the second will emerge with the amplitude

$$A_{m,n} = \sigma_1^2\sigma_2^2(\rho_1^2)^m(\rho_2^2)^n. \tag{14.1}$$

For the calculations of the phases, we use the phase differences between the direct wave and the waves with $2m$ and $2n$ reflections. In the case of the simple interferometer, the phase difference between two consecutive waves is $2\pi p$, where p is the order number (§2). Therefore a wave, after $2m$ reflections in the first etalon, will show a phase difference of $2\pi m p_1$, and if the wave has to undergo $2n$ additional reflections in the second etalon, the phase difference with respect to the direct wave will be

$$\Phi_{m,n} = 2\pi(mp_1 + np_2), \tag{14.2}$$

where

$$p_1 = (2t_1 \cos\phi)/\lambda$$

TABLE VI. Amplitudes of multiply reflected rays in units of the amplitude $\sigma_1^2\sigma_2^2$ of the transmitted direct ray.

n \ m	0	1	2	3	4	5
0	1	ρ_1^2	ρ_1^4	ρ_1^6	ρ_1^8	ρ_1^{10}
1	ρ_2^2	$\rho_1^2\rho_2^2$	$\rho_1^4\rho_2^2$	$\rho_1^6\rho_2^2$	$\rho_1^8\rho_2^2$	$\rho_1^{10}\rho_2^2$
2	ρ_2^4	$\rho_1^2\rho_2^4$	$\rho_1^4\rho_2^4$	$\rho_1^6\rho_2^4$	$\rho_1^8\rho_2^4$	$\rho_1^{10}\rho_2^4$
3	ρ_2^6	$\rho_1^2\rho_2^6$	$\rho_1^4\rho_2^6$	$\rho_1^6\rho_2^6$	$\rho_1^8\rho_2^6$	$\rho_1^{10}\rho_2^6$
4	ρ_2^8	$\rho_1^2\rho_2^8$	$\rho_1^4\rho_2^8$	$\rho_1^6\rho_2^8$	$\rho_1^8\rho_2^8$	$\rho_1^{10}\rho_2^8$
5	ρ_2^{10}	$\rho_1^2\rho_2^{10}$	$\rho_1^4\rho_2^{10}$	$\rho_1^6\rho_2^{10}$	$\rho_1^8\rho_2^{10}$	$\rho_1^{10}\rho_2^{10}$

and

$$p_2=(2t_2\cos\phi)/\lambda. \tag{14.3}$$

Knowing the amplitudes and phases of the partial waves, we are able to write the equation for the vibration which all the partial waves produce at infinity or at the focal plane of the projecting system:

$$A\exp(i\omega\tau)=(\sigma_1^2\sigma_2^2\sum_{m=0}^{\infty}\sum_{n=0}^{\infty}(\rho_1^2)^m(\rho_2^2)^n \times\exp[-2\pi i(mp_1+np_2)])\exp(i\omega\tau). \tag{14.4}$$

The amplitude A is found by the following summation:

$$\begin{aligned}A&=\sigma_1^2\sigma_2^2\sum_{n=0}^{\infty}[\rho_2^{2n}\exp(-2\pi inp_2)\times\sum_{m=0}^{\infty}\rho_1^{2m}\exp(-2\pi imp)]\\&=\sigma_1^2\sigma_2^2\sum_{n=0}^{\infty}[\rho_2^{2n}\exp(-2\pi inp_2)\times(1-\rho_1^2\exp(-2\pi ip_1))^{-1}]\\&=\sigma_1^2\sigma_2^2(1-\rho_1^2\exp[-2\pi ip_1])^{-1}\times(1-\rho_2^2\exp(-2\pi ip_2))^{-1}.\end{aligned} \tag{14.5}$$

From the last expression for the amplitude, we get the intensity $I=A\bar{A}$, where $\bar{A}$ is the complex conjugate of A. Introducing the transmission and reflection power, $s=\sigma^2$ and $r=\rho^2$, respectively, we obtain the following result:

$$I=s_1^2(1+r_1^2-2r_1\cos 2\pi p_1)^{-1}\times s_2^2(1+r_2^2-2r_2\cos 2\pi p_2)^{-1} \tag{14.6}$$

or by replacing $\cos 2\pi p$ by $(1-2\sin^2\pi p)$

$$I=(s_1^2/(1-r_1^2))[1+(4r_1/(1-r_1)^2)\sin^2\pi p_1]^{-1}\times(s_2^2/(1-r_2)^2)[1+(4r_2/(1-r_2)^2)\sin^2\pi p_2]^{-1}. \tag{14.7}$$

This is just the product of the intensity expressions of the separate etalons (see formula (4.3)).

The discussion of formula (14.7) confirms the previous explanation of the action of the compound interferometer given in §13, and gives quantitative details.

As the second term of the denominators is always positive, principal maxima will be observed if both denominators become simultaneously unity. This is possible only if both p_1 and p_2 are whole numbers. These are the order numbers of the fringes belonging to the same angle of incidence φ_i. As these order numbers have to fulfill the fundamental equations (14.3), the relation will hold:

$$p_2/p_1=t_2/t_1=k \tag{14.8}$$

and as p_1 and p_2 are integers, k must be a rational number.

It is clear that there are other angles φ_i for which principal maxima will result. For the angle which follows the innermost coincidence, the order numbers may be $p_1'=p_1-x$ and $p_2'=p_2-y$, respectively, for which the relation (14.8) will hold also:

$$p_2'/p_1'=t_2/t_1=k=(p_2-y)/(p_1-x). \tag{14.9}$$

The combination of the two last equations yields the following relation between x and y:

$$kx=y. \tag{14.10}$$

From this relation one can see that several coincidences of the fringes of the smaller and thicker etalon, producing principal maxima, can be observed in the restricted field of view only if k is a fraction with small numerator and denominator. But we will not discuss this general case, and we will restrict ourselves to the case realized in the compound interferometer where k is a small integer. In this simplest case, where the thickness of the thicker etalon is a multiple of the thickness of the thinner etalon, all the maxima of the thinner etalon belonging to the orders p_1, $(p_1\pm1)$, $(p_1\pm2)$, $\cdots$ will appear. According to (14.10) however, only the orders p_2, $(p_2\pm k)$, $(p_2\pm 2k)$, $\cdots$ of the thicker etalon will be obtained with the maximum intensity

$$I_{\max}=s_1^2s_2^2/(1-r_1)^2(1-r_2)^2.$$

The other orders of the thicker etalon $(p_2\pm1)$, $(p_2\pm2)$, $\cdots$ $(p_2\pm(k+1))$, $(p_2\pm(k+2))$, $\cdots$ $(p_2\pm(2k-1))$, which give rise to a maximum of the second factor in (14.7) will appear also, but with very much weaker intensity, because the first factor in (14.7) becomes very small for these orders.

Between the maxima there are minima of intensity, occurring approximately when $\sin^2\pi p_2$ in the second factor of (14.7) becomes unity,

thus making the second factor a minimum. This will take place for the orders $(p_2 \pm \frac{1}{2})$, $(p_2 \pm \frac{3}{2})$, $\cdots$, but the exact positions of the minima are slightly different from these values due to the influence of the first factor. Generally, these minima do not coincide with minima of the thinner etalon; only if $k=1, 3, 5, \cdots$, there is one minimum half-way between the principal maxima for which both factors in (14.7) are a minimum. In this case the minimum intensity becomes

$$I_{\min} = I_{\max}/(1+4r_1/(1-r_1)^2)(1+4r_2/(1-r_2)^2).$$

The intensity of the other minima cannot be given by a simple expression but can be numerically calculated for a given case.

It should be mentioned that the exact positions of the intermediate maxima are also slightly influenced by the first factor so that their positions are shifted towards the neighboring principal maximum.

For the elucidation of all the statements given above, a special case is treated in Table VII. It is assumed that the thickness of one etalon is four times that of the other. The reflection power is assumed to be the same, $r_1=r_2=0.8$, so that $4r/(1-r)^2=80$.

Although the intensities of the suppressed orders are very much weaker than those of the principal maxima, they are strong enough for producing patterns on a spectrogram if long exposure times are employed. This can be a source of error, as a confusion with weak lines of the transmitted orders is possible. However, the application of different combinations of etalon gaps will eliminate every doubt as the patterns of lines of the transmitted orders will not change their relative positions, whereas the suppressed orders will do this if the thick etalon gap is kept constant and the thinner one is varied.

The intensities of the intermediate maxima depend upon the reflection power and on their position relative to the principal maxima. The closer they are to these maxima, the stronger they are, and therefore they may easily cause confusion with weak lines. In order to avoid this, the ratio k must not be too large. The greater the value of k, the greater will be the number of small, intermediate maxima, and if k is appreciably large, these maxima will be so close to the neighboring principal maxima that their intensity is strong enough to act on a photographic plate during normal exposure times. A maximum value of $k=4$ usually will increase the spectral range of the thicker etalon satisfactorily.

TABLE VII. Position and relative intensity of the maxima and minima.

Exact order of the thin etalon	Approximate order of the thin etalon	Approximate order of the thick etalon	$I/I_{\max}$	Remarks
				Principal
p_1	p_1	$p_2=4p_1$	1	Maximum
$p_1 \pm 0.156$	$p_1 \pm 1/8$	$p_2 \pm 1/2$	1/1300	Minimum
$p_1 \pm 0.244$	$p_1 \pm 2/8$	$p_2 \pm 1$	1/41	Maximum
$p_1 \pm 0.383$	$p_1 \pm 3/8$	$p_2 \pm 3/2$	1/5600	Minimum
$p_1 \pm 0.500$	$p_1 \pm 4/8$	$p_2 \pm 2$	1/81	Maximum
$p_1 \pm 0.617$	$p_1 \pm 5/8$	$p_2 \pm 5/2$	1/5600	Minimum
$p_1 \pm 0.756$	$p_1 \pm 6/8$	$p_2 \pm 3$	1/41	Maximum
$p_1 \pm 0.844$	$p_1 \pm 7/8$	$p_2 \pm 7/2$	1/1300	Minimum
$p_1 \pm 1.000$	$p_1 \pm 8/8$	$p_2 \pm 4$	1	Principal Maximum

The theory of the multiplex interference spectroscope obviously is the same as for the compound interferometer. For the evaluation of the patterns, however, the refractive index of the plate material has to be known, while in the case of the compound interferometer, the procedure for wave-length or interval measurements remains the same as for the simple interferometer.

As we saw, the thickness of the thicker etalon has to be exactly a multiple of that of the thinner etalon. Naturally, this condition can be fulfilled only with a limited accuracy in advance and therefore an accurate adjustment must be performed when the final set-up is made.

In the case of the multiplex interference spectroscope, the fine adjustment can be made by a slight inclination of the plates against each other until the right orders are in coincidence.

The simplest way to adjust the compound interferometer is to put one of the etalons in an air-tight chamber in which the density of the air, and herewith the position of the different orders, can be varied until the right orders are in coincidence. For the preliminary adjustments, the phenomenon of the "superposition fringes" is used. These appear in white light as soon as the thicknesses of the etalons are in a simple ratio, as Fabry and Perot pointed out.[1]

[1] Fabry and Perot, Ann. Chim. Phys. **12**, 459 (1897).

§15. Resolving Power of the Compound Interferometer

The resolving power of the compound interferometer can be derived in the same way as was done in §6 for the simple interferometer. But, in order to avoid too complicated expressions, we restrict ourselves to the treatment of the approximation which corresponds to *Childs'* treatment of the simple interferometer (see end of §6); we neglect the overlapping of the intensity curves at the maximum of the lines (see Fig. 7 in Part I). Regarding the relations (13.3) and (13.7), we write the intensity expression (14.7) in the form

$$I=(s_1^2 s_2^2/(1-r_1^2)(1-r_2^2))$$
$$\times(1+\eta_1\sin^2\pi p_2/k)^{-1}(1+\eta_2\sin^2\pi p_2)^{-1}, \quad (15.1)$$

where

$$\eta_1=4r_1/(1-r_1)^2 \quad \text{and} \quad \eta_2=4r_2/(1-r_2)^2.$$

The subscript 2 refers to the greater etalon.

As in §6, we consider two close lines, λ and $\lambda+\Delta\lambda$ which may be just resolved. The maximum of the line λ may have the integral order p; the maximum of the other line may be situated at a distance which corresponds to the order $p+\Delta p$ in the order scale of the line λ. Then, the maximum intensity will be obtained from the intensity formula by replacing p_2 by p:

$$I_{\max}=I(p).$$

Similarly, the intensity at the saddle of the superimposed intensity curve is found as

$$I_{\text{saddle}}=2I(p+\Delta p/2).$$

TABLE VIIIa. Increase of the resolving power of the compound interferometer in comparison with the larger single interferometer.

η_1/η_2 \ k	1	2	3	4
$\frac{1}{3}$	1.28	1.09	1.04	1.03
$\frac{1}{2}$	1.38	1.13	1.06	1.04
1	1.61	1.25	1.12	1.07
2	1.94	1.38	1.20	1.09
3	2.22	1.50	1.28	1.18

TABLE VIIIb. $\eta=4r/(1-r)^2$.

r	0.6	0.65	0.7	0.75	0.8	0.85	0.9
η	15	23	31	48	80	155	360

According to the modified *Rayleigh* condition for resolution (§6), it must be:

$$I_{\max}=1.25\, I_{\text{saddle}},$$

and therefore,

$$I(p)=2.5\, I(p+\Delta p/2).$$

Thus, with the intensity formula (15.1), we get as condition for resolution

$$(1+\eta_1\sin^2\pi p/k)^{-1}(1+\eta_2\sin^2\pi p)^{-1}$$
$$=2.5(1+\eta_1\sin^2\pi(p+\Delta p/2)/k)^{-1}$$
$$\times(1+\eta_2\sin^2\pi(p+\Delta p/2))^{-1}.$$

Considering that p and p/k are whole numbers, we get:

$$1=2.5(1+\eta_1\sin^2\pi\Delta p/2k)^{-1}(1+\eta_2\sin^2\pi\Delta p/2)^{-1}$$

or

$$\eta_1\sin^2\pi\Delta p/2k+\eta_2\sin^2\pi\Delta p/2$$
$$+\eta_1\eta_2(\sin^2\pi\Delta p/2k)(\sin^2\pi\Delta p/2)=1.5. \quad (15.2)$$

Furthermore, introducing the relation $|R|=p/\Delta p$ between resolving power R, order number p, and the order interval Δp which is just resolved, we can write the condition for resolution in the final form:

$$\eta_1\sin^2(\pi p/2kR)+\eta_2\sin^2(\pi p/2R)$$
$$+\eta_1\eta_2\sin^2(\pi p/2kR)\sin^2(\pi p/2R)=1.5.$$

Under normal conditions, the metal films of the etalons have such high reflecting power that, in the neighborhood of the maxima, the intensity drops rapidly. Therefore, within the limit of accuracy of our approximation, the sines can be replaced by the corresponding angles:

$$\eta_1(\pi p/2k)^2R^{-2}+\eta_2(\pi p/2)^2R^{-2}$$
$$+\eta_1\eta_2(\pi p/2k)^2R^{-4}=1.5. \quad (15.3)$$

The solution of this equation yields the resolving power of the compound interferometer, for which the notation R_C may be used:

$$R_C=6^{-\frac{1}{2}}\pi p_2\eta_2^{\frac{1}{2}}\cdot 2^{-\frac{1}{2}}[1+(\eta_1/\eta_2)k^{-2}$$
$$+(1+8(\eta_1/\eta_2)k^{-2}+(\eta_1/\eta_2)^2k^{-4})^{\frac{1}{2}}]^{\frac{1}{2}}. \quad (15.4)$$

We use p_2 instead of p in order to show that the order number of the thicker etalon is meant.

The formula (15.4) yields the resolving power of the single thicker etalon if we put $\eta_1=0$, or $k=\infty$, which means that there is no thin etalon or an infinitely thin one:

$$R_{\text{single}}=6^{-\frac{1}{2}}\pi p_2\eta_2^{\frac{1}{2}}=2.56p_2r_2^{\frac{1}{2}}/(1-r_2)$$

in accordance with Childs' result (§6, end). Using the last relation, we can write the Eq. (15.4) in the form:

$$R_C=R_{\text{single}}C_2, \tag{15.5}$$

where C_2 is given by formula (15.4).

Taking $k=1$, we obtain the resolving power of two etalons of the same thickness in series ($p_1=p_2=p$):

$$R_C'=6^{-\frac{1}{2}}\pi p\eta_2^{\frac{1}{2}}\cdot 2^{-\frac{1}{2}}[1+\eta_1/\eta_2 + (1+8(\eta_1/\eta_2)+(\eta_1/\eta_2)^2)^{\frac{1}{2}}]^{\frac{1}{2}}. \tag{15.6}$$

This means an appreciably higher resolution than that of the single etalon. In the case of identical etalon plates ($\eta_1=\eta_2=\eta$), we find

$$R_C''=6^{-\frac{1}{2}}\pi p\eta^{\frac{1}{2}}\cdot 2^{-\frac{1}{2}}[2+10^{\frac{1}{2}}]^{\frac{1}{2}}=4.12pr^{\frac{1}{2}}/(1-r)$$

or

$$R_C''=1.61\ R_{\text{single}}. \tag{15.7}$$

The expression (15.4) for R_C has been written in such a way that it contains the resolving power of the single thicker etalon as a factor. However, we can write it in such a way that the resolving power R_1 of the thinner etalon occurs. Introducing the relation $p_2=p_1k$, we can easily transform (15.4) into:

$$R_C=6^{-\frac{1}{2}}\pi p_1\eta_1^{\frac{1}{2}}\cdot C_1, \tag{15.8}$$

where

$$C_1=k(\eta_2/\eta_1)^{\frac{1}{2}}\cdot C_2.$$

Formulae (15.5) and (15.8) show that there are two possibilities of describing the combined action of the two etalons, depending upon whether we regard the thinner or the thicker etalon as the auxiliary instrument. Regarding the thinner etalon as a complementary outfit, as we did in §13, we can say that the resolving power of the compound interferometer is mainly determined by that of the thicker etalon, and that the thinner etalon has the function of increasing the spectral range of the thicker one. However, as we see, it is possible to regard the thicker etalon as the auxiliary instrument; then the thicker etalon has to be described as an enlarger of the resolving power, the spectral range of the smaller etalon remaining unchanged.

Table VIIIa gives a compilation of the factor C_2 in formula (15.5) for different values of k and η_1/η_2, occurring in practical work. The values of η as functions of r can be taken from the attached Table VIIIb. The choice of the k and η_1/η_2 values depends upon the special problems.

It may be mentioned that W. V. Houston, who invented the compound interferometer, derived an approximate expression for its resolving power. His expression is different from that given in this report, because the definition of resolution is different. Houston made the assumption that "two fringes can be recognized as distinct if their maxima are separated by a distance equal to the width of one image where its intensity has dropped to one-half its maximum value." As it will be shown in §16, this width, the so-called "apparatus width," can be expressed by

$$A_\lambda=2\pi^{-1}(\eta_1+k^2\eta_2)^{-\frac{1}{2}}\langle\Delta\lambda\rangle,$$

where the range of dispersion $\langle\Delta\lambda\rangle$, according to (5.2), equals λ/p_1, p_1 being the order of the smaller etalon. Therefore, the resolving power as defined by Houston is given by

$$R^*_C=\lambda/A_\lambda=2^{-1}p_1\pi(\eta_1+k^2\eta_2)^{\frac{1}{2}}.$$

For $\eta_1=\eta_2=4r/(1-r)^2$, we get

$$R^*_C=p_1\pi r^{\frac{1}{2}}(1-r)^{-1}(1+k^2)^{\frac{1}{2}}.$$

This is Houston's formula, written in the notation of this report. Using order numbers $p_2=kp_1$ of the thicker etalon, we can transform this expression into

$$R^*_C=p_2\pi r^{\frac{1}{2}}(1-r)^{-1}(1+k^{-2})^{\frac{1}{2}}.$$

§16. Apparatus Half-Width

In close connection with the treatment of the resolving power is that of the apparatus half-width, which for the simple interferometer has been treated at the end of §4. The half-width is defined as the total width of the intensity curve for an intensity equal to $\frac{1}{2}I_{\max}$. It can be expressed in order numbers of the thicker or thinner etalon, or in wave numbers, or in

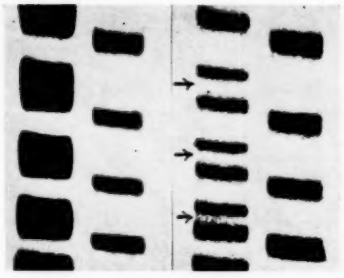

(a) (b)

FIG. 11. Absorption of neon line 6402A.

angstrom units. For the derivation, we use order numbers of the thicker etalon.

An approximate value of the half-width, sufficient for most of the practical applications, can be found from an approximation of the general intensity formula (15.1). Putting $p_2=p_2'+\gamma$, where p_2' (and also $p_2'/k=p_1'$) is a whole number, we write (15.1) in the form

$$I_\gamma=I_{\max}(1+\eta_1\sin^2(\pi\gamma/k))^{-1}\times(1+\eta_2\sin^2(\pi\gamma))^{-1}. \quad (16.1)$$

In the neighborhood of the principal maxima, we can use the approximation

$$I_\gamma=I_{\max}(1+\eta_1(\pi\gamma/k)^2)^{-1}(1+\eta_2(\pi\gamma)^2)^{-1}. \quad (16.2)$$

For $\gamma=\gamma_h$, the intensity may be $\frac{1}{2}I_{\max}$, so that γ_h is determined as a root of the equation

$$(1+\eta_1(\pi\gamma/k)^2)(1+\eta_2(\pi\gamma)^2)=2.$$

Neglecting the term with γ^4, one derives as first approximation the total width $2\gamma_h$, measured in order numbers of the thick etalon

$$2\gamma_h=2k\pi^{-1}(\eta_1+k^2\eta_2)^{-\frac{1}{2}}. \quad (16.3)$$

In order numbers of the thinner etalon as units, we get

$$2\gamma_h'=2\pi^{-1}(\eta_1+k^2\eta_2)^{-\frac{1}{2}}. \quad (16.4)$$

The apparatus width can be expressed in wave numbers by transformation of (16.3) or (16.4) with the same relations as we used in (5.6):

$$A_\nu=2\gamma_h/2t_2=2\gamma_h/2kt_1=2\gamma_h'/2t_1=2\pi^{-1}(\eta_1+k^2\eta_2)^{-\frac{1}{2}}/2t_1. \quad (16.5)$$

Introducing the spectral range in wave numbers $\langle\Delta\nu\rangle=1/2t_1$, we can write

$$A_\nu=2\pi^{-1}(\eta_1+k^2\eta_2)^{-\frac{1}{2}}\langle\Delta\nu\rangle \text{ cm}^{-1}. \quad (16.6)$$

The half-width expressed in angstrom units will be correspondingly:

$$A_\lambda=2\pi^{-1}(\eta_1+k^2\eta_2)^{-\frac{1}{2}}\langle\Delta\lambda\rangle A. \quad (16.7)$$

Putting $\eta_2=0$, we have to get the half-width of the thinner etalon. Equation (16.6), for instance, yields the value

$$A_\nu'=2\pi^{-1}\eta_1^{-\frac{1}{2}}\langle\Delta\nu\rangle=\pi^{-1}r_1^{-\frac{1}{2}}(1-r_1)\langle\Delta\nu\rangle \quad (16.8)$$

in accordance with formula (5.6). With $\eta_1=0$, we obtain in the same way the half-width of the thicker etalon

$$A_\nu''=\pi^{-1}r_2^{-\frac{1}{2}}(1-r_2)\langle\Delta\nu\rangle/k, \quad (16.9)$$

where $\langle\Delta\nu\rangle/k$ is the spectral range of the thicker etalon.

Formula (16.6) in connection with (16.8) and (16.9) shows that the fringes are sharper with the compound interferometer than with the thicker etalon alone, a conclusion we have already drawn from the treatment of resolving power.

It is easy to derive expressions of higher approximations, but for practical purposes the given formulae are sufficient, the accuracy for normal η values being within 1 to 2 percent.

III. SOME APPLICATIONS OF THE FABRY AND PEROT INTERFEROMETER

§17. Application for the Investigation of Absorption Spectra (Solar Spectrum)

In the treatment of the Fabry-Perot and of the compound interferometer, we considered their application exclusively in the investigation of emission lines. It is obvious that these instruments can be used for the investigation of absorption lines without any change in the arrangements described in §8, as long as the continuous background has a smaller extension than the spectral range. An example is reproduced in Fig. 11 which shows strong absorption for the neon line 6402A. Light emitted by the capillary part of a neon discharge tube passed through a second neon tube of larger cross section, excited by a very weak glow discharge. The width of the

lines emitted by the latter tube is smaller than the width of the lines emitted by the capillary part. Therefore, narrow absorption lines appear in the middle of the broader patterns produced by the capillary tube. The lines belonging to metastable states as final levels show especially strong absorption. The neighboring line 6382A does not show absorption because no metastable states are involved in the emission of this line.

As soon as the continuous background covers a wave-length interval slightly greater than the spectral range, the different orders of the background overlap. Then the region of the absorption line will be masked, but not quite extinguished, by the light of different wave-lengths belonging to the neighboring orders. As long as we have to deal only with the position of absorption lines, a partial overlapping is not serious, but, as soon as conclusions about the intensity of absorption lines need be drawn, the overlapping of the background patterns can be a serious source of error. For such purposes, the proper width of the background must be chosen very carefully.

When the background covers a great wave-length region. e.g., as in the case of the solar spectrum, the use of interferometric methods seems to be impossible. However, Fabry and Buisson[2] have pointed out in what manner the interferometer can be applied to this case also.

The method is important for the determination of Standard solar wave-lengths,[3] and may, therefore, be described in detail.

Let us suppose a Fabry-Perot interferometer to be crossed in the usual manner with a stigmatic spectroscope and to be adjusted in such a manner that the center of the interference rings of emission lines coincides with the middle of the slit image.

We furthermore assume that the spectroscope is furnished with a slit of the symmetric type, the center line of which always traverses the center of the interference rings, whatever the width of the slit may be.

At first the slit may be very narrow. When light of a continuous source is sent through this arrangement, the spectrum consists of bright, narrow fringes of parabolic shape which are separated by broader, dark intervals (See Fig. 12a).

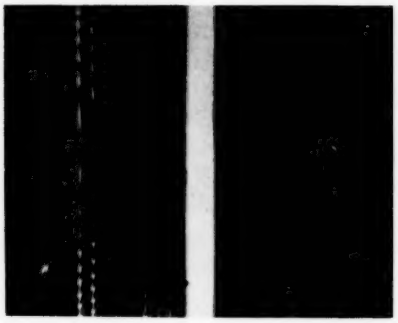

(a) (b)

FIG. 12. Channeled spectrum with solar absorption lines (negative). The dark line in (b) is a neon emission line. Publ. Allegheny Obs., reference 17.4.

The formation of this so-called "channeled spectrum" can easily be understood, if one regards a continuous spectrum as consisting of a continuous series of narrow, monochromatic spectral lines. Under the action of the interferometer, in each of these narrow lines the familiar Fabry-Perot patterns are formed. Along a line of the average wave-length λ, there will be spots of maximal intensity in such distances R for which the fundamental formula (2.6) $p\lambda = 2t(1 - R^2/2f^2)$ is fulfilled. The patterns of the adjacent regions of the continuous spectrum will show a slight change of the radii of the rings which shrink with increasing wave-length. One can easily see that the bright spots of consecutive lines merge, forming bright curves which are nothing else but the interference lines of the channeled spectrum. The sharpness of these lines depends upon the resolution of the interferometer and the auxiliary spectroscope.

A certain bright interference fringe of the channeled spectrum is characterized by a constant order p, while the neighboring fringes have the orders $(p \pm 1)$. When the interferometer is crossed with a grating, producing an approximately constant dispersion, the shape of the channel interference fringes can be calculated. The fundamental formula (2.6) can be regarded as the equation of a family of curves, the λ and

[2] Ch. Fabry, Comptes rendus **140**, 1136 (1905). Ch. Fabry and H. Buisson, J. de phys. **9**, 197 (1910).

[3] K. Burns and Wm. F. Meggers, Pub. Allegheny Obs. **6**, 105 (1925).

R values being the abscissae and the ordinates, respectively, and p being the parameter. Within the approximation of the formula (2.6), valid for small values of R/f alone, the curves can be regarded as parabolas, their vertices being situated at wave-lengths determined by $\lambda = 2t/p$. The vertices of two consecutive parabolas have a separation $\Delta\lambda$ equal to the range of dispersion of the interferometer. The higher the order of interference, the closer the channels will be. It is obvious that, for the production of fine channels, the resolving powers of the auxiliary spectroscope and of the interferometer must be of the same order of magnitude.

If now the continuous spectrum contains absorption lines, the appearance of the channeled spectrum will be changed. In this case the bright channels will be interrupted by dark regions, the positions of which correspond to the wave-lengths of the absorption lines (Fig. 12a). In other words, they are determined by the intersection of the parabolas with the absorption lines. These dark spots have exactly the same positions as bright interference patterns would have if they were formed by emission lines of the same wave-lengths as those of the absorption lines. Therefore, principally, it is possible to measure the relative position of the dark spots of an absorption line, to calculate the R values, and to use the same methods of wave-length calculations as for emission lines (§9 and §10). Practically, however, the measurement is very difficult because the spots have a very small extension in the direction of the grating dispersion. It would be very much more convenient if the spots could be broadened in this direction.

This can easily be accomplished by opening the slit of the spectral apparatus. As soon as we do this, the bright parabolic channels become broader. At the same time, the dark spots due to the absorption lines spread out with respect to the grating dispersion. When the slit is so wide that consecutive channels touch each other, the channels coalesce and disappear. At this point, the spectrum has the appearance of a continuous spectrum, containing the dark "interference fringes" of the absorption lines (Fig. 12b). The appearance of this spectrum is exactly the same as the negative of a spectrum with emission lines. The measurement of the ring systems is very much more convenient and exact than it was in the presence of the distinctly visible channels.

The optimum slit width at which the channels coalesce depends upon the spectral region because the vertex separation of consecutive channels equals $\lambda^2/2t$. When, by the proper choice of the slit width, the channels are invisible for short wave-lengths, they will still be separated for longer wave-lengths. Therefore, if one has to deal with the investigation of absorption spectra covering a large range of wave-lengths (solar spectrum, e.g.), a great number of exposures with different slit widths must be made.

For a clear understanding of the influence of the slit width on the appearance of the channeled spectrum, it may be mentioned that the spectrum obtained at the time of disappearance of the channels is not a real continuous spectrum. By the combined action of interferometer and grating, the radiation of a certain wave-length interval covers only a small region of a channel. The horizontal extension of this region, due to the dispersion of the grating, is determined by the width of the slit, the vertical extension by the wave-length interval. The neighboring radiations of different wave-length are continuously arranged one upon another, simultaneously shifted in the direction of the spectroscope dispersion. If the slit width is increased, the horizontal extension of a monochromatic region is increased, the vertical remaining unchanged. When the slit is opened to such a degree that the neighboring channels coalesce, the wave-length changes discontinuously from one channel to the adjacent one. For the center of the interference system, this wave-length change is equal to the spectral range of the interferometer. The continuous spectrum, therefore, is not a real one; we could call it a pseudo-continuum.

If there is no interferometer present, the continuous spectrum is influenced quite differently by the slit width. In this case, opening of the slit causes a superposition of the different neighboring wave-lengths. The resulting spectrum is an impure continuum.

C. D. Shane applied this method for the study of the structure of solar spectrum lines.

It is obvious that the compound interferometer can be used in the same way as the simple Fabry-

Perot instrument for the investigation of absorption spectra.

§18. Intensity Distribution in Spectral Lines

In the first part of this report, we did not take into account that a spectral line has a certain intensity distribution. When we spoke of the wave-length of a line, there was always implied that the wave-length value referred to the center of gravity of the line patterns. However, there are many radiation problems which cannot be treated satisfactorily by the measurement of wave-lengths alone. Very often the intensity distribution of a line, or at least the half-width of the line, is of interest. The latter is defined as the total width of the intensity-frequency curve ($I=f(\nu)$) for an intensity equal to half the maximum intensity.

As preferably interferometric methods are in use for the solution of such problems, a brief outline of the subject may be given.

Experimentally, the intensity distribution curve is obtained by means of direct or photographic photometry of the patterns produced by a powerful spectral apparatus. The intensity distribution $I=F(\nu)$, gained in this manner, is not the true one of the light source, $I=f(\nu)$, because of the restricted resolving power of the spectroscope.

An ideal spectroscope, having an infinitely high resolving power, would analyze the radiation of a light source perfectly. According to the individual law of dispersion of the spectroscope, $\nu=f(\varphi)$, each frequency corresponds to a definite deviation angle φ, and, therefore, a small band $\Delta\nu$ of frequencies between ν and $(\nu+\Delta\nu)$ would be reproduced by a quite definite angular interval between φ and $(\varphi+\Delta\varphi)$. If, furthermore, the incident intensities would be diminished by the spectrograph equally for all wave-lengths, the intensity distribution of the light source would be reproduced without distortion also.

A real spectroscope acts quite differently. Owing to the peculiar interference or diffraction effects occurring in the apparatus, the light of a small frequency band $\Delta\nu$ covers a greater geometrical interval than one would expect according to the dispersion law of the apparatus. Radiation of frequency ν is thrown into regions of other frequencies and the intensity distribution is spuriously distorted. In order to obtain the true distribution, one must reduce the experimental distribution.

This would be possible if one knew the intensity distribution produced by the apparatus with strictly monochromatic light. In the case of the Fabry-Perot interferometer, the calculation of the distribution function is possible (§4) and also for the other instruments, suitable for the analysis of spectral lines. The apparatus distribution function can be described by giving the intensity ratio $I/I_{\max}$ as a function of wave-lengths, wave numbers, or order numbers. As the origin of these scales, one usually applies the point of maximum intensity.

In formula (4.6), the intensity distribution in the neighborhood of the maximum is described by using the order distance from the maximum. The approximation of this formula is sufficient for the treatment of the usual intensity distri-

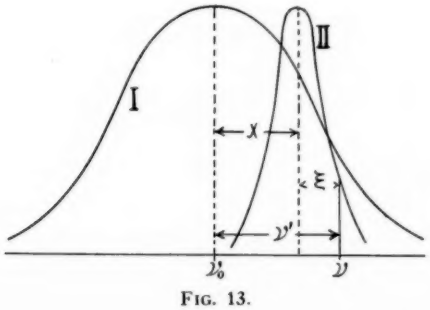

FIG. 13.

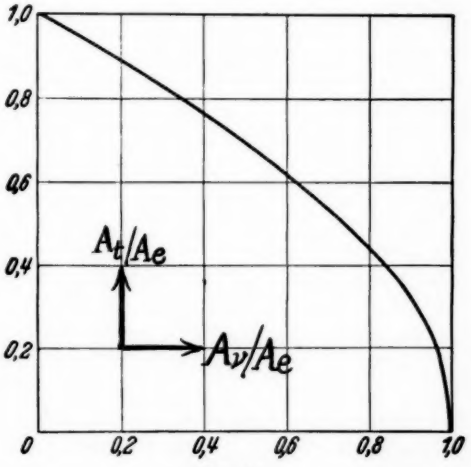

FIG. 14.

bution problems. Sometimes, one prefers the distribution function in the form $I=\varphi(\nu)$ or $I=\varphi(\nu-\nu_0)=\varphi(\xi)$, where ν_0 is the frequency of the maximum. The latter form for the Fabry-Perot instrument can easily be obtained by transformation of Eq. (4.6). By using the relations (4.5), (5.6), and $\Delta\nu=\langle\Delta\nu\rangle\cdot\gamma$, formula (4.6) becomes:

$$I(\xi)/I_{\max}=1/(1+4\xi^2/A_\nu^2), \qquad (18.1)$$

where A_ν is the apparatus half-width.

The observed intensity distribution of a somewhat broad spectral line is the result of the addition of the overlapping monochromatic areas in which the narrow strips $F(x)dx$ of the true intensity curve are distorted by the spectral apparatus ($x=\nu-\nu_0$ is the frequency distance from the maximum of the line). If the true distribution $f(x)$ and the apparatus distribution are known, it is possible to calculate the experimental distribution.

The true intensity distribution may be represented by the curve I of Fig. 13, the apparatus distribution by the curve II. The analytical expression for the first may be $I=f(x)$ and for the latter $I=\varphi(\xi)$. A small interval between x and $(x+dx)$, having an intensity proportional to $f(x)dx$, produces, by the action of the spectroscope, at a place attributed to a frequency ν, an intensity proportional to

$$dI=f(x)dx\varphi(\xi)=f(x)\varphi(\nu-\nu_0-x)dx$$
$$=f(x)\varphi(\nu'-x)dx,$$

where we put $\nu'=(\nu-\nu_0)$. The summation of the contributions of all the other intervals dx will give the relative intensity observed at a distance ν' from the maximum; therefore, the observed intensity distribution will be:

$$I(\nu')=\int_{-\infty}^{+\infty} f(x)\varphi(\nu'-x)dx. \qquad (18.2)$$

§19. Half-Width of Spectral Lines

It is not intended to treat here the general problem of determining the true distribution from the experimental and apparatus distribution. Only this question may be discussed: How does the half-width of the observed distribution depend upon the apparatus half-width, and how

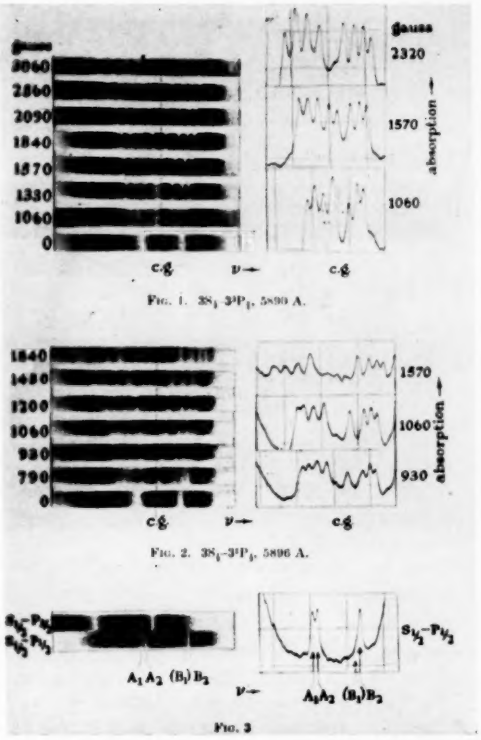

FIG. 15. Zeeman effect of the hyperfine structure of the sodium D lines. (Jackson and Kuhn, courtesy of Proc. Roy. Soc. London.)

can the true half-width of a spectral line be found from the observed intensity distribution?

The most common reason for the broadening of spectral lines is the Doppler effect. The intensity distribution due to the random motion of the emitting particles is called Doppler distribution, and has the form

$$I(x)=\exp(-x^2/q^2). \qquad (19.1)$$

The half-width of this distribution (we call it the true half-width A_t) is given by

$$A_t=2q(\log_e 2)^{\frac{1}{2}}.$$

In order to see how a line with Doppler distribution is distorted when analyzed by means of a Fabry-Perot interferometer, one can calculate, by means of (18.2) and of the distributions (18.1) and (19.1), the distribution which one would obtain experimentally. Furthermore, it is

FIG. 16. Patterns of Cd 6438A obtained with 18-cm etalon and with an atomic beam of Cd excited by electron impact.

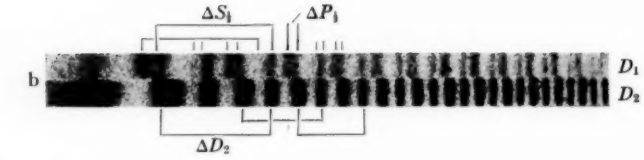

FIG. 17. Hyperfine structure of sodium D lines (atomic beam and 12-cm etalon).

FIG. 18. Structure of sodium lines. (a) λ5682A and 5688A. $\nu = 3^2P_{3/2,1/2} - 4^2D_{5/2,3/2}$. 60-mm etalon. (b) λ6154A and 6160A. $\nu = 3^2P_{3/2,1/2} - 5^2S_{1/2}$. 36-mm etalon.

possible to derive the half-width A_e of this distribution and to investigate the relation between true width A_t, experimental width A_e, and apparatus width A_ν. This has been done by Burger and van Cittert and, more generally, by Minkowski and Bruck. The latter summarized the results of their calculations, which we do not reproduce, in a curve, shown in Fig. 14. As the abscissae the ratios A_ν/A_e are chosen, and as ordinates A_t/A_e. This curve, principally valid only for lines with Doppler distribution, can be used for the reduction of the measured half-width to the true one, if A_ν is known.

As we see, A_e is not simply the sum of A_ν and A_t. In the range $0.5 < A_t/A_\nu < 1$, for instance, is

$$A_e = 0.80A_\nu + 0.81A_t \quad \text{or} \quad A_t \approx 1.25A_e - A_\nu.$$

A very simple relation exists between the three widths when a line with natural width or a width due to damping by collision is analyzed with an etalon. For this case, Minkowski and Bruck derive that $A_e = A_\nu + A_t$. For details, the reader must be referred to the original papers quoted in the bibliography.

Some experimental remarks, however, should be added. The half-width A_e of the patterns is usually obtained by means of photographic photometry. The recorded curves must be reduced to intensity curves by means of intensity marks. Furthermore, a reduction of the abscissae to a wave number scale is necessary. As a recording photometer usually furnishes the intensities as a function of a linear scale, the simplest method of reduction is to plot the intensity values against the squares of the radii of the patterns and to use formula (9.3) for the reduction to ν values.

The apparatus width A_ν can be calculated from the reflectivity according to formula (5.6), but it is more advisable to determine it in the following manner: With very small spacers of the etalon the patterns of very sharp lines are investigated in the way described above. These measurements yield immediately the apparatus width for the given etalon distance. It is $A_\nu = A_e$, because $A_\nu \gg A_t$. The apparatus width for any larger etalon distance then can be calculated with formula (5.6). This method also takes account of slight inhomogeneities of the metal coating and of slight variations of the thickness of the etalon. Both deviations from the ideal state decrease the resolving power of the interferometer and cause it to act as though a smaller reflection power were present.

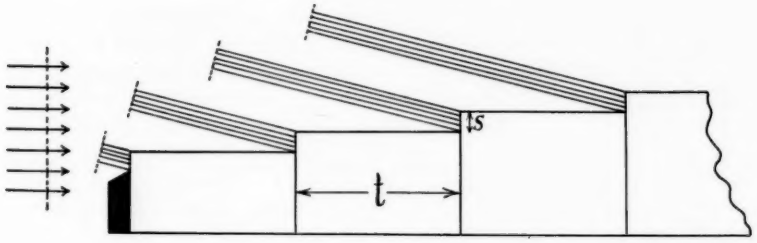

FIG. 19. Reflection echelon; principle.

A very simple method for the determination of the half-width of Fabry-Perot patterns without knowing the whole density curve of the photographic plate is described in the quoted paper of Burger and van Cittert.

§20. Some Recent Investigations by Means of Interferometers and Atomic Beams

It is not intended to go into details of the numerous investigations in the field of interference spectroscopy. Only a few examples may be given in order to show the trend of the development in the last few years.

From the results of §6 and §15, it can be seen that it is not difficult to obtain a resolving power of several millions by means of interferometers, if only a sufficiently high reflectivity of the metal films and large spacers is applied. However, interferometers of such a high resolving power are useless for the investigation of spectral lines which are emitted by the common light sources. As the temperature of these sources is rather high, the lines show such a great Doppler width that very close fine structures remain unresolvable.

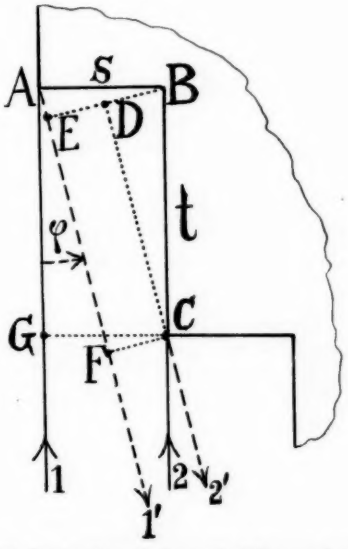

FIG. 20. Derivation of the path difference between consecutive waves.

In order to make use of the obtainable high resolving power, it is necessary to develop light sources with extremely reduced Doppler width. There is the possibility of operating the light sources at extremely low temperatures, but many experimental difficulties arise. Another possibility is the application of atomic beams which can be used very easily for the production of absorption lines. But also the production of emission lines is possible, when the beams are excited by light or electron impact. By observing such a beam in a direction perpendicular to it and by using a sufficiently small angular aperture of the light rays, one can diminish the broadening of the lines to such a small amount as would be obtained with a light source at a few degrees Kelvin.

During recent years Jackson and Kuhn have investigated the hyperfine structure of the resonance lines of several elements in absorption by means of unexcited atomic beams, and interferometers. The background for the production of the absorption lines was furnished by an emission tube which contained the vapor of the corresponding element. As an example of these investigations, we give in Fig. 15 a reproduction of the photographs and intensity curves obtained by these authors in an investigation of the Zeeman effect of the hyperfine structure of sodium. These patterns allow one to determine the nuclear spin of Na and were obtained with a compound interferometer in which a 2-cm and an 8-cm etalon were combined. The spectral

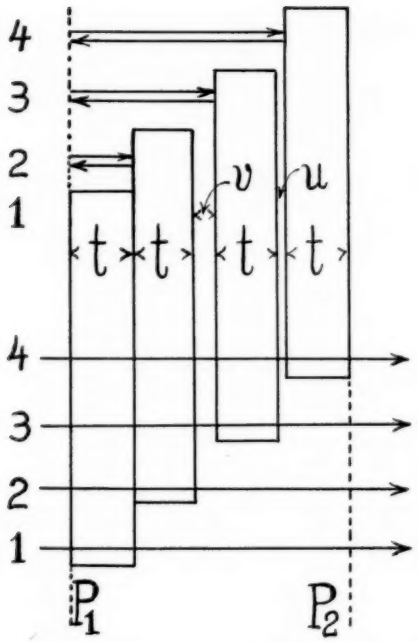

FIG. 21. Comparison of reflection and transmission echelon. The path differences between consecutive waves is affected by the air spaces u and v in the case of the reflection type.

range is about 0.25 cm^{-1} and the possible resolution about 0.003 cm^{-1}.

The absorption method is restricted to resonance lines alone. In order to produce the whole spectrum of an element it is necessary to excite the atoms of the beam by electron impact. This method was developed by Minkowski and Bruck and by Meissner and Luft independently. Bogros and Esclangon, and R. A. Fisher excited the beam by a high frequency discharge in the presence of argon at low pressure.

Minkowski and Bruck used the method for the investigation of the structure of the red cadmium line 6438A which was found to be asymmetric, probably due to unresolved isotopic shifts of the lines belonging to different isotopes. The half-width obtained with the atomic beam was about 1.9×10^{-2} cm^{-1}. Figure 16 is a reproduction of patterns of this line obtained by Meissner and Luft with a cadmium beam and by means of an 18-cm Fabry-Perot etalon. The asymmetry of the lines can be seen clearly. In this case, the resolving power was about four million.

Meissner and Luft investigated the hyperfine structure of the sodium D emission lines and were able to resolve the hyperfine structure of the $^2P_{\frac{1}{2}}$ level, the interval of which is only 0.0053 cm^{-1}, corresponding to a wave-length difference of 0.0020A (Fig. 17). In these experiments, the intensity of the atomic beam could be increased to such an amount that the investigation of all the stronger lines of the Na spectrum was possible. The ^2D term could be resolved. The separations involved vary from 0.03 to 0.01A and cannot be resolved when the usual light sources are applied. In Fig. 18 the patterns of two doublets are reproduced. The satellite present in the $^2P^2D$ line has a separation of 0.011A from the stronger component. The other doublet belongs to the sharp series and has, therefore, no satellite.

Other examples were given in Fig. 9 of Part I, showing the isotopic shift of Mg lines. Also in this case, the superiority of the atomic beam source over other light sources can be demonstrated. By employing a Schueler tube, the line attributed to Mg (25) could not be detected.

There is no doubt that the further development of the atomic beam light source is very important for interferometric investigations in the future.

IV. THE REFLECTION ECHELON DIFFRACTION GRATING

§21. Principle of the Instruments

Although only a few years have passed since the reflection echelon was introduced into spectroscopic research, the principle of the instrument is not new. When Michelson, in 1898, conceived the idea of the echelon principle, the device which was first considered was the reflection echelon. But the manufacture of the

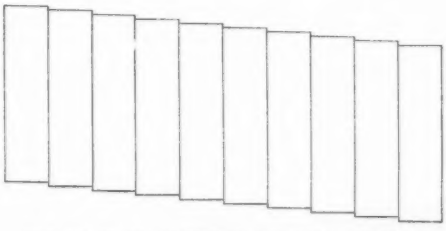

FIG. 22. Profile of Williams' reflection echelon.

instrument had been found impossible until the endeavors of W. E. Williams, in collaboration with Adam Hilger Ltd., London, were crowned with success.

The basic idea of Michelson started from the fact that the resolving power of an ordinary diffraction grating is given by the product of the order p of the spectrum, and the number N of the diffracting elements. With ordinary gratings, p is usually restricted to small values; N is large, but, for practical reasons, it cannot be increased sufficiently to obtain the high resolving power necessary for investigations of many problems arising in modern spectroscopy. Michelson's idea was to build an instrument which would enable one to work with orders so high that even a few diffracting elements would be sufficient to accomplish a great resolving power.

The new device was the following: A certain number (20 to 40) of plane parallel glass plates of exactly the same thickness t are built up in steps, each plate projecting beyond the last by a small equal amount s, and each plate being in direct contact with the neighboring ones. Furthermore, the small faces of the steps are coated with a very thin metal film (silver or platinum) in order to obtain sufficient reflectivity (Fig. 19).

A plane wave, produced by a collimator, may be incident normally to the steps. The incident wave front will be split by the single steps and will originate wavelets in each step, forming secondary, diffracted wave fronts. In the focus of a lens are formed diffraction spectra, the orders of which depend upon the angles of diffraction φ, the width of the steps s, and the thickness of the plates (height of the steps) t. The order of interference p, the path difference Δl of corresponding rays of two consecutive steps, and the wave-length λ are connected by the relation $\Delta l = p\lambda$. By inspection of Fig. 20, one can easily see that the path difference between the rays 1′ and 2′ is given by:

$$\Delta l = GA + AF = BC + DC + AE$$

or by introducing observable quantities,

$$p\lambda = t + t\cos\varphi + s\sin\varphi. \qquad (21.1)$$

For small diffraction angles, the order, therefore, will be:

$$p = (2t + s\varphi)/\lambda. \qquad (21.2)$$

In order to estimate the resolving power one could obtain in a special case, let us assume $t = 1$ cm and $\lambda = 5000$A. Then the order in the direction of the normal will be 40,000. Therefore, an instrument with 25 plates would have in this spectral region a resolving power of one million, very much more indeed than one can obtain with ordinary gratings.

Michelson himself has already pointed out the difficulties connected with the manufacture of these instruments. Even if the plates could be worked equal in thickness within $1/20\lambda$, it would be very difficult, or even impossible, to join the plates without distortion so that they lie on each other in perfect contact, or with an exactly constant air space between them. Indeed, this difficulty, which Michelson foresaw, was surmounted only ten years ago.

The difficulty of obtaining a perfect contact between the plates does not arise in the realization of Michelson's modified original idea, employing the echelon as a transmission instrument. This can easily be understood from Fig. 21 where several plates of equal thickness t are put together separated by unequal air spaces, and where it is assumed that the upper part is used in reflection and the lower part in transmission. For the sake of simplicity, the incident and diffracted rays are assumed to be normal to the steps. If one calculates the optical paths of the waves between plane P_1 and the steps for the reflection instrument, and between P_1 and P_2 for the transmission instrument, and from them the path differences between consecutive waves, one will find that they are independent of the air spaces for the transmission instrument, whereas they vary for the reflection echelon.

In the case of the transmission echelon, the path difference for $\varphi = 0$ is $(n-1)t$, in comparison with $2t$ for an ideal reflection echelon. Therefore, we understand that the accuracy of the plate thickness does not have to be so high as for a perfect reflection echelon. According to Williams, "the accuracy of workmanship in the reflection instrument is between three and four times higher than that of the transmission instrument when used in the same spectral region. A standard at least ten times higher than before has to be aimed at" for the use of the instrument in the Schumann region. These are the reasons why the

original idea of Michelson could not be realized, although the transmission type has been in use for over forty years.

In 1929, E. W. Williams accidentally found that plane plates of quartz or fused silica contact very easily without any pressure and without any distortional effect. In this case, the contact is so perfect that plates fitted together can barely be separated again, even after having been soaked in petrol for several days. This experience with quartz plates showed that by the use of this material the reflection echelon would become a practical possibility, if plane parallel quartz or silica plates of equal thickness could be worked. The final success proved that the hopes entertained in this direction were legitimate.

The construction of Williams' reflection echelon differs from the old transmission type as far as plates of equal size are put together. The profile of the assembled echelon is that of a double stair (Fig. 22). This construction is necessary in order to avoid distortions. The area of the plates is about 4×4 cm^2 and the thickness t varies from 6 to 8 mm and the step width is usually 1 mm. The number of the plates varies from 20 to 40.

As we restrict ourselves to the description of high resolving instruments suitable exclusively for absolute measurements, the transmission type will not be treated in the following. Readers interested in such instruments may be referred to the papers quoted in the bibliography.

§22. Intensity Distribution in the Echelon Patterns

The intensity distribution and the shape of the fringes formed by a reflection echelon at an infinitely distant point P_0, or at a point in the focal plane of a lens, can be found in two steps: (a) first, we calculate the amplitude of the vibration which is produced at point P_0 by the diffraction at the single echelon elements, (b) then, by summation of these vibrations, we obtain the amplitude and intensity at point P_0. Hereby, the phase difference of the vibrations originated by consecutive elements is involved. The first problem is a diffraction problem, the latter a pure interference problem, principally the same as we treated in §4 for the etalon.

In the case of the latter, the summation concerns an *infinite* number of vibrations with gradually *decreasing amplitudes*, whereas in the case of the echelon, a *finite* number of vibrations of *equal amplitudes* are superimposed. However, there is an important difference between the two cases: The echelon, as a diffraction instrument, requires the incidence of a plane wave, wherefore a collimator is needed; the plane parallel plate, on the other hand, must be illuminated by an extended light source or with convergent light rays in order to obtain fringes covering a suitable area of the focal plane of the projecting lens.

In order to obtain the formulae in a general form from which we can easily derive the formulae for special cases we do not restrict the treatment to the case where the rays involved are situated only in a principal section of the echelon. This simplified treatment, similar to that in §21, can be found in elementary books on optics.

The echelon may be placed in a coordinate system as indicated by Fig. 23. Step width, plate thickness (step height), and the length of the long edges are denoted by the letters s, t, and h, respectively. A plane wave of strictly monochromatic light may be incident. The direction of propagation is determined by the direction cosines α_0, β_0, γ_0 of the wave normal, the positive direction of which coincides with the direction of propagation. The normal of the diffracted wave, or better the direction in which the infinitely distant point P_0 is situated is given by corresponding cosines α, β, and γ. We assume that the angle of incidence is small, as it is in all practical cases. Then we are allowed to treat the reflecting faces (hs) as the diffracting elements.* They are equivalent to rectangular openings in a screen.

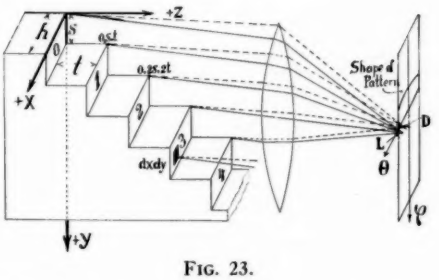

FIG. 23.

* It is easy to introduce the small corrections which for the transmission type have been calculated by H. C. van Geel (reference (21.4)).

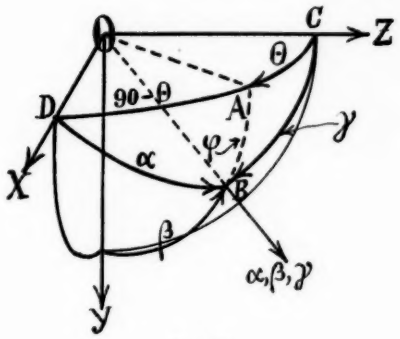

FIG. 24.

The incident wave

$$\exp\left[i\omega\tau - ik(x\alpha_0+y\beta_0+z\gamma_0)\right], \quad \gamma<0, \quad k=2\pi/\lambda,$$

produces at a point $P(x, y, 0)$ of the first step the vibration $\exp\left[i\omega\tau - ik(x\alpha_0+y\beta_0)\right]$. At a point $P(x, y+\mu s, \mu t)$ at the face of the μth step, correspondingly the excitation will be

$$\exp\left[i\omega\tau - ik(x\alpha_0+y\beta_0+\mu s\beta_0+\mu t\gamma_0)\right].$$

From the area element $dx \times dy$ at point P of the μth step a diffracted wave will start and produce at a very distant point $P_0(x_0, y_0, z_0)$, situated in direction α, β, γ, a vibration which we can write

$$dU = \text{Const.} \exp\left[i\omega\tau - ik(x\alpha_0+y\beta_0 + \mu s\beta_0+\mu t\gamma_0) - ik(d_0-d)\right],$$

where (d_0-d) is the distance between the wave fronts of the diffracted waves which traverse the points $P_0(x_0, y_0, z_0)$ and $P(x, y+\mu, \mu t)$. Therefore the partial vibration in P_0 is given by

$$\begin{aligned} dU &= \text{const.} \exp\left[i\omega\tau - ik(x\alpha_0+y\beta_0+\mu s\beta_0+\mu t\gamma_0)\right. \\ &\quad \left. - ik(x_0\alpha+y_0\beta+z_0\gamma) + ik(x\alpha+y\beta+\mu s\beta+\mu t\gamma)\right]dxdy \\ &= \text{const.} \exp\left(i\omega\tau - ikd_0\right)\cdot \exp ik\left[x(\alpha-\alpha_0)\right. \\ &\quad \left. + y(\beta-\beta_0)+\mu s(\beta-\beta_0)+\mu t(\gamma-\gamma_0)\right]dxdy. \end{aligned}$$

The superposition of the vibrations of all elements and steps gives the total vibration in P_0. By integration over the area of the single element, we obtain the excitation in P_0 due to the diffraction at a single step. The summation of the N single vibrations, which differ only with respect to the phase, gives the total vibration in P_0. The content of this statement is expressed in the following expression for the resultant vibration in P_0:

$$\begin{aligned} U_{P_0} &= \text{const.} \exp\left[i\omega\tau - ikd_0\right] \\ &\quad \cdot \int_0^h \exp\left[ikx(\alpha-\alpha_0)\right]dx \int_0^s \exp\left[iky(\beta-\beta_0)\right]dy \\ &\quad \sum_{\mu=0}^{\mu=N-1} \exp\left[ik(\mu s(\beta-\beta_0)+\mu t(\gamma-\gamma_0))\right]. \end{aligned} \tag{22.1}$$

The evaluation of the integrals and of the sum furnishes the expression:

$$\begin{aligned} U_{P_0} &= \text{const.} \exp\left[i\omega\tau - ikd_0\right] \\ &\quad \cdot \frac{\exp\left[ikh(\alpha-\alpha_0)\right]-1}{ik(\alpha-\alpha_0)} \cdot \frac{\exp\left[iks(\beta-\beta_0)\right]-1}{ik(\beta-\beta_0)} \\ &\quad \cdot \frac{1-\exp\left[ikN(s(\beta-\beta_0)+t(\gamma-\gamma_0))\right]}{1-\exp\left[ik(s(\beta-\beta_0)+t(\gamma-\gamma_0))\right]}. \end{aligned}$$

The observable intensity in P_0, given by $I = U\cdot\bar{U}$, can be written as

$$\begin{aligned} I_{P_0} &= I_0\left(\frac{\sin kh(\alpha-\alpha_0)/2}{kh(\alpha-\alpha_0)/2}\right)^2 \cdot \left(\frac{\sin ks(\beta-\beta_0)/2}{ks(\beta-\beta_0)/2}\right)^2 \\ &\quad \times \left(\frac{\sin kN[s(\beta-\beta_0)+t(\gamma-\gamma_0)]/2}{\sin k[s(\beta-\beta_0)+t(\gamma-\gamma_0)]/2}\right)^2, \end{aligned} \tag{22.2}$$

where we put

$$I_0 = (\text{const.}\ hs)^2.$$

Before we discuss the formula, we will transform it into a form which fits practical purposes better. First, we introduce instead of α_0, β_0, γ_0, the cosines

$$\alpha' = (\alpha_0-180), \quad \beta' = (\beta_0-180), \quad \gamma' = (\gamma-180).$$

This means that we measure the inclination of the incident rays in the same manner as the diffracted rays by reversing the sign of the normal of the incident wave. Furthermore, we will introduce the angles φ and θ which the rays make with the (xz) and (yz) planes, respectively (Fig. 24). The necessary relations are

$$\cos\alpha = \cos\varphi\sin\theta, \quad \cos\beta = \sin\varphi, \quad \cos\gamma = \cos\varphi\cos\theta.$$

After these transformations, the intensity

expression becomes:

$$\left.\begin{aligned} &I=I_0((\sin u)/u)^2\cdot((\sin v)/v)^2 \\ &\qquad\cdot((\sin Nw)/\sin w)^2=I_0\cdot F_1\cdot F_2\cdot F_3 \\ &\text{where, by replacing of } k \text{ by its value } 2\pi/\lambda, \\ &u=\pi h(\cos\varphi\sin\theta+\cos\varphi_0\sin\theta_0)/\lambda, \\ &v=\pi s(\sin\varphi+\sin\varphi_0)/\lambda, \\ &\text{and} \\ &w=\pi[s(\sin\varphi+\sin\varphi_0) \\ &\qquad+t(\cos\varphi\cos\theta+\cos\varphi_0\cos\theta_0)]/\lambda. \end{aligned}\right\} \quad (22.3)$$

The factors F_1 and F_2 describe the intensity distribution of the Fraunhofer patterns which we observe when a plane wave is diffracted by a rectangular opening of height h and width s. Factor F_3 describes the interference effect obtained by the cooperation of the N steps of the echelon grating.

As we will learn from the following, in the practical application of the echelon the angles φ and θ are small. Within the limit of accuracy of high precision measurements, we are allowed to put $\sin\varphi=\varphi$, $\cos\varphi=1$, and $\cos\theta=(1-\theta^2/2)$. Therefore, before we discuss the formula, we will introduce these approximations. Then the factors F become:

$$F_1=((\sin u)/u)^2 \quad \text{where} \quad u=\pi h(\theta+\theta_0)/\lambda,$$

$$F_2=((\sin v)/v)^2 \quad \text{where} \quad v=\pi s(\phi+\phi_0)/\lambda,$$

and $F_3=((\sin Nw)/\sin w)^2$, where

$$w=\pi[s(\phi+\phi_0)+t(2-\theta^2/2-\theta_0^2/2)]/\lambda.$$

The discussion of the functions F yields the following results:

$$\left.\begin{aligned} &F_1\text{: Principal maximum, } F_1=1, \\ &\qquad\qquad\qquad\qquad \text{for } \theta=-\theta_0 \\ &\text{Minima, } F_1=0 \quad \text{for } \theta=-\theta_0\pm m\lambda/h, \end{aligned}\right\} \quad (22.4)$$

Intermediate maxima of small values about halfway between consecutive minima.

$$\left.\begin{aligned} &F_2\text{: Principal maximum, } F_2=1, \\ &\qquad\qquad\qquad\qquad \text{for } \varphi=-\varphi_0 \\ &\text{Minima, } F_2=0 \qquad \text{for } \varphi=\varphi_0\pm n\lambda/s \end{aligned}\right\} \quad (22.5)$$

Intermediate maxima of small amount about halfway between consecutive minima.

For the description of the patterns it is convenient to introduce rectangular coordinates, ξ and η, in the focal plane of the projecting lens (focal length f). We put

$$(\theta_0+\theta)f=\xi \quad \text{and} \quad (\varphi+\varphi_0)f=\eta$$

and can describe the patterns as follows:

The illumination of the focal plane is restricted to certain areas limited by two orthogonal systems of dark lines parallel to the ξ- and η-axes. The intervals in both groups are constant, except one. The separation of the lines parallel to the η-axis is $\Delta\xi=f\lambda/h$, the distance between the lines parallel to the ξ-axis is $\Delta\eta=f\lambda/s$. For $\xi=0$ and for $\eta=0$, however, we obtain the maximal possible intensity. Therefore, the first dark fringes in both systems are separated by distances $2f\lambda/h$ and $2f\lambda/s$. The principal maximum is present in the central rectangle, terminated by the lines $\xi=\pm f\lambda/h$ and $\eta=\pm f\lambda/s$.

The values of h and s for an echelon are about 40 mm and 1 mm, respectively. Therefore the dark fringes parallel to the η-axis are very narrow in comparison with the fringes parallel to the ξ-axis. As soon as we do not use a point source in the focus of the collimator lens, but a relatively short slit parallel to the long edges of the echelon, the patterns parallel to the η-axis will coalesce, due to the illumination of the dark regions by light coming from neighboring points of the slit, for which θ_0 varies. Therefore, by using a sufficiently long slit, one will become independent of the variation of the light intensity with θ. The intensity distribution we obtain is the same as for a slit illuminated with a line shaped light source the extension of which is parallel to the diffracting slit.

TABLE IX.

Maxima	0		$\pm1.430\pi$		$\pm2.459\pi$		$\pm3.470\pi$
Intensity	1		0.047		0.017		0.008
Minima		$\pm\pi$		$\pm2\pi$		$\pm3\pi$	
Intensity		0		0		0	

Table IX gives quantitative data about the values of the maximum and minimum intensities and their location for which we use the values of v. Appreciable intensity can be obtained only in the central region between $v=+\pi$ and $v=-\pi$. This is the region which is important for practical purposes.

The intensity distribution produced by one single element, discussed above, is now con-

siderably changed by the cooperation of more elements, in our case N. This is described by the interference factor $F_3=((\sin Nw)/(\sin w))^2$.

This function has principal maxima for $w=\pm p\pi$, where $p=1, 2, \cdots 20{,}000, 20{,}001\cdots$. The value of all these maxima is N^2. Between two principal maxima, there are $(N-1)$ values of w for which F_3 becomes zero. They are given by the relation $Nw=p\pi$, or $w=p\pi/N$, where $p=p=1, 2, 3\cdots N-1; N+1, N+2, \cdots 2N-1; \cdots$. Furthermore, there exist $(N-2)$ maxima of F_3, situated between the zero values and approximately determined by the relation $w=(p+\frac{1}{2})n/N$. These values of F_3, however, are so small that the corresponding light intensities, in comparison with those of the principal maxima, are too weak to be observable with customary instruments ($N\geqq 20$). The higher the number of steps the sharper the interference fringes will be, because the neighboring minima confine the principal maximum to smaller regions of w.

Let us summarize the results by using the detailed intensity formula (22.3) which we modify for the practical case in which a slit parallel to the edges is applied. The slit may be just long enough to make one independent of the fluctuations of factor F_1 (see above). If θ_0 is the angle which determines the center of the slit, the patterns due to factor F_3 will be situated mainly in a direction $\theta=-\theta_0$ (22.4). Therefore we are allowed, to replace the item $(2-\theta^2/2-\theta_0^2/2)$ by $(2-\theta^2)$, and we can write Eq. (22.3) in the specialized form:

$$I=I_0\left(\frac{\sin\pi s(\varphi+\varphi_0)/\lambda}{\pi s(\varphi+\varphi_0)/\lambda}\right)^2 \cdot\left(\frac{\sin N\pi(s(\varphi+\varphi_0)+2t(1-\theta^2/2))/\lambda}{\sin\pi(s(\varphi+\varphi_0)+2t(1-\theta^2/2))/\lambda}\right)^2, \quad (22.6)$$

where I_0, different from the original I_0, is the maximal possible intensity we can get for $F_2=F_3=1$.

There will be appreciable intensity only in the surrounding of the direction of regular reflection in a region between the angles $(-\varphi_0+\lambda/s)$ and $(-\varphi_0-\lambda/s)$. Due to factor F_3, however, there will be sharp and strong interference maxima only in such directions φ for which the relation holds:

$$s(\varphi+\varphi_0)+2t(1-\theta^2/2)=p\lambda, \quad (22.7)$$

which, for angles $\vartheta\approx 0$ becomes

$$s(\varphi+\varphi_0)+2t=p\lambda. \quad (22.8)$$

The order of interference is very high. For $t=0.5$ cm and $\lambda=5000$A it becomes about 20,000.

But only a few orders of those allowed by formula (22.7) are observable. The number is restricted by the action of the intensity factor F_2. The angular order separation, that is the angular distance of two consecutive orders, $\langle\Delta\varphi\rangle=d\varphi/dp$ is

$$\langle\Delta\varphi\rangle=\lambda/s. \quad (22.9)$$

This is just half the angular separation of the first minima due to the diffraction at one single element. Therefore, only two of the orders allowed by formula (22.7) will appear with appreciable intensity. They belong to angles between $(-\varphi_0\pm\lambda/s)$.

The other allowed orders, appearing between zero values of factor F_2, are very weak, because, according to Table IX, F_2 is very small in these regions.

The two fringes in the central region generally appear with different intensities, but they will be equally strong if their positions are symmetric to the direction $\varphi=-\varphi_0$. This special position is called (symmetric) "two-order position."

In another special case, for $\varphi=-\varphi_0$, one order alone will appear if the wave-length is favorable for the fulfilment of the equation $2t(1-\theta^2/2)=p\lambda$. In this case all the other orders coincide with the zero values of factor F_2 and have, therefore, the intensity zero. This position of a line is called "single-order position."

A simple way of bringing the patterns of a line into any position is described in §26 (pressure chamber).

The different possibilities are illustrated by Fig. 25. The curve $(\sin^2 v)/v^2$ is the envelope of all intensity curves of the interference fringes produced by a line in the different positions. This curve is very important if one deals with intensity measurements by means of an echelon.

Shape of the Fringes

If we apply a long slit parallel to the long edges of the echelon, in an autocollimation arrangement for instance, the fringes show a curvature. This can easily be understood from the general

equation (22.7). To each point of the slit, determined by the angles φ_0 and θ_0, a pattern point determined by corresponding angles φ and θ, is attributed. As we can put $\theta=-\theta_0$, the relation between φ and θ for a fringe is given by (22.7). If we suppose that a light point moves along a slit (φ_0 remaining constant), the correspondent pattern point will move along a curve, the shape of which we will calculate. For this purpose, we use the same coordinate system, as above. Putting $(\varphi+\varphi_0)=\psi$ and introducing the coordinates $\xi=f\vartheta$ and $\eta=f\psi$, we obtain from (22.7) the relation

$$\eta=f(p\lambda-2t)/s+(t/fs)\xi^2.$$

For $p=$const., this equation is nothing else but the equation of the iso-order lines. The curves are parabolas their concave side directed towards the $+\eta$-axis (Fig. 23).

A short piece of the slit in an average distance $-\xi'$ will produce an inclined fringe the slope of which is determined by

$$(d\eta/d\xi)_{\xi'}=(2t/fs)\xi'=(2t/s)\vartheta'.$$

Such patterns are observed when the echelon is used in place of the back reflecting mirror of a Littrow spectrograph (see §26).

The corresponding calculations for the transmission echelon have been made by M. Lane (reference 22.1).

§23. Dispersion, Spectral Range, Order Distance

One great advantage of the reflection echelon, in comparison with other instruments of high resolving power, is the simple relation between angles, wave-lengths, and order numbers. The approximation of the fundamental formula (22.5) is sufficient for all measurements of highest accuracy, as long as we deal with very sharp lines. In these cases, the formulae derived in the following are correct.

(1) The *angular dispersion*, D_a, defined by $d\varphi/d\lambda$, is

$$D_a=p/s \quad \text{or} \quad \text{approx.}=2t/\lambda s. \qquad (23.1)$$

(2) The *linear dispersion*, determined from the separation of the patterns of two close lines with the wave-length difference $\delta\lambda$, is defined as

$$D_l=\delta x/\delta\lambda=\delta x/\delta\beta\cdot\delta\beta/\delta\lambda=fp/s=f\cdot D_a, \qquad (23.2)$$

where f is the focal length of the objective which projects the fringes on the spectrograph slit.

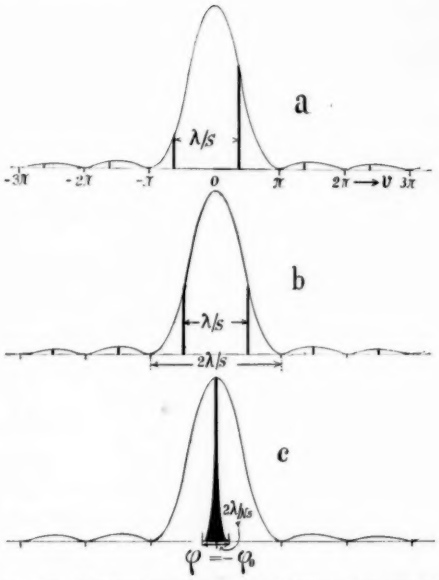

FIG. 25. Illustration of three different line positions. (a) Two-order position (asymmetric), (b) Two-order position (symmetric), (c) Single-order position, showing also schematically the intensity distribution of the pattern.

(3) The *angular order distance* has been derived in (22.9).

$$\langle\Delta\varphi\rangle=\lambda/s. \qquad (23.3)$$

(4) The *linear order distance*, therefore, becomes

$$\langle\Delta x\rangle=f\lambda/s. \qquad (23.4)$$

(5) The *spectral range* $\langle\Delta\lambda\rangle$, defined as the wave-length difference of two lines separated by an angle equal to the angle of the angular order distance, is given by

$$\langle\Delta\lambda\rangle=\delta\beta/D_a=\lambda/p=\lambda^2/2t. \qquad (23.5)$$

(6) The spectral range, expressed in wave numbers, correspondingly becomes

$$\langle\Delta\nu\rangle=|\langle\Delta\lambda\rangle|\lambda^2|=1/2t. \qquad (23.6)$$

§24. Apparatus Half-Width

The apparatus half-width is defined as the total width of the theoretical intensity curve for

an intensity equal to $I_{max}/2$. It can be derived from the general intensity formula (22.4). We restrict ourselves to the case of the single-order position and of very small angles θ.

If we measure the deviation angles from the single-order position, that is, if we introduce angles $\psi=(\varphi+\varphi_0)$, the intensity formula (22.6) in our simple case becomes

$$I=I_0[(\sin(\pi s\psi/\lambda))/(\pi s\psi/\lambda)]^2 \times[\sin(\pi N(s\psi+2t)/\lambda)/\sin(\pi(s\psi+2t)/\lambda)]^2.$$

For $\psi=0$ we obtain $I_{max}=N^2I_0$, the order being $p_0=2t/\lambda$. The intensity drops to $\frac{1}{2}$ of this value for the angular displacement ψ_h which is one-half of the angular half-width. Remembering that $2t/\lambda$ is a whole number and using the abbreviation $\pi s\psi_h/\lambda=u$, we can write the condition equation for ψ_h in the form:

$$(\sin u/u)^2(\sin Nu/\sin u)^2=N^2/2,$$

or

$$(\sin Nu/Nu)^2=\tfrac{1}{2}.$$

The solution of this equation gives

$$Nu=\pi Ns\psi_h/\lambda=1.39$$

or

$$\psi_h=0.442\lambda/sN.$$

By application of formula (22.5) and of the relations (23.5) and (23.6), we find the half-width in the usual units:

Apparatus half-width	
in order numbers:	$2\gamma_h=0.883/N$
in angstrom units	$A_\lambda=0.883\langle\Delta\lambda\rangle/N$
in wave numbers	$A_\nu=0.883\langle\Delta\nu\rangle/N$

where $\langle\Delta\lambda\rangle$ and $\langle\Delta\nu\rangle$ is the spectral range.

§25. Resolving Power of the Echelon

The derivation of the resolving power of the echelon is very much simpler than in the case of the interferometer, for we can apply immediately Rayleigh's criterion. We assume that two infinitely sharp and equally strong lines of wave-length λ and $\lambda+\delta\lambda$ are resolved when the maximum of one line coincides with the minimum of the other. According to §22, the angular distance between the maximum and the following minimum is $\delta\varphi=\lambda/sN$. On the other hand, according to (22.8), a shift of the wave-length λ by $\delta\lambda$ would produce an angular displacement $\delta\varphi=\delta\lambda p/s$. Therefore, between the wave-length difference of two just resolved lines and their angular separation the relation $\lambda/sN=\delta\lambda p/s$ will hold. Therefore:

$$\text{Resolving power } R=\lambda/\delta\lambda=Np\approx 2tN/\lambda. \quad (25.1)$$

The echelon which Williams and Middleton used for the determination of the wave-lengths of iron lines consists of forty plates of 6.87-mm thickness. For light of 5500A the theoretical resolving power is about one million.

Let us compare this instrument with a Fabry-Perot interferometer of the same resolving power. The latter can be calculated by formula (6.3), according to which $R\approx 3p\sqrt{r}/(1-r)$. Assuming a reflectivity $r=0.90$ we obtain $R=28.5p$. As R shall be 10^6 for 5500A, we get $p=35{,}000$ and for the thickness of the etalon $t=3.18$ cm. As the effective number of rays is smaller than in the case of the echelon the thickness of the etalon must be larger in order to furnish the same resolving power as with the echelon. If the separation of the etalon would be equal to the echelon plate thickness, the reflectivity r of the etalon should be 0.93 in order to obtain the same resolving power as with the 40-plate echelon. The application of such a high reflection power is impossible, especially in the short wave region. The resolving power of the echelon is not affected by the reflectivity of the steps and is superior to the interferometer.

§26. Arrangement of the Echelon

Details of the manufacture and the testing of the single plates and the finished echelon will not be described here. Readers interested in such details are referred to Williams' paper where all of these interesting questions are treated.

After the finished echelon bloc has been platinized it is mounted very carefully in a rectangular, optically worked Invar box in such a way that each plate takes its part of support. Otherwise, by the sagging of the central part of the pile, the focus of the patterns would be changed. The whole instrument is mounted in a housing in such a way that it can be turned about an axis perpendicular to the reflecting faces. In

this way it is very easy to use the instrument with horizontal or vertical dispersion.

Furthermore, the instrument is placed in an air-tight chamber in order to keep it in vacuum for vacuum wave-length determinations. The chamber also can be used as a constant pressure chamber. For long exposure times, it is absolutely necessary to be independent from variations of the atmospheric pressure and also from temperature changes. The latter are eliminated by using a pressure chamber provided with double walls between which water of constant temperature is flowing.

For work in the Schumann region, the echelon together with the auxiliary spectroscope must be set up in a greater vacuum chamber. It is remarkable that it is possible to use the echelon in a vacuum without any change of its constants. This proves that the contact between the plates is perfect.

The use of a pressure chamber is very advantageous in another respect. Often it is necessary to place a line at different distances from the single-order position. Without any mechanical change in the set-up, this can be performed by a slight change of the gas pressure in the chamber, for, the refractive index of the gas, and hence, the path difference, is a function of the gas density.

It is easy to calculate beforehand what pressure change is necessary in order to obtain a certain change of the order of interference.

Let us introduce into the fundamental formula (22.5) the vacuum wave-length $\lambda_0 = n\lambda$, and let us calculate the change of the order p due to a variation of the pressure b. For a constant direction φ the relation will be:

$$p\lambda_0 = n(s(\varphi+\varphi_0)+2t) = n\cdot\text{const.}$$

Hence $dp/db = (dp/dn)(dn/db) \approx p(dn/db)$, because n is approximately $=1$. Therefore a change in pressure Δb producing a change Δp of the order is given by

$$\Delta b = (\Delta p/p)/(dn/db) = \lambda\Delta p/2t(dn/db).$$

According to the known relations

$$(n-1)/d = (n_0-1)/d_0, \quad \text{and density } d \sim b,$$

we have

$$(n-1) = b(n_0-1)/b_0 \quad \text{and} \quad dn/db = (n_0-1)/b_0$$

and finally

$$\Delta b = \Delta p\lambda/2t(n_0-1).$$

For air and sodium light and for a plate thickness of 0.7 cm we find $\Delta b/\Delta p = 113$ mm Hg/order. From this example, we can see that it is easily possible to shift a line within the total spectral range by small pressure changes.

Crossing of Echelon and Auxiliary Spectroscope

Because of the small spectral range, the echelon, like all other interference spectroscopes, must be used in combination with an auxiliary apparatus, the dispersion of which is large enough for a proper separation of the radiations of different wave-lengths.

The simplest way is to use the auxiliary spectroscope as a monochromator. Then the collimator slit of the echelon is illuminated only with the light of the spectral line which one wishes to investigate. But, as one usually is interested in a greater part of a spectrum, it is more convenient to combine the echelon with the auxiliary instrument in one of the manners which we have described in §8 for the use of the etalon.

The most natural way seems to be, at first sight, the application of the echelon as the back-reflecting mirror in a Littrow spectrograph. Such an arrangement would have great advantages because it is most compact and because the light losses are at a minimum. However, for exact measurements and for the utilization of the full power of the echelon this arrangement is not advisable. In order to understand the disadvantage of this arrangement, tempting at first, let us suppose the echelon to be set up in such a manner that the edges of the steps are perpendicular to the refracting (vertical) edge of the prism of the spectrograph and vertical to the rays emerging perpendicular to the second face of the prism. The slit of the spectrograph is in horizontal position and its length is kept so small that the patterns of the spectral lines are sufficiently separated. The echelon has such an inclination that the single-order position is in a suitable range of the photographic camera. It is obvious that the simplified fundamental formula (22.8) can be applied for such patterns only which belong to rays incident perpendicular to the edge of the echelon steps. For all the other

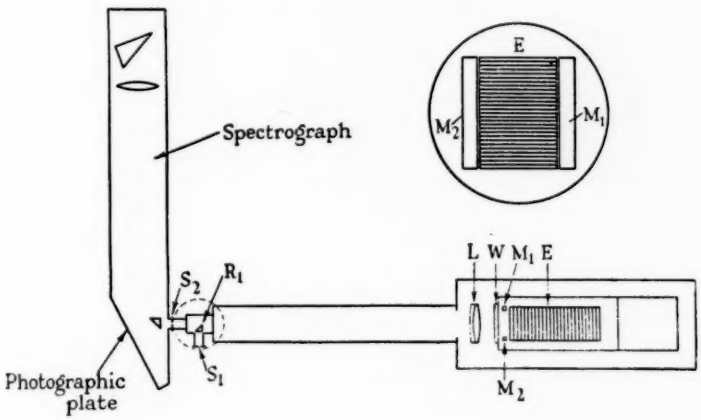

FIG. 26. Arrangement of W. E. Williams (reference 26.5).

patterns the exact formula (22.7) must be applied. This would mean a slight increase of calculation work only, but more serious is the fact that the patterns show an inclination which grows larger as they depart from the axis of the spectrograph. Hand in hand with this inclination goes a decrease of the resolving power (see §22, shape of the fringes).

In order to avoid these disadvantages, the standard arrangement for high precision work is made in the following manner: The echelon is set up in front of a stigmatic spectrograph. A separate autocollimation system, consisting of a slit and an objective (or mirror arrangement), projects the patterns on the spectrograph slit. In Fig. 26 the arrangement used by Williams and his co-workers is reproduced. The slit S_1 of the autocollimation system is perpendicular to the spectrograph slit S_2 and is located in the focal plane of the objective L. Light entering S_1 is reflected by means of the total reflecting prism R_1 and falls, after traversing the lens L, on the echelon E, the dispersion of which is crossed with that of the spectrograph. The patterns are projected by L on the slit S_2. As only the central part of the fringes enters the spectrograph slit, no curvature of the patterns can be observed. The angle θ is practically zero in this case, wherefore the simple formula (22.8) can be applied for all lines of the spectrum. An arrangement with mirrors has the advantage that no chromatic aberration can deteriorate the patterns. The focal lengths of the systems must be long in order to obtain a suitable linear dispersion (23.2); lengths of $f=150$ cm to 300 cm are in use.

For investigations in the vacuum region, the reflection echelon must be combined with a stigmatic grating mounting. A very compact vacuum apparatus has been developed in the Spectroscopy Laboratory of M.I.T. A fused quartz reflection echelon (25 plates) has been combined with a concave grating (30,000 lines/inch and $R=200$ cm) and concave mirror, forming together the stigmatic Runge-Paschen mounting. MacAdam has shown that this arrangement is applicable for high precision work in the vacuum region. He applied crossed dispersions as well as parallel dispersions. By means of the latter arrangement he performed wave-length measurements of Cu II lines in the ultraviolet region (2404A–2013A) and in the Schumann region (1621A–1488A). As the echelon plates are 7.3 mm thick, the order numbers for short wave-length are very high and therefore, the determination of the correct order number is rather difficult (see §27).

§27. W. E. Williams Method of Wave-Length Measurements

The method employed by Williams for the evaluation of echelon patterns is related to Babcock and St. John's treatment of Fabry-Perot fringes (§10, p. 421). In the latter, the principal point is to determine the order number of the center of the ring system for which the relation between wave-length, etalon separation, and order has the simplest form. In this method,

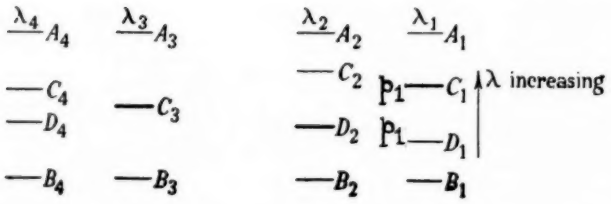

FIG. 27. Schematic patterns of four different wave-lengths (after Williams). The order of D_1 must be replaced by (p_1-1).

the center of the ring system is a natural reference mark.

Such a natural reference mark does not exist in the patterns obtained by means of an echelon. It has to be furnished artificially. For this purpose, Williams provided the echelon with two narrow, platinized plane mirrors M_1 and M_2 on either side of the echelon (Fig. 26). By means of screw adjustments, they can be tilted until two images (A and B in Fig. 27) of the auxiliary slit S_1 are formed on the spectrograph slit S_2 in suitable positions. Usually the mirrors are adjusted in such a way that the images A and B are about symmetrical with and close to the echelon patterns. When the echelon dispersion is crossed with the spectroscope dispersion (e.g., echelon steps horizontal, refracting edge of the prism vertical, the photographic plate will show patterns similar to Fig. 27.

The patterns of the four wave-lengths λ_1, λ_2, λ_3, λ_4 consist of the fiduciary marks A_1, A_2, A_3, A_4; B_1, B_2, B_3, B_4, which are the images of S_1 formed by the mirrors. The lines C_1 and D_1 represent the interference fringes of the p_1th and (p_1-1)th order for a standard line of known wave-length λ_1. Similarly, C_2 and D_2, C_4 and D_4 are consecutive orders of other lines λ_2 and λ_4. The patterns of these lines are assumed to be in double-order position, whereas the line λ_3 shows only one order, corresponding to the single-order position.

Every fringe C and D is distinguished by an integral order p and $(p-1)$, but order numbers also can be attributed to the marks A and B. These order numbers, regularly non-integral numbers, can be expressed by the order p of the neighboring fringe and a fractional part ϵ.

The determination of the fractional part is much easier with echelon than with etalon patterns because the relation between order and displacement is linear according to (22.8). The procedure may be explained by using the patterns of Fig. 27. The measurement of the patterns gives the distances involved on an arbitrary scale. From these values the fractional parts are easily found for lines which are not in single-order position. The distance CD, the linear order distance $\langle\Delta x\rangle$, corresponds to the change of order unity, the distance AC to the change of the fractional part ϵ. Therefore, we have for the lines λ_1 and λ_2:

order number in A_1:

$$(p_1+\epsilon_1)=p_1+A_1C_1/C_1D_1, \quad (27.1)$$

order number in A_2:

$$(p_2+\epsilon_2)=p_2+A_2C_2/C_2D_2. \quad (27.2)$$

In the case of a line in single-order position, however, this method cannot be applied. But if the order distance of a neighboring line is known the interorder distance of the other line can be calculated, as the separation of orders varies directly as λ (23.4). This method applied to the patterns of λ_3 and λ_4 gives for the order separation of λ_3:

$$\langle\Delta x\rangle_3=(C_4D_4\lambda_3/\lambda_4)\cdot(A_3B_3/A_4B_4). \quad (27.3)$$

The last term in this expression is the ratio of the magnification factors of the spectrograph for the two lines. The necessity of this reduction explains the use of a second mirror M_2. In this way, we find:
order number in

$$A_3: (p_3+\epsilon_3)=p_3+A_3C_3/\langle\Delta x\rangle_3. \quad (27.4)$$

When the fractional parts are determined, the further procedure of the wave-length determination is exactly the same as described for the etalon method. Therefore, we may refer to §10.

One point, however, must be mentioned in this connection. For the calculation of the correct wave-length of an unknown line, we must know an approximate value which may be known from grating measurements. If those preliminary measurements are not exact enough, we can be

in doubt about the order of interference within one unit. In the case of the interferometer, every doubt can be eliminated by applying another spacer; in the case of the echelon, however, such a simple method does not exist, except if another echelon with different plate thickness is at our disposal. Therefore, for high precision measurements by means of the echelon, reliable measurements must be at hand. The degree of accuracy of these measurements depends upon the order of the echelon patterns. For work in the Schumann region, where no other instrument is at our disposal, the plate thickness should be smaller than they are in the instruments built until now.

The wave-length values obtained in this manner must be reduced to normal conditions (§12). But, as the instrument usually is employed in a vacuum chamber, the measurements give the vacuum wave-lengths directly.

Correction for phase change is unnecessary because a phase change or the dispersion of phase change does not affect the position of echelon patterns. This is a great advantage over the etalon method in which the elimination of the phase change is always a very annoying task.

As for the accuracy of the method, we can estimate it from data given in the paper of Williams and Drinkwater which deals with the determination of vacuum wave-lengths of iron lines. The focal length of the lens which projected the patterns on the spectrograph slit was 170 cm. With this value and with echelon steps of 1 mm the inter-order distance in the red region is about 1 mm, and $\frac{1}{2}$ mm at 3000A. By means of a good micrometer microscope, the fractional parts can be determined with an accuracy of ± 0.001 to ± 0.002. With a plate thickness of 6.87 mm, the order of interference is about 22,000 in the red and about twice as much at 3000A. Therefore, one is in a position to compare sharp lines in any part of the spectrum with an accuracy of 5×10^{-8}.

But this high degree of accuracy can be obtained only with sharp lines. If we have to deal with broader lines, we must remember that the character of the apparatus intensity distribution may cause a distortion of the true intensity distribution of a spectral line. Preferably echelon spectroscopes cause an appreciable distortion if the patterns of somewhat broad lines are not in single-order position. As we learned from the formula (22.6) for the intensity distribution in the patterns of monochromatic light, the intensity depends upon the position of the fringes between the first minima of factor F_2. For a broad line, this factor will vary for the different sections of the line and therefore the shape of the intensity distribution curve will be distorted. Obviously, for the single-order position the location of the center of gravity remains. For other positions, however, especially for the symmetric double-order position, the centers of gravity of the two patterns are spuriously displaced towards each other. In connection with this shift, the value of the order distance will become too small and, therefore, the fractional part ϵ too large, and the final wave-length value too small. However, there are two possibilities of obtaining the correct wave-length values: (a) By taking several sets of photographs at different pressures in the pressure chamber and by measuring broad lines in the single-order position only; (b) by applying a correction. The latter is the only way if vacuum wave-lengths are determined.

A relatively simple method of obtaining such a correction has been proposed by Williams. It is simpler than an older one, used for transmission echelons by Merton and Barratt.[4] Williams' method is as follows: Employing the designations: Δm = mirror image distance, Δx = linear inter-order distance, we have, according to formula (23.4)

$$\Delta m/\Delta x = S \cdot \Delta m/f\lambda,$$

therefore

$$\lambda \Delta m/\Delta x = S\Delta m/f = \text{const.} = 1/k.$$

This relation is valid for all sharp lines of a spectrogram. A broad line of wave-length λ_b should produce patterns with an order separation

$$\Delta x_b = k \cdot \lambda_b \cdot \Delta m_b.$$

The experimental value $\Delta' x_b$, however, will be smaller than the calculated Δx_b because of the spurious shift. It is easy to be seen that the value of $(\Delta x_b - \Delta' x_b)/2$ will be the correction which has to be applied for the readings of the fringe belonging to the higher order. If the value of the fringe position is corrected in this manner,

[4] T. R. Merton and S. Barratt, Phil. Trans. **222**, 380 (1922).

the fractional part is correct and independent of the width of the line.

The distortion of the patterns by an echelon grating is a serious disadvantage in comparison to the Fabry-Perot interferometer. In this case, such a distortion cannot arise, as far as the innermost asymmetric ring is omitted in the measurements. On the other hand, the advantages of the echelon are so overwhelming, especially with respect to the application in the vacuum region, that we have to put up with this disadvantage.

Measurement of Small Wave-Length Differences

According to the linear relations involved in formula (0.0) the measurement of wave-length differences of close, sharp lines is very simple. Between the linear separation δx and the wave-length difference $\delta\lambda$ of two lines exists the relation

$$\delta\lambda/\delta x = \langle\Delta\lambda\rangle/\langle\Delta x\rangle = \lambda^2/2t\langle\Delta x\rangle,$$

where $\langle\Delta x\rangle$ is the linear inter-order distance and $\langle\Delta\lambda\rangle$ the spectral range. If the lines are not in single-order position, $\langle\Delta x\rangle$ can be obtained from their patterns. For lines in single-order positions $\langle\Delta x\rangle$ can be determined from neighboring lines as described above. (27.3).

BIBLIOGRAPHY

II. Compound Interferometer and Multiplex Interference Spectroscope

(*§13–§16*)

(13.1) W. V. Houston, Phys. Rev. **29**, 478 (1927).
(13.2) D. A. Jackson and H. Kuhn, Proc. Roy. Soc. **A167**, 205 (1938).
(13.3) E. Gehrcke and E. Lau, Zeits. f. tech. Physik **8**, 157 (1927); Physik. Zeits. **31**, 973 (1930).
(13.4) E. Lau, Zeits. f. Physik **63**, 313 (1930).
(13.5) E. Lau and E. Ritter, Zeits. f. Physik **76**, 190 (1932).
(13.6) P. Görlich and E. Lau, Zeits. f. Physik **77**, 746 (1932).
(13.7) P. H. van Cittert, Ann. d. Physik **13**, 753 (1932).

III. Some Applications

§17. Absorption Spectra

(17.1) Ch. Fabry, Comptes rendues **140**, 1136 (1905).
(17.2) E. Gehrcke and O. Reichenheim, Verh. d. D. Phys. Ges. **4**, 209 (1906).
(17.3) Ch. Fabry and H. Buisson, J. de phys. **9**, 197 (1910).
(17.4) K. Burns and Wm. F. Meggers, Pub. Allegheny Obs. **6**, 105 (1925).
(17.5) K. Burns, Wm. F. Meggers, and C. C. Kiess, Bur. Stand. J. Research, 297 (1928).
(17.6) C. D. Shane, Lick Obs. Bull. **16**, 76 (1932).

§18–§19. Intensity Distribution

(18.1) P. P. Koch, Ann. d. Physik **42**, 1 (1913).
(18.2) A. J. Dempster, Ann. d. Physik **47**, 791 (1915).
(18.3) M. N. Saha, Phys. Rev. **10**, 782 (1917).
(18.4) L. Gilchrist, Phys. Rev. **27**, 596 (1926).
(18.5) H. C. Burger and P. H. van Cittert, Zeits. f. Physik **44**, 58 (1927).
(18.6) J. K. Robertson, Can. J. Research **4**, 305 (1931).
(18.7) R. Minkowski and H. Bruck, Zeits. f. Physik **95**, 299 (1935).

§20. Some Recent Investigations

(20.1) D. A. Jackson and H. Kuhn, Nature **134**, 25 (1934); Proc. Roy. Soc. **A148**, 335 (1935); **154**, 679 (1936); **165**, 303 (1938); **167**, 205 (1938).
(20.2) R. Minkowski and H. Bruck, Zeits. f. Physik **95**, 274 (1935).
(20.3) R. A. Fisher, Phys. Rev. **51**, 381 (1937).
(20.4) K. W. Meissner and K. F. Luft, Ann. d. Physik **28**, 667 (1937); Ann. d. Physik **29**, 698 (1937); Zeits. f. Physik **106**, 362 (1937).
(20.5) K. W. Meissner, Ann. d. Physik **31**, 505 and 518 (1938).

IV. Reflection Echelon

§21. Principle of the Instrument

(21.1) A. A. Michelson, Astrophys. J. **8**, 37 (1898); J. de phys. **8**, 305 (1899); Am. J. Sci. **5**, 215 (1898). Proc. Am. Acad. **35**, 111 (1899).
(21.2) W. E. Williams, Nature **127**, 816 (1931).
(21.3) W. E. Williams, Proc. Phys. Soc. London **45**, 699 (1933).
(21.4) Transmission echelon: A. A. Michelson, reference (22.1); R. A. Houston, Phil. Mag. **7**, 456 (1904); H. C. Burger and P. H. van Cittert, Proc. Amst. Akad.; B. Galitzin, Bull. Petersburg **23**, 67 (1905); Zeits. f. Instrumentenk. **27**, 224 (1907); H. C. van Geel, Rev. d'optique **2**, 445 (1923); P. H. van Cittert, Ann. d. Physik **77**, 372 (1925).

§22. Intensity Distribution

(22.1) M. Laue, Physik. Zeits. **6**, 283 (1905).

§26. Arrangement of the Echelon

(26.1) W. E. Williams, reference (21.3).
(26.2) D. A. Jackson, Proc. Roy. Soc. London **A128**, 508 (1930).
(26.3) R. Ritschl, Zeits. f. Physik **79**, 1 (1932).
(26.4) D. L. McAdam, Physics Thesis, M.I.T. 1936; Phys. Rev. **50**, 185 (1936).
(26.5) W. E. Williams and A. Middleton, Proc. Roy. Soc. **A172**, 157 (1939).
(26.6) J. W. Drinkwater, Sir Owen Richardson, and W. E. Williams, Proc. Roy. Soc. **A174**, 164 (1940).

§27. Williams Method of Wave-Length Measurements

(27.1) W. E. Williams, references (21.2), (21.3), (26.4), (26.5).
(27.2) W. E. Williams and A Middleton, reference (26.4).

Errata: Interference Spectroscopy. Part I

(J. Opt. Soc. Am. 31, 405 (1941))

KARL WILH. MEISSNER
Worcester Polytechnic Institute, Worcester, Massachusetts

FORMULA (4.2), page 411: The + sign in the second factor of the denominator must be replaced by —.

Page 413, third line from the bottom: replace semicolon with colon.

Page 414: The two equations preceding Eq. (6.1) must be replaced by the following expressions:

$$(1+\eta \sin^2 \pi(p_0+\langle\Delta p\rangle/2))(2+\eta \sin^2 \pi(p_0+\langle\Delta p\rangle)) = 2.5(1+\eta \sin^2 \pi(p_0+\langle\Delta p\rangle))$$
$$(1+\eta \sin^2 \pi\langle\Delta p\rangle/2)(2+\eta \sin^2 \pi\langle\Delta p\rangle) = 2.5(1+\eta \sin^2 \pi\langle\Delta p\rangle).$$

Equation (6.1) becomes:

$$(1+\eta \sin^2 \pi p/2R)(2+\eta \sin^2 \pi p/R) = 2.5(1+\eta \sin^2 \pi p/R).$$

Page 427: in reference (6.2) read: W. V. Houston.

APRIL, 1942 J. O. S. A. VOLUME 32

On the Performance of Optical Instruments with Coated Lens Systems*

J. E. TYLER, R. S. MORSE, AND F. B. JEWETT, JR.
National Research Corporation, Boston, Massachusetts

(Received January 17, 1942)

THE performance of optical instruments with coated lens systems has received considerable attention in the last few years, with most of the emphasis on the increase in transmission or "speed" effected by the coatings.

In some experiments on a Schneider-Kreuznach *f*:2 lens having ten air-glass surfaces, Cartwright[1] observed "A slight increase in contrast . . . under normal lighting conditions and a large increase . . . under adverse lighting conditions" as well as an increase in detail. Turner[2,3] also mentions the effect of coating on contrast. Other than this no detailed work seems to be available concerning the improvement in contrast obtained by coating the surfaces of an optical system.

There are many instances where it is desirable if not imperative to see or register detail in the presence of a relatively large sky area. Any foreground subject against a background of sky, clouds, white sand, snow, or brightly illuminated water is an excellent example. When a lens system forms an image of such an object, the image will suffer from what might be termed "selective flare"—that is, light from the bright area of the object after being multiply reflected within the lens system will contribute an approximately constant amount of light to all parts of the image. This veil of light will decrease the contrast of the image by an amount which will depend upon the design of the optical system, particularly upon the number of glass-air surfaces it contains, and upon the brightness of the sky area.

The purpose of this investigation was to determine the extent of the loss in contrast in an image when one-half the object consisted of a relatively bright diffuse area, called the sky area, the other half being a relatively darker area, called the foreground area, in which detail existed, and then to determine the improvement obtained by coating the lens.

* Delivered before the Optical Society on October 25, 1941.

[1] C. H. Cartwright, J. Opt. Soc. Am. **30**, 110–114 (1940).
[2] A. F. Turner, *Photo Technique* (October, 1940).
[3] A. F. Turner, *The Educational Focus* (1941).

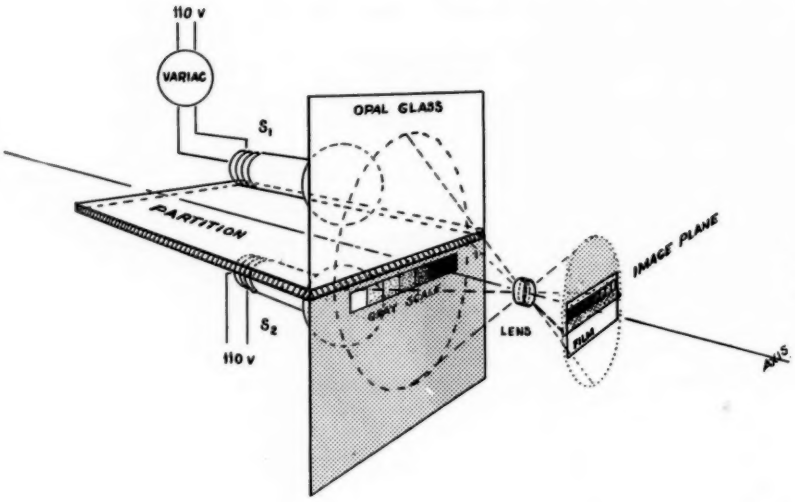

FIG. 1. Diagram of apparatus used to record variations in contrast of the gray scale with varying "sky" brightness.

In order to simulate the conditions of the problem in the laboratory an experiment was chosen which embraced the following features:

1. One-half the field angle of the lens was filled with a diffuse source whose brightness could be varied.
2. A step-wedge having constant contrast was inserted in the other half of the field angle.
3. The lens system was well designed and in common use.
4. The recording medium was chosen so as to be similar in response to the human eye in order that the results obtained would be comparable with visual observation, at least to a first approximation.

The experimental apparatus is shown diagrammatically in Fig. 1.

S_1 is a photoflood bulb whose brightness can be varied from 0 to a maximum by means of the Variac. S_2 is a 100-watt frosted bulb; the voltage across this lamp could be kept constant by means of a Variac and volt meter. The two lamps are separated by a partition designed to eliminate light leakage from the source S_1 to the gray scale. The lens under test was placed close enough to the target to insure that the whole upper half of the field angle would be filled with diffuse light as shown, and the film was then focused in the image plane.

By photographing this target at various values for "sky" brightness, first with an uncoated lens and then with the same lens coated, and by observing all the necessary precautions to insure identical emulsion, exposure time, development, etc., data were obtained which gave the change in density of the wedge steps—or foreground detail—with increasing "sky" brightness. The curves in Fig. 2 are typical of the results obtained:

It will be seen from the curves that the increase in transmission and decrease in flare, that are characteristic of a lens system after it has been coated, are both operating to increase the contrast in the image of the gray scale. Curves A and A' are from the densest step of the wedge, hence of the various steps they received the greatest

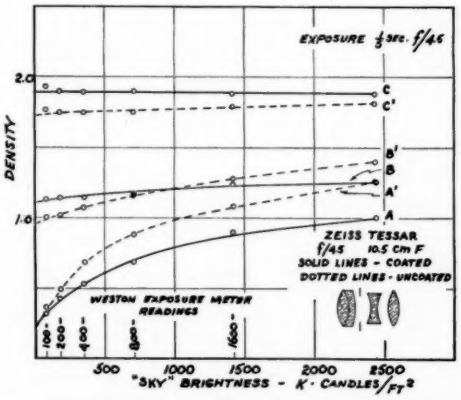

FIG. 2. Showing the effect of flare on the negative record obtained from the individual steps of the wedge. In Figs. 2 and 3 a scale of readings taken with a Weston Master Exposure Meter is superimposed on the brightness grid to facilitate interpretation of the graphs. A minus sign following the Weston meter reading means that the arrow pointed to the unnumbered step below the figure given; a plus sign, to the unnumbered step above the figure given.

percent increase in exposure due to whatever flare existed. Densities obtained with the coated lens (curve A) are considerably less than those obtained with the uncoated lens because of the great reduction in flare which in this case is the important factor. Curves C and C' are from the lightest step in the wedge and contain the least percent increase in exposure due to flare. In this case, the increase in transmission effected by the low-reflecting films results in greater densities from the coated lens system (curve C.) Curves B and B' represent the intermediate case. Where the curves cross, the contribution from flare in one approximately offsets the increase in transmission of the other.

By employing the difference between maximum and minimum density of the wedges as a measure of their contrast, it is possible to plot the change in contrast of the step wedge with sky brightness. This is given in Fig. 3. The initial gain due to increased transmission is evident at the 0 level of sky brightness and the additional gain due to elimination of flare is shown by the difference in slope between the two curves.

One of the most interesting facts shown by these curves is that the rate of loss in contrast is greatest at the low levels of "sky" brightness. In Fig. 2, this is indicated by the slope of curve A relative to curve A' and in Fig. 3 also by the

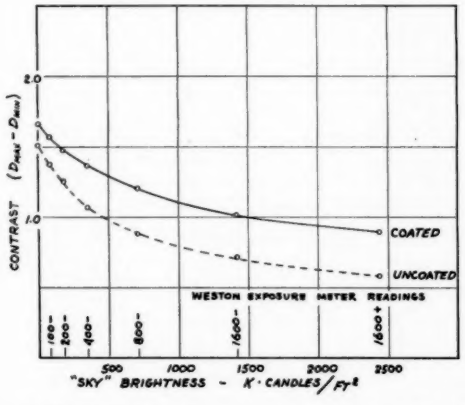

FIG. 3. Showing change in contrast of the step wedge with increasing "sky" brightness.

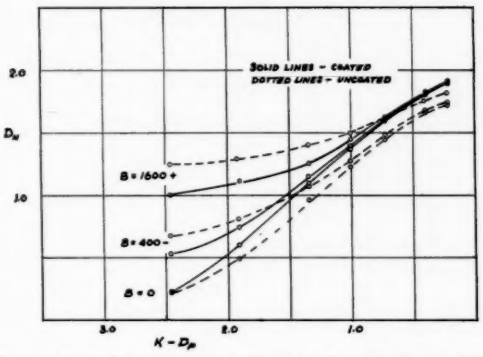

FIG. 4. Variation in contrast illustrated in the form of H and D curves.

relative slopes of the two curves which is nearly 0 after $B = 350$.

An interesting method of comparing the results is given in Fig. 4. If the densities of the negative steps, (D_n) are plotted against a constant minus the densities of the original positive steps, $(K - D_p)$ a curve will result which will have the form of the characteristic curve. For a contact print, this curve becomes the true characteristic curve of the negative material. For projection prints, the nearest approach to the true H and D curve will come from the coated lens system at 0 sky brightness. The other curves in the figure show clearly the effect of sky brightness and the arguments for coated *vs.* uncoated lens systems.

As a supplement to this work, an investigation was made to discover the effect of aperture on the contrast of the image detail in the experiment. So far as could be determined, the effect is substantially independent of aperture.

Measurements were also made of the total transmissions of the lens systems to diffuse green light from an extended source. These measurements were made with a Mcbeth illuminometer equipped with a Wratten No. 58 green filter, and are in agreement with published results. For example, the Zeiss Tessar of Fig. 2 (6 air-glass surfaces) showed an increase of 26.5 percent. Another Zeiss Tessar f:4.5, 11.5-cm focal length showed similar increase and a Laak Dialytar (8 air-glass surfaces) f:3.5, 30-cm focal length showed 29.3 percent increase.

The Effect of Temperature upon the Spectral Sensitivity of Photographic Emulsions*

C. H. EVANS
Kodak Research Laboratories, Eastman Kodak Company, Rochester, New York
(Received January 12, 1942)

Spectral sensitivities at three different temperatures (approximately +25°C, −75°C, and −185°C) were determined for seven commercial emulsions. For the six optically sensitized emulsions, it was found that the efficiency of optical sensitization decreased as temperature was lowered, except that for three of the emulsions this decrease commenced only somewhere below −75°C. Efficiencies found at approximately −185°C ranged from 1/4 to 1/550 of their values at +25°C. The decrease apparently pertains to the transfer of the action of light from the dye to the silver halide.

INTRODUCTION

SOME information on the effect of temperature on the spectral sensitivity of photographic materials has been published. Sheppard, Wightman, and Quirk presented results of exposures made at +20°C, −70°C, and −180°C on Wratten Panchromatic plates and at +20°C and −180°C on Eastman Process plates.[1] By using filters to isolate the two regions they found, for the panchromatic material, that inertia speeds ($10/i$) in the region of natural sensitivity (blue exposing radiation) and in the region of optical sensitization (red exposing radiation) were about equally decreased by lowering the temperature of the emulsion during exposure.

Ungar published spectrograms made at several different times of exposure, at both room temperature and −180°C, on variously sensitized samples of a commercial photographic paper.[2] On the basis of just perceptible densities he concluded that in each case the sensitivity in the region of optical sensitization was depressed at −180°C to a greater degree than that in the region of natural sensitivity of the silver halide. The magnitude of this differential effect varied from a factor of about 25 down to a factor probably not far different from 1, among the different sensitizers.

Sheppard, Wightman, and Quirk mention a change in the color of their panchromatic plate upon exposure to vapor from liquid air, and attribute this to the action of ozone present in the vapor. Ungar tested his strips of sensitized paper for similar effects by dipping them in liquid air, but could see no change except for the strip sensitized with eosin, which changed color reversibly with changing temperature.

In the present paper are presented spectral sensitivity curves for seven different commercial emulsions exposed at room temperature (~+25°C) and also at temperatures near those of solid carbon dioxide (−79°C) and of liquid air (−186°C) or liquid nitrogen (−196°C). For one of these emulsions determinations of spectral transmission were also made, at the temperatures +26°C and −187°C.

EXPERIMENTAL PROCEDURE

The sensitometer regularly employed in these Laboratories for the determination of spectral sensitivity in the visible and infra-red was used.[3] This yields intensity-scale monochromatic exposures with ten power-of-two steps. For the present work an unsilvered wide-mouthed Dewar flask was set up just behind the usual exposure plane. An aluminum cylinder slightly smaller in diameter than the flask was inserted in it. This was supported at the upper end through an insulating material which also closed the flask against moisture from the air. The cylinder has a chamber bored in along its axis from the top, and can be filled from outside with a cooling liquid. Vapors from this liquid have no access to the film. The latter is held against a flat face recessed in the cylinder, and can be readily in-

* Communication No. 838 from The Kodak Research Laboratories.
[1] S. E. Sheppard, E. P. Wightman, and R. F. Quirk, J. Phys. Chem. **38**, 817 (1934).
[2] G. Ungar, Zeits. f. Physik **106**, 322 (1937).
[3] C. H. Evans, J. Opt. Soc. Am. **30**, 118 (1940).

serted and removed without allowing moisture from the air to enter the flask. Temperatures of the cylinder, and hence of the film, are read by means of a mercury or pentane thermometer inserted in a hole in the cylinder near the exposure plane.

By the use of a thermocouple cemented to a film strip, it was found that even at −190°C only about 30 seconds were required for the film to come down to temperature after insertion, but, in all cases, 90 seconds were allowed prior to exposure.

A separate strip of film was exposed at each wave-length. Times of exposure of 15 seconds were used throughout, with the exceptions noted below. This use of a constant exposure time prevents errors which would otherwise appear because of reciprocity law failure.[4] The exceptions are for films I and II, for which exposures at wave-lengths of 500 mμ and longer at the temperature −180°C were of 4 minutes' duration. However, this does not introduce reciprocity failure effects, as it has been shown that reciprocity failure has disappeared at this temperature.[5] The intensity of the exposing radiation for each exposure was determined by use of a thermopile.

Strips of the same emulsion exposed at the same temperature were developed together, along with check strips exposed in the Dewar flask apparatus at room temperature. The spectral sensitivity curve of each emulsion at room temperature was determined in the regular routine fashion, using the standard plate holders. The check strips, mentioned above, enabled corrections to be applied to the low temperature data to take into account losses by reflection at the walls of the Dewar flask, differences caused by the displacement of the exposure plane from its usual position, and differences in development. These corrections were not large (~0.10 log unit) and were the same for all wave-lengths. All films were developed for 5 minutes in Eastman D-19b developer at 65°F.

Densities of the resulting sensitometric strips were read and plotted in the form of intensity-scale characteristic curves. From these were read the exposures (ergs/cm²) required to produce a density of 0.40 above fog. Sensitivities as here defined are the reciprocals of these values. Spectral sensitivity curves were then obtained by plotting the logarithm of sensitivity as a function of wave-length.

For one emulsion the spectral transmission was measured at +26°C and at −187°C by a photographic method. Two strips of this film, which had no antihalation backing, were placed in the apparatus, one in front of the other. The emulsion side of the second strip was in close contact with the film base of the front one. An exposure was then made in the usual manner, the second strip thus being exposed by light transmitted by the first. This was done at several wave-lengths, at both +26°C and −187°C. For each wave-length, the transmission of the film was found by comparison of the intensity-scale characteristic curves obtained from the two strips. A correction was applied at each wave-length to take into account the extra exposure received by each film strip as a result of interreflections. This correction varied with wave-length, but was never larger than 15 percent of the value computed without the correction.

RESULTS

Spectral sensitivity curves for seven emulsions at three different temperatures are shown in Figs. 1 and 2. The temperatures of the film during exposure are indicated on the curves. Descriptions of the emulsions appear in Table I.

In Fig. 2 are also shown the reflection and transmission curves (solid lines) of a sample of emulsion VII, obtained at room temperature with a General Electric Recording Spectrophotometer by Mr. E. E. Richardson of these Laboratories. The triangles plotted along the transmission curve show values of transmission obtained photographically at +26°C, while the crosses represent values obtained in the same way at −187°C.

DISCUSSION OF RESULTS

The curves for the optically sensitized emulsions II–VII (Figs. 1 and 2) show that lowering the temperature of these films decreases the efficiency of their optical sensitization. For some

[4] J. H. Webb, J. Opt. Soc. Am. **23**, 316 (1933); **25**, 4 (1935).

[5] W. F. Berg and K. Mendelssohn, Proc. Roy. Soc. **A168**, 168 (1938); C. H. Evans and E. Hirschlaff, J. Opt. Soc. Am. **29**, 164 (1939).

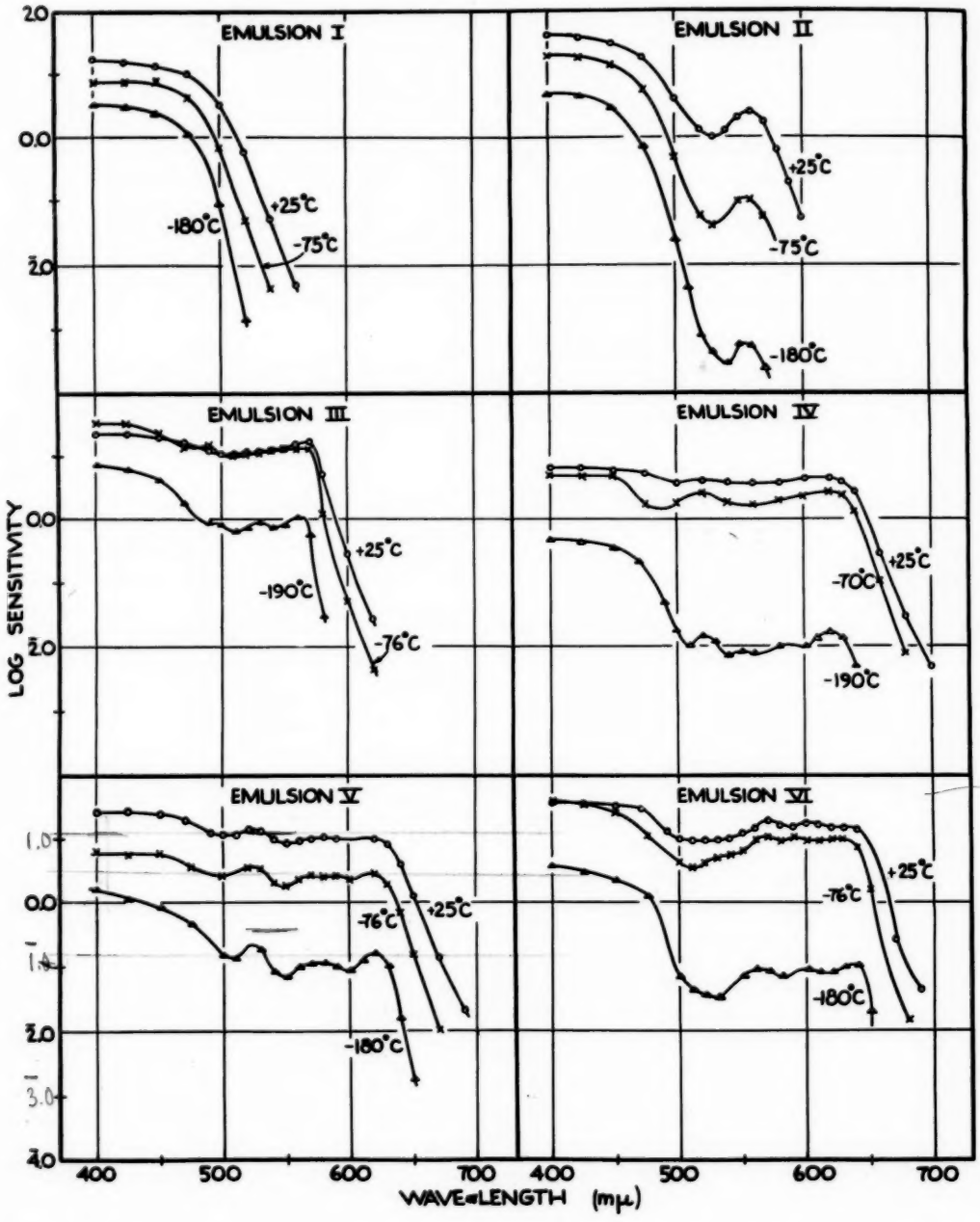

FIG. 1. Effect of temperature upon spectral sensitivity. Sensitivity defined as the reciprocal of the exposure (ergs/cm²) required to produce a developed density of 0.4 above fog.

of the emulsions, this decrease commences only somewhere below −75°C. Curves of spectral sensitivity at different temperatures for the unsensitized emulsion I (Fig. 1) are included for completeness.

To evaluate the efficiency of optical sensitization at low temperatures relative to that at room temperature, it is necessary to obtain the ratio of the loss in sensitivity in the region of natural sensitivity to that in the sensitized region. This may be seen from the following simplified picture:

The final stages in the formation of the latent image are taken to be the same, irrespective of the wave-length of exposing radiation. Electrons raised into the conduction levels of the silver halide lattice of the photographic grain by the action of light are trapped at sensitivity specks on the grain. These trapped electrons attract silver ions from the silver halide (electrolytic conduction), neutralizing them at the sensitivity specks to form the latent image.[6] For a given intensity of radiation of a wave-length lying well within the region of natural sensitivity, changing the temperature of the grain changes the rate of formation of latent image chiefly by its effect on the electrolytic conduction. The absorption of light by the silver halide is but little affected by temperature,[7] and the quantum yield of electrons at −185°C is approximately unity.[8] The change in the rate of formation of the latent image for a constant rate of elevation of electrons to conduction levels is reflected in the change, with temperature, of the natural sensitivity.

It is assumed that attainment of equal densities in equal exposure times with radiations of different wave-lengths corresponds to the same average rate of elevation of electrons to the conduction levels. This assumption follows from consideration of Webb's[4] findings that the shape of the reciprocity failure curve (drawn for constant density) of an emulsion, although altered by temperature, remains the same at any given temperature for different wave-lengths of exposing radiation. The curves for two different wave-lengths are separated by a constant amount, measured along lines of constant time. The shape of the reciprocity failure curve is directly associated with the rate of liberation of conduction electrons within the grain.[6,9,10] For present purposes, it is immaterial whether the conduction

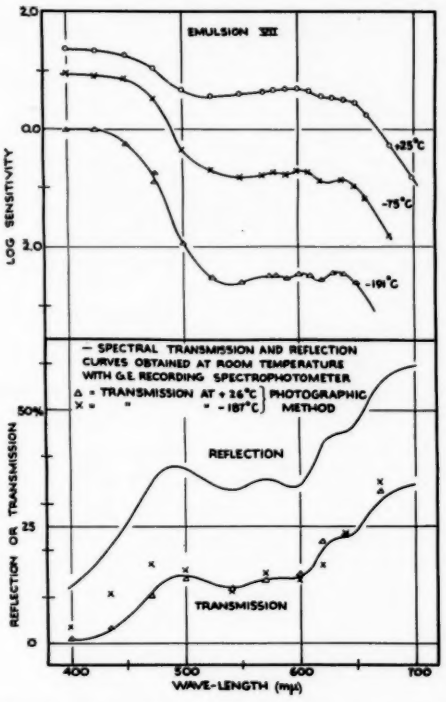

FIG. 2. *Above:* Effect of temperature upon spectral sensitivity of a panchromatic emulsion. *Below:* Reflection and transmission curves for same emulsion as above, determined at room temperature on G.E. Recording Spectrophotometer. Spectral transmission determined photographically at +26°C shown by triangles, and at −187°C by crosses.

TABLE I. Description of emulsions.

Number assigned to emulsion	Sensitization	Speed	Grain
I	Unsensitized	Medium	Fine
II	Orthochromatic	Medium	Coarse
III	Orthochromatic	Very high	Coarse
IV	Panchromatic	Medium	Fine
V	Panchromatic	High	Coarse
VI−	Panchromatic	Very high	Coarse
VII	Panchromatic	Medium	Medium

[6] For more detail see the following: R. W. Gurney and N. F. Mott, Proc. Roy. Soc. **A164**, 151 (1938); J. H. Webb and C. H. Evans, J. Opt. Soc. Am. **28**, 249 (1938).
[7] H. Fesefeldt, Zeits. f. Physik **64**, 741 (1930).
[8] W. Lehfeldt, Nachr. Ges. Wiss. Gött. Math.-Phys. Kl. **1**, 171 (1935).
[9] J. H. Webb and C. H. Evans, J. Opt. Soc. Am. **28**, 431 (1938).
[10] W. F. Berg, A. Marriage, and G. W. W. Stevens, J. Opt. Soc. Am. **31**, 385 (1941).

TABLE II. Effect of temperature upon efficiency of sensitization. Ratio of efficiency of sensitizer at temperature T to its efficiency at room temperature.

Emulsion	Wave-length in sensitized region $\lambda(m\mu)$	$T(C°)$	Ratio	$T(C°)$	Ratio
II	560	−76	1/10	−190	1/550
III	560	−76	1	−190	1/5
IV	620	−70	1	−190	1/20
V	620	−76	1	−180	1/4
VI	630	−76	1/2	−180	1/15
VII	600	−75	1/10	−191	1/60

electrons freed by action of light absorbed by the dye originate in the dye itself or whether they are freed from the silver halide by some mechanism.

Referring now to the spectral sensitivity curves of Figs. 1 and 2, it may be said that the factor by which sensitivity drops at wave-length 400 mμ measures the increase in the rate at which conduction electrons must be produced to give the same developed density with an exposure of equal duration at the lower temperature. The drop in sensitivity at wave-lengths in the region of optical sensitization, however, is composed of two factors, one representing this same required increase in production of electrons, and the other representing a loss in efficiency of the sensitizer at low temperature as compared with its efficiency at room temperature.

To separate these factors, it is necessary to take the ratio of the loss in sensitivity at wave-length 400 mμ to that incurred at the wave-length in the sensitized region by the lowered temperature. This ratio measures the efficiency of sensitization at the low temperature with respect to the efficiency at room temperature. Its reciprocal is the factor by which an intensity of exposing radiation in the sensitized region must be increased, at the low temperature, to produce conduction electrons at the same rate as did the initial intensity at room temperature.

Table II shows the ratios for the sensitized emulsions tested. All these ratios were obtained for a density of 0.4 above fog, although it was found that they varied relatively little with density level.

As an example, we may say that for emulsion VII at wave-length 600 mμ, approximately sixty times as many quanta are required at −191°C to produce a given number of conduction electrons as are required at +25°C to produce the same number.

In Fig. 2, we have evidence that this decreased efficiency pertains to the transfer of the action of light from the dye to the silver halide, rather than to the absorption of light by the dye. Although high accuracy is not claimed for the transmission values of emulsion VII measured photographically at +26°C and at −187°C, it does appear that the absorption by the dye through the main region of optical sensitization is but little affected by temperature. Since absorption (A) is related to transmission (T) and reflection (R) by the expression $A=(1-T-R)$, this involves the assumption that changes in reflection are of the same order as changes in transmission. This assumption was checked qualitatively by observing a strip of the film as it was inserted in the low temperature apparatus at −187°C. No changes could be seen. Any changes in absorption are of a different order of magnitude from the observed drop in sensitivity. It appears, therefore, that the dye of emulsion VII absorbs about sixty times as many quanta to produce one conduction electron in the silver halide lattice at −187°C as it does to produce one when the grain is at +25°C.

In conclusion, it may be stated that the results shown in Figs. 1 and 2 agree with those of Ungar with respect to both the general order of magnitude of the effect and the fact that this magnitude varies among different sensitizers. It also appears probable that the effect is dependent upon the basic emulsion as well as upon the sensitizer.

The panchromatic emulsion tested by Sheppard, Wightman, and Quirk was evidently one which showed the differential effect but slightly, being somewhat comparable in this respect with emulsions III and V.

Mercury Sensitization and the Optical and X-Ray Latent Images

ALBERT MAY
The Catholic University of America, Washington, D. C.
(Received January 28, 1942)

INTRODUCTION

ONE of the simplest methods known for increasing the optical sensitivity of a photographic film or plate beyond the value that it has at the completion of the manufacturing processes is that of hypersensitization in mercury vapor.[1] The procedure consists simply in exposing the film in a light and air-tight box to the vapor from a small amount of mercury for a period which may vary from a few hours to a few days. While some emulsions have been found to be unaffected by this treatment or to suffer decreases of speed,[2] increases in speed of 25 to 150 percent have usually been reported for optical exposures of short duration. Increases up to 600 percent have been obtained[3] for sixteen-hour exposures to very weak light. Apparently the only mention in the literature of the application of this process to x-ray exposures is the mere statement[4] that an increase of speed was obtained.

It was felt that information concerning the x-ray and optical latent images might be obtained by a further study of this effect and mercury-sensitized x-ray emulsions have been tested with exposures to x-rays and to visible light.

THEORETICAL

The generally accepted theory of latent image formation is essentially as follows.[5] On the surface of the silver bromide grains and probably within the grains in the unexposed emulsion are sensitivity centers or nuclei consisting probably of silver sulphide with a small accumulation of metallic silver. Photoelectrons produced in the grains by the photographic exposure wander through the lattice and are trapped at the centers since their energy when in the center is less than when they are in the silver bromide lattice. The resulting negative charge attracts interstitial silver ions which travel to the centers and accumulate there as atoms, thus increasing the size of the center. If the amount of silver at the center becomes sufficiently great the center becomes developable. Centers which contained this amount of silver prior to exposure will be developable whether there is an exposure or not, giving rise to inherent fog.

The reciprocity law assumes that the developable density depends upon the product of the intensity of illumination and the duration of the exposure and not upon these two quantities separately. Actually at very low and very high intensities a greater value of the product is required to produce a given density than at some intermediate intensity. These failures of the reciprocity law have been explained[5] by the facts that low intensity light is relatively inefficient in building up the smaller centers and that high intensities favor the formation of many small centers instead of one large one.

A quantum of visible light has sufficient energy to produce only one photoelectron and hence one silver atom. A single x-ray quantum may produce thousands of silver atoms and may thus render a grain developable.[6]

An explanation of the hypersensitization by mercury vapor has been given by Dersch and Dürr.[1] Atoms of mercury are undoubtedly adsorbed to silver nuclei on the surface of the grains, effectively increasing their sizes as though silver had been added. Less optical exposure is then needed to bring the nuclei to a size at which they will be developable.

PROCEDURE

The exposures were made on Eastman Ultraspeed Blue Brand and No Screen x-ray film which are designed for use with and without fluorescent screens, respectively. They will be designated as US and NS film. These films are coated on both

[1] F. Dersch and H. Dürr, J. Soc. Mot. Pict. Eng. **28**, 178 (1937).
[2] C. Emmerman, Brit. J. Phot. **84**, 440 (1937); Kleinfilm Photo (May-June, 1937).
[3] I. S. Bowen and L. T. Clark, J. Opt. Soc. Am. **30**, 508 (1940).
[4] Reference 1, discussion p. 186.
[5] R. W. Gurney and N. F. Mott, Proc. Roy. Soc. **A164**, 151 (1938); J. H. Webb. J. App. Phys. **11**, 18 (1940); N. F. Mott, Phot. J. **81**, 63 (1941).
[6] J. Eggert and W. Noddack, Naturwiss. **15**, 57 (1927).

sides of the base and the emulsions are non-color-sensitized. The US film is fifteen or twenty times as sensitive to visible light as the NS film probably due to a larger average size of the silver nuclei, which is indicated by its higher inherent fog.

Numerous tests were made with both films by exposing them to either visible light or to x-rays. The source of visible light was white light filtered through an Eastman OA (bromide) safelight filter except for the most intense illuminations for which white light was used. The x-ray exposures were made to the "white" radiation from a tube operated at about 35 kv.

In each test two film strips were irradiated and developed side by side. One of these strips was exposed to mercury vapor either before or after exposure to radiation. The development was for five minutes in Eastman D19 at 18.5°C approximately. Step exposures with a step-ratio of 2 : 1 were used.

The intensities were judged (neglecting reciprocity law failure) by the time required to produce a developed density of unity above fog. These times varied from one-half second to two hours for the x-ray exposures and from 0.01 second to an hour and a half for visible exposures.

The densities were measured on a simple comparison densitometer[7] and D-log t curves (where t is the exposure time) were plotted for the unsensitized strips. The relative speeds for the various steps of the sensitized strips were estimated by finding from the curves what exposure time on the unsensitized strip would have been required to give the density obtained on the sensitized one. This method permits the evaluation of speed for different exposure times and does not require that the full characteristic curve be available. The speed change is indicated by a speed factor s which has a value of unity if no change of speed occurs, a value of 2 if the speed is doubled, etc.

Various periods of exposure to mercury vapor were tried and the optimum times as judged from the maximum increases of speed with visible light were found to be slightly less than one day for the US film and perhaps five days for the NS. Considerable fog is obtained by the hypersensitization of the US film, the fog being increased by about 0.1 after nineteen hours in the mercury vapor and reaching prohibitive values after several days. The fogging varies considerably for a given sensitizing time, depending undoubtedly on humidity[8] and other factors. Only slight fogging is produced on the NS film, the density increase seldom exceeding 0.005. A decrease of background fog due to mercury hypersensitization has been reported[9] for certain spectrographic plates. Several tests on NS film gave this result but the difference in background is so small that it is probably due to some slight difference in development or humidity conditions during the time of sensitization rather than to the sensitization itself.

[7] The author is indebted to Mr. Joseph F. Mullaney for the construction of this densitometer.

RESULTS

Figure 1 shows the average speed increase factors s for presensitized film, that is, film which was hypersensitized before exposure, as a function of density above fog. Each point plotted indicates, for a given density, the average speed factor of 13 to 21 tests made with various intensities of x-rays or visible light. It will be seen that only in the case of US film exposed to visible light is any considerable increase of speed obtained. This same film when exposed to x-rays suffers, on the average, a reduction of speed. On the other hand a very small increase of speed is obtained for NS film exposed to visible light and a still smaller increase when x-rays are used.

The reason why hypersensitization, followed by exposure to visible light causes an increase of speed has already been discussed. The small increase of speed and small sensitization fog of NS film indicates small silver nuclei. While the increase of effective size of the nuclei by the addition of mercury atoms would cause considerable increase of speed for such an emulsion, the small size of the nuclei prevents any considerable adsorption of these atoms. The fogging produced in the US film indicates that it contains many silver nuclei large enough to be brought to a developable size by the addition of a few mercury atoms.

As we have seen, a single absorbed x-ray

[8] F. L. English, Am. Phot. **33**, 90 (1939).
[9] F. L. Whipple, D. Norman, and R. Loevinger, Harvard Coll. Obs. Bull. No. 907, p. 36 (1938).

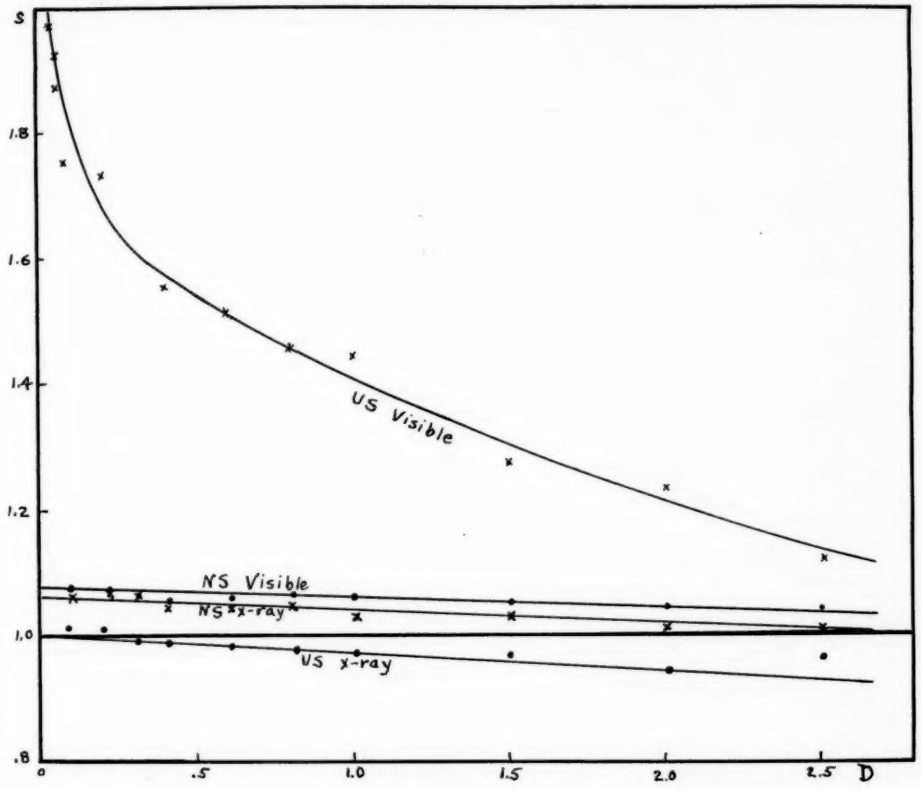

FIG. 1. Average speed factors of presensitized film as functions of density.

quantum produces hundreds of available electrons and the initial size of the silver nucleus is of less importance than for quanta of visible light. If, however, a center is very small the energy of an electron in it may be so little below the energy it would have when in the lattice that the center will have little tendency to trap electrons. It is probably the building up of such centers by the addition of mercury atoms that accounts for the small increase of speed of the NS film with x-ray exposures.

The explanation of the decrease of speed of US film when exposed to x-rays can be found in the fact that although the densities above fog are less in the sensitized than in the unsensitized film, the total densities of the sensitized film are greater than the unsensitized densities. In other words the small increase of speed naturally produced is more than counterbalanced by the destruction of available centers by sensitization fog.[8]

The general decrease of the speed factor s with increased density is explained by the fact that the larger centers are more likely to adsorb mercury atoms and hence have their speed increased. These are the nuclei most likely to be made developable by small exposures. At higher densities the remainder, consisting generally of only slightly sensitized centers, are involved.

It will be seen that the results for visible light are in agreement with those of most experimenters[10] who have found either a reduction of slope of the characteristic curve or no appreciable change.

Curves plotted for postsensitized film are quite similar to those of Fig. 1 but the graphs are lower. The increase of speed of US film for visible

[10] E.g. references (2) and (7).

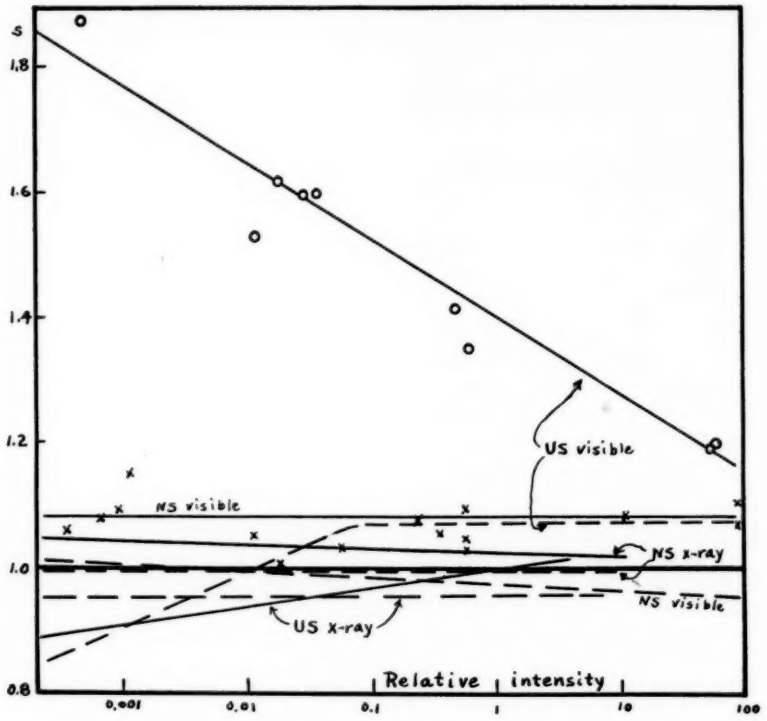

FIG. 2. Average speed factors as functions of intensity of irradiation.
——— presensitized
– – – – postsensitized
○ US visible presensitized
× NS visible presensitized

light is about forty percent at unit density for presensitized film and only about six percent when postsensitized. The graphs for NS film are depressed about four percent and that for US film with x-ray exposures one or two percent.

These lower s values are to be expected for postsensitization. When an increase of speed is obtained with postsensitization it results from an increase of the effective nucleus size by the adsorbed atoms so that some are rendered developable but the increase in size is that due only to a number of mercury atoms. For presensitization, on the other hand, the increase in effective size of the nuclei gives them the potentiality of attracting a large number of silver atoms to the nuclei. Some investigators have found[11] a greater increase in speed for postsensitization than for presensitization and others report[9] that the results of post- and presensitization are the same. These experimenters used dye-sensitized emulsions.

Graphs for postsensitized film show decreases of the speed factor at higher densities similar to those seen in Fig. 1 for the presensitized film. These decreases are ascribable to the fact that when a film is already developable to a high density the probability that a mercury atom will adsorb to those nuclei which it could make developable is small compared to the probability of adsorption to one of the larger centers already developable.

In Fig. 2 the speed factors for presensitized and postsensitized film are plotted against the intensities of the light or x-rays. These speed factors are averages for various densities, whereas in Fig. 1 values averaged over different light

[11] C. Emmerman, Brit. J. Phot. **84**, 378 (1937); Kleinfilm Photo (March-April, 1937); reference 1.

intensities were plotted against the developed densities. As already mentioned the intensities were judged by the exposure times required to produce unit density and the abscissas in Fig. 2 are the reciprocals of these times in seconds on a logarithmic scale. The points from which the graphs were determined are plotted in Fig. 2 only for presensitized films exposed to visible light. The effect of the hypersensitization varies so much from test to test principally because of the slightly different history of the film that the slopes and curvatures cannot be obtained with accuracy. For this reason most of the graphs have been given as straight lines. Each point plotted in Fig. 2 represents one test and eight to sixteen such tests were used in determining the various graphs. The spreads of the points for all graphs were substantially similar to those for which the points are shown.

The greater increase of speed of presensitized film at weak illuminations with visible light has been described by Bowen and Clark[3] who call it a reduction of the low intensity reciprocity law failure. The effect of presensitization is to enlarge the small centers involved in this failure and so to bring about its reduction.

There is little doubt that the most intense visible light illuminations used were in the region of high intensity reciprocity law failure. Some evidence of a decrease of this failure is seen from the points for presensitized NS film exposed to visible light in Fig. 2. Such a decrease might be expected since the presensitization increases the average size of the surface centers and thus permits the simultaneous trapping of more electrons per center.

The outstanding feature in the graphs for postsensitized film in Fig. 2 is the decrease of the speed factor for US film sensitized after exposure to light as the light intensity is reduced. The reduction of low intensity failure will not be present in postsensitized film so that we should not expect an increased speed factor at weak illuminations. The actual decrease is due to the fact that with weak light it is principally the large centers that are built up (by the mechanism of low intensity failure), while at higher intensities many of the smaller centers are enlarged. Comparatively more of the smaller centers will need mercury atoms to bring them to a developable size.

It is to be expected that US and NS films should have similar graphs for similar exposures, and no change of speed factor is probable with change of the intensity for x-ray exposures. The fact that these expectations are not fulfilled indicates that the slopes given the graphs are probably inaccurate.

Tenth Summer Conference on Spectroscopy and Its Applications

LETTER ballots to all persons who have attended the recent Summer Spectroscopy Conferences, held at the Massachusetts Institute of Technology, have shown that in spite of the emergency there is a widespread desire that another conference be held this summer, and an interesting program has been assured. Accordingly, the tenth Summer Conference on Spectroscopy and Its Applications has been scheduled, to be held in Cambridge on July 20, 21, and 22, 1942, under the joint auspices of the Optical Society of America and the Massachusetts Institute of Technology.

Since the air-conditioned room in which the Conference will be held will seat only 225 persons, and since two-thirds of the seats have already been reserved as a result of the balloting, those who expect to attend the Conference should write as soon as possible for reservations to the Chairman of the Program Committee, PROFESSOR G. R. HARRISON, *Massachusetts Institute of Technology, Cambridge, Massachusetts.*

An Intensity-Scale Sensitometer that Works at Intensity-Time Levels Used in Practical Photography*

WM. BORNEMANN AND CLIFTON TUTTLE
Kodak Research Laboratories, Eastman Kodak Company, Rochester, New York

(Received December 12, 1941)

A new intensity-scale sensitometer capable of producing a top maximum exposure of about 100 meter-candle-seconds in 1/50 second has been designed and built. The instrument exposes twenty steps, one step at a time. The individual steps are the same size as those produced by the IIb instrument. Every effort has been made to make this sensitometer reproducible to specifications and free from variability with age and use. Instead of the absorbing step tablet ordinarily found in high intensity instruments of the variable-intensity type, this sensitometer produces its exposure series by the interposition of metal diaphragms in an optical system. The size of these diaphragms was determined by computation and the results have been checked experimentally.

TO be of the greatest usefulness in the interpretation of practical photographic results, sensitometry should be carried out under conditions approaching as closely as possible to those applying to the practical exposure. In picture taking or in printing, exposure is produced almost invariably at a constant time while the variation in density from point to point in the image results from variation in intensity. In both picture taking and printing on film materials, the great majority of exposures are of short duration and at correspondingly high intensity levels. Most amateur snapshots and motion picture photographs, which together make up undoubtedly the greatest number of exposures, are made at exposure times of 1/25 to 1/100 second. Time values in motion picture printing are of the same order.

Although the desirability of duplicating in sensitometry the practical conditions of exposure has been recognized almost from the beginnings of scientific photography, the most widely used precision sensitometers have been of the constant-intensity, variable-time type. The Eastman IIb sensitometer[1] is probably the most popular instrument of this kind. The most common variable-intensity sensitometers are of the tablet type. These have always been regarded with some mistrust because they depend upon light-absorbing materials to produce the intensity variation. It has been a difficult matter to produce absorbing tablets that are non-selective and stable.

In order to avoid the limitations of absorbing tablets other means of varying the intensity of the exposing light have been proposed. A precise means, of course, is the application of the inverse square law, a method which may be above reproach theoretically, but which in practice leads to a cumbersome design undesirable in an instrument for routine work.

Jones and Morrison[2] devised a sensitometer utilizing a cylindrical optical system diaphragmed by a series of slit openings. The result is a compact instrument capable of an intensity level high enough and an exposure range great enough to meet the requirements, but it is admittedly difficult to calibrate and to maintain in calibration. It cannot, moreover, be said to be reproducible to specification.

The instrument which we shall describe was designed to meet the requirements of practical sensitometry: as to its intensity level, simplicity of calibration, convenience of operation, and dimensions of the strip produced.

Much equipment now exists for the processing and reading of sensitometric strips of the dimensions used by the IIb instrument. These strips measure $1\frac{3}{8}\times 12$ inches. The exposed area consists of two rows of steps, each 0.4 inch square, the rows being separated by an unexposed

* Communication No. 839 from the Kodak Research Laboratories.

[1] Loyd A. Jones, "A motion picture laboratory sensitometer," J. Opt. Soc. Am. **17**, 536 (1931).

[2] Loyd A. Jones and C. A. Morrison, "Sensitometry of photographic papers," J. Frank. Inst. **228**, 445 (1939); **228**, 605 (1939); **228**, 755 (1939).

area 0.2 inch wide. It is desirable that these dimensions should be maintained.

Slow positive film materials now on the market require a top exposure value of about 100 meter-candle-seconds. Thus at an exposure time of 1/50 second, the problem of sensitometer design is resolved into one of producing a maximum intensity of about 5000 meter-candles. It is of course necessary that this intensity be uniform over the step being exposed.

It was decided in the case of this sensitometer to expose each step separately and between exposures (while the strip is being indexed from one step to the next) to adjust the aperture of an optical system to give the correct intensity level to the following exposure. The step-by-step method, since it involves uniform illumination of only relatively small areas, considerably simplifies the problem of securing an adequate amount of light.

Because we feel that this instrument, or one built according to the same general principles, might be useful in standardizing sensitometric technique, we shall describe the essential features in considerable detail.

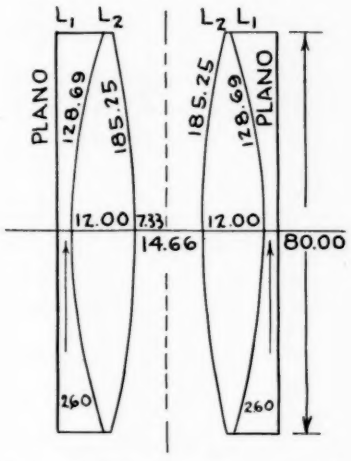

Component	Glasses	D	G'	V
1	B & L DF-2	1.61700	1.63929	36.6
2	B & L LBC-2	1.57250	1.58521	57.4

Equivalent focus 363.25 mm. Back focus 353.07 mm.

Spherical aberration	Coma
F 4.5 −0.044	−0.004
F 6.43–0.332	−0.012
Color: C−D+0.476	F−D −0.104

FIG. 2. Objective lens (all dimensions in mm).

THE LIGHT SOURCE

A rectangle of uniform brightness radiating according to the cosine law would be the most satisfactory source. An incandescent sheet of tungsten of the same area and proportions as the area to be illuminated would be ideal, but such tungsten filaments are not uniformly bright. A rectangular window in an integrating sphere would be a possible source but such a device would waste light and the sphere coating would probably deteriorate in color and reflectance. The device adopted is the so-called integrating bar—a bar of white optical borosilicate crown glass 1 inch square and $2\frac{9}{16}$ inches long. Both ends of the bar are fine ground and for additional diffusion the exit end is covered by a square of glass fine ground on its outer surface. A monoplane filament lamp is mounted on a base plate and the bar is supported on a bracket. The lamp may be moved back and forth from the end of the bar so that variations in light output between lamps operated at given color temperature values may be compensated in the original calibration of the light source. With this lamp operated at a current value such that the color temperature at the bar end is 2660°K, the luminance[3] is 30.6 candles per square centimeter. Because of the slight color of the bar the lamp itself operates at a color temperature slightly below that of the bar end. Other lamps of the same rating and type

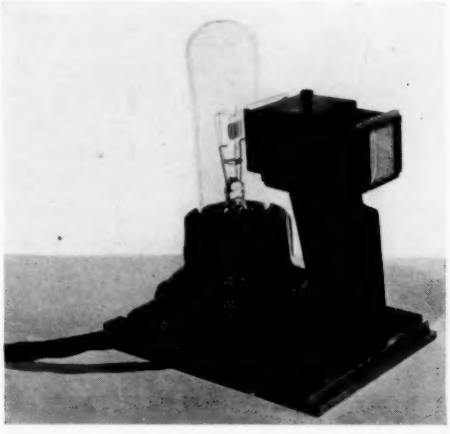

FIG. 1. Photograph of light source.

[3] "Colorimetry: Preliminary draft of a report on nomenclature and definitions," J. Opt. Soc. Am. **27**, 207 (1937).

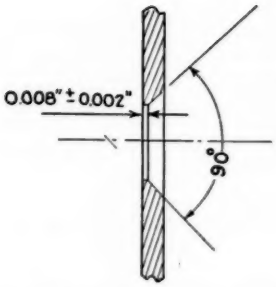

FIG. 3. Cross section drawing on an aperture plate.

may have an output differing from that of the average lamp by ±10 percent.

A photograph of the complete light source unit is shown in Fig. 1. In this case a 500-watt projection type lamp with an offset filament furnishes the light to the bar. The luminance of the window may, however, be adjusted to a standard value by movement of the lamp. Once set, the bar and lamp are anchored firmly in position with respect to each other on a base which is later accurately positioned in the instrument itself. Lamps of lower wattage are used for negative sensitometric light sources, but whatever the lamp used, the whole unit is calibrated in the photometric standardizing laboratory. The lamp is locked in position and the current to be used to produce the specified color temperature is noted.

THE LENS SYSTEM

The condensing system consists of two identical telescope objectives face to face. The objective was designed specifically for this system by Dr. Max Herzberger of these Laboratories. The materials used and the essential dimensions are shown on the drawing and in the caption of Fig. 2.

Each half of the system has a relative aperture of $f/4.5$ and is corrected independently for chromatic and spherical aberrations within 0.025 percent of the focal length. Because of the symmetry of the layout, the combined system is free from coma. The design of this lens system and the dimensions employed make it certain that the intensity of the image formed in the image plane will be directly proportional to the area of diaphragming apertures inserted in the parallel light between the components.

The series of diaphragm diameters computed to give $\sqrt{2}$ steps in intensity is shown in column 2 of Table I. Columns 3 and 4 of this table will be discussed later. To obtain mechanical accuracy, all of the diaphragm holes were bored out, and the nine smallest holes were lapped to dimensions using hardened steel plugs of the correct diameters. This method should give a dimensional accuracy within ±0.3 percent, which would be about 0.01 mm at 2.97 mm, the diameter of the smallest hole.

The diaphragm holes are countersunk from the rear side to a thickness of 0.008 inch and the brass is chemically blackened. The cross-sectional view of one of these apertures is shown in Fig. 3.

SET-UP OF OPTICAL SYSTEM

The complete optical system of the sensitometer consists of the light source, the two lens components with their diaphragming plates, a shutter, and a mask in front of the film. Provision is also made between the light source and the lens for insertion of either a solid or a liquid filter. A blower directs a stream of air on the lamp and bar-end to prevent over-heating.

The first lens is set at its focal distance from the source and the second lens at its focal distance

TABLE I. Diaphragm dimensions and intensities* produced in the exposing plane when the source luminance is 30.6 candles per square centimeter.

Step No.	Diaphragm Diameter (mm)	Intensities in Film Plane (meter-candles) Computed	Measured
1	80.00	9402	9400
2	67.28	6649	6635
3	56.57	4701	4701
4	47.57	3324	3270
5	40.00	2350	2350
6	33.64	1662	1630
7	28.28	1175.0	1155
8	23.79	831.4	830.0
9	20.00	587.5	587.5
10	16.82	415.6	416.0
11	14.14	293.7	287.0
12	11.90	207.8	205.0
13	10.00	146.9	147.0
14	8.41	103.9	103.5
15	7.07	73.43	74.5
16	5.95	52.00	53.0
17	5.00	36.72	37.5
18	4.20	25.92	26.5
19	3.54	18.42	18.5
20	2.97	12.96	13.0

* In sensitometry of positive materials a color temperature of 3000°K is customary. The filter to convert the 2660°K source to 3000°K has a transmission slightly greater than 50 percent. Thus the top intensity available with this source is about 5000 meter-candles.

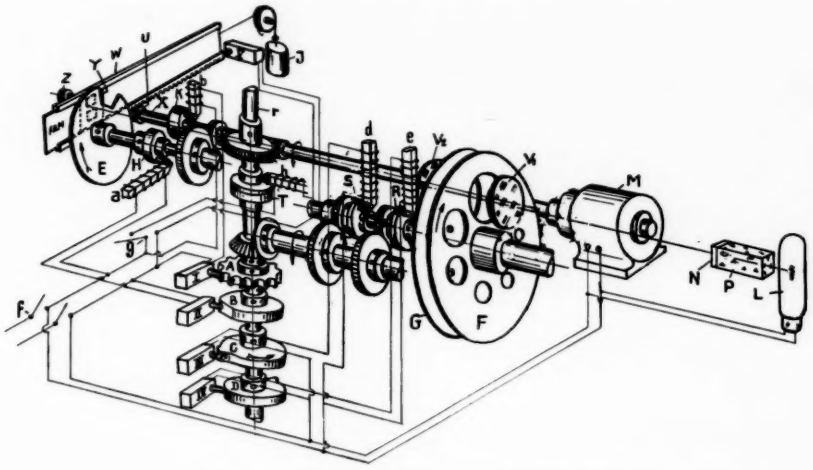

FIG. 4. Schematic layout of electromechanical system.

from the film plane. The separation between the components is as shown in Fig. 2.

THE MECHANICAL AND ELECTRICAL SYSTEMS

Given the optical system just described, a number of different mechanical devices may be built to produce the necessary diaphragm changes, to control the exposure time, and to transport the sensitive film from step to step.

The system actually used in this instrument is illustrated schematically in Fig. 4. The light source, consisting of the lamp L, glass bar P, and the ground glass N, is imaged by the lens V_1V_2 on the film plane. Modulation of the exposure is produced by the set of diaphragms arranged in series about the periphery of two disks, F and G. One disk carrying all the apertures, would, of course, serve the same purpose, but the size of a single disk carrying the whole diaphragm series would be large and cumbersome. Each diaphragm hole is cut in a metal plate which is used as an inset in the disk. This allows the removal for checking or replacement of any of the diaphragms without disturbing the rest.

A continuously rotating shutter E near the plane of the film controls the length of exposure and keeps light from falling on the film during the film-indexing part of the cycle.

The film is held in a carriage so designed that it is easily loaded in the dark. The carriage moves in gibs and is driven by a pinion U which meshes with a rack to which the carriage is attached. The pinion is driven by a shaft X, one revolution of which moves the carriage the required distance (0.4 inch). The single revolution of X is accomplished by a one-turn clutch mechanism and is released to make this one revolution whenever solenoid b is energized. The time of indexing is 0.2 second. After the carriage has moved the whole length of the sensitometric strip, the pinion may be disengaged by pulling knob Z. This frees the carriage for manual resetting. A weight I takes out backlash in the gears.

In operation, the main switch f is closed, energizing a $\frac{1}{8}$-hp synchronous motor M, and lighting the lamp L. By means of a variable transformer, the lamp is brought to its calibrated current reading at which it produces a source of the required candlepower and color.

The exposure cycle is initiated by closing switch g thus energizing solenoid h, allowing the one-turn clutch T to rotate. This clutch drives a shaft upon which are mounted cams A, B, C, and D. The function of these cams is to operate four switches, I, II, III, and IV, in pretimed sequence. As the cams start to rotate, switch II is closed, energizing solenoid a thus allowing clutch H and the sector shutter E to rotate as long as switch II is held closed. Cam B is cut so as to keep this switch closed during the whole exposure cycle, i.e., until twenty steps are exposed.

As the leading edge of the shutter opening cuts

FIG. 5. Photograph of completed sensitometer.

into the light beam, the riser on cam C closes switch III which through the medium of the solenoid d engages the clutch S, thus starting the rotation of the diaphragm disk F. This disk continues to rotate throughout the remainder of the exposure cycle. The diaphragm openings are never stationary even while the exposure-timing shutter is open. The slight movement of a diaphragm between the lens elements which takes place during exposure is of no consequence since there is no zonal error in the lens. The advantage in mechanical design of moving the fairly heavy diaphragm disk continuously rather than intermittently is obvious.

The second disk G is set in motion through the action of cam D shortly before the first disk has completed one revolution. Thereafter it continues to rotate at the same speed as disk F with its smaller set of diaphragms located concentrically to the diaphragms in disk F.

The cam A, through the medium of the switch I, and solenoid b, indexes the film during each dark portion of the shutter cycle.

The exposure cycle is completed as soon as the shaft r has made one revolution. This occurs 8 seconds after switch g is closed. The switch V which is in series with the starting switch g is opened by the film carriage at the extremity of its travel and it thus prevents starting of the machine until the carriage has been manually returned to its starting position.

A photograph of the instrument is shown in Fig. 5.

PRACTICAL TESTING OF SENSITOMETER

With this sensitometer we have attempted to produce an instrument which would conform to the ASA proposed standards of sensitometric procedure[4] and we have designed it so that it could be reproduced to specifications. The proof of success in achieving these aims rests in a comparison of the results expected from a computation of exposing intensities* with the results actually measured in the instrument.

Results to be expected in this sensitometer can be computed directly from the lens constants and the luminance of the source. The photometric formula is:

$$I=\pi LT\times 10^4/(4f^2),$$

where I is the intensity in meter-candles, L is the luminance in candles per square centimeter, T is the transmission factor of the lens, and f is the effective f-value of the lens. Rewriting this equation in terms of d (the aperture diameter in millimeters), and substituting the value 0.81 for T as computed from the glass indices, gives

$$I=0.048\times B\times d^2.$$

The whole instrument was set on a bench photometer. The intensities actually produced in the film plane by the series of diaphragms were read by visual means and the readings were checked by a calibrated photo-cell. The probable error of photometric readings is about 1 percent. At the low intensity steps an error in the visual reading of 1.5 percent is possible. The results are given in column 3 of Table I. The agreement between computed and measured results is reasonably good in all cases.

As a secondary check, a series of photographic measurements was made, using a refined inverse-square-law sensitometer for comparison. In this instrument a light source operated at the same color temperature and an exposure time of 1/50 second was used and the other well-known requirements of photographic photometry were followed carefully. Several different kinds of emulsions were used and in all about forty different strips were exposed. These data indicate

[4] American Standards Association, "Proposed American Standard: Specifications for determining photographic speeds of roll films, film packs, and miniature camera films," J. Opt. Soc. Am. **31**, 87 (1941).

* The time factor of the exposure with a synchronous motor actuating a sector shutter is subject to so small an error that it can be neglected.

that the new sensitometer is in very good agreement with the standardizing inverse-square-law instrument.

It is believed that the only likely cause of change in an instrument of this type, aside from that of the unavoidable deterioration of the lamp itself, is the possible effect of deformation of the lamp filament. It is conceivable that enough filament sagging will occur in the source of highest color temperature to cause a variation in the brightness distribution of the end of the integrating bar. Such an effect will upset the uniformity of illumination of the sensitometric area, which, in the instrument as originally set up, is very good. Should this prove to be serious, it is proposed to limit the exposed area to a 0.4-inch square spot with the center of the square located on the optical axis of the instrument, whereupon filament deformation would no longer be a source of material error.

APRIL, 1942 J. O. S. A. VOLUME 32

A Logarithm-of-Wave-Length Scale for Use in Absorption Spectrophotometry

WILLIAM A. SHURCLIFF
Research Department, Calco Chemical Division, American Cyanamid Company, Bound Brook, New Jersey
(Received December 22, 1941)

Some advantages of a logarithm-of-wave-length scale for spectrophotometric absorption curves are indicated. A system arranged so as to provide 100 units per spectral octave has been found especially convenient, particularly so in connection with instruments which can plot over a number of different ranges and at different magnifications.

INTRODUCTION

ALTHOUGH the question of what abscissa scale is most suitable for presentation of spectrophotometric data has been the object of discussion for over fifty years, it is apparent that no general agreement on any one system, whether wave-length, frequency, or logarithm-of-wave-length, has yet been arrived at. Thus, a survey of articles on infra-red spectrophotometry in the 1940 numbers of the *Journal of the Optical Society of America*, *The Journal of Chemical Physics*, and *Journal of Applied Physics*, shows that a small majority of the writers (14 to 10) favor a frequency scale, although the arrangement of the plots such that wave-length increases to the right is also (if somewhat inconsistently) favored by a small majority (15 to 9).

In favor of the wave-length system reference is commonly made to the fact that wave-length is a very familiar and easily understood parameter, and that it may be experimentally evaluated in more straightforward manner than other abscissas. The use of frequency as abscissa was first proposed by Stoney, according to Rayleigh,[1] this variable now being most conveniently and commonly used in problems involving Planck's law: $E=h\nu$.

Lord Rayleigh[1] pointed out in 1883 that a logarithm-of-wave-length scale had the advantage of allotting equal space to each spectral octave. In this respect, the logarithm-of-wave-length scale avoids the difficulties inherent in the wave-length or frequency scales, as indicated in Fig. 1, in that, using the logarithm-of-wave-length scale, neither of the ranges, ultraviolet nor infra-red, is expanded at the expense of the other. For this reason, the logarithm-of-wave-length

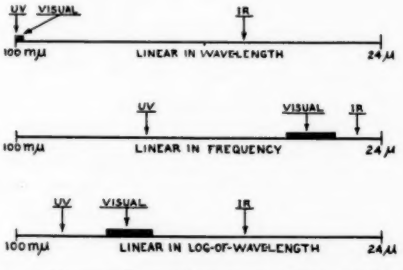

FIG. 1. Diagram illustrating space allotted to the ultraviolet, visual, and infra-red ranges by the three commonest linear abscissas.

[1] Lord Rayleigh, Nature (1883).

scale has been used by a number of authors, including Wood[2] and Hardy and Perrin,[3] in presenting data covering a wide spectral range.

Another convenient property of the logarithm-of-wave-length scale is that if one desires to retain roughly constant spectral resolution ($\lambda/d\lambda$) over a broad range, one needs merely to maintain the slit-width ($d(\log \lambda)$) approximately constant. (Resolution is, of course, far from constant when, over a broad spectral range, the wave-length-system or frequency-system slit width ($d\lambda$ or $d\nu$) is held constant.)

A further obvious property of the logarithm-of-wave-length system (i.e., minus-logarithm-of-frequency system) is that harmonics (lines or bands occurring at ν, 2ν, 3ν, etc.) have spacings (log 2, log 3, etc.) which are independent of the location of the fundamental, in analogy with the common (logarithmic) musical scale.

CURRENT CONSIDERATIONS

In weighing the merits of the three systems as applied to absorption spectrophotometry, it is apparent at the outset that wave-length and frequency are both satisfactory when the instrument at hand operates over a fixed and relatively narrow range. Thus in the use of the recording spectrophotometers operated by the company with which the writer is associated, several hundred thousand curves were obtained satisfactorily using wave-length and frequency abscissas extending from 400 to 700 millimicrons.

However, spectrophotometric equipment has now reached a stage of development where common wave-length and frequency scales have been found to present serious constraints of two types, as discussed below.

1. Constraint Related to the Extension of the Spectral Range

Several recording spectrophotometers with which the writer is concerned operate in routine manner over a range from 375 to 1200 millimicrons. It was found at an early stage that for such a range of a little less than two octaves, a fixed wave-length scale allotted relatively too much space to the infra-red range (750 to 1200 millimicrons), whereas a fixed frequency scale, on the other hand, gave too little space to this range. Improved proportioning resulted when a logarithm-of-wave-length scale was adopted.

The argument might be advanced that inequalities of abscissa space allotment could be obviated satisfactorily by dividing a curve into several segments each of which would be presented at a different, appropriate magnification. While this sort of corrective procedure has been resorted to frequently,[4] it presents several serious drawbacks.

The principal disadvantage of requiring progressive changes in abscissa magnification is that it greatly complicates the making of small shifts of range. Thus in operating spectrophotometers covering the visual and near infra-red ranges, it has been found desirable to provide means of effecting shifts in the range covered in a single plot (see Fig. 2). To "fit" the range to the characteristics of the particular curve to be drawn,—i.e., to make it possible to include in a single plot a majority of the salient features of the curve—it has been found necessary to make provision for shifting the range by small or large amounts, the actual scheme involved being one in which shifts of 1/10, 2/10, 3/10, etc., octave may be effected. Naturally, if it were necessary to change magnification discontinuously at arbitrary spectral positions, the complexities of instrument design and data presentation would be enormously increased. It appears that the ideal system would be one analogous to that employed in cartography, where contiguous regions are presented on maps which are identical in scale and which can thus be joined together conveniently to describe any region near to or including the borderline.

2. Constraints Related to Providing a Choice of Abscissa Magnification

It appears well recognized that there are certain problems in colorimetry which cannot be solved by visual range spectrophotometers operating at but a single abscissa magnification. That is, while the usual type of curve allotting

[2] R. W. Wood, *Physical Optics* (The Macmillan Company).

[3] A. C. Hardy and F. H. Perrin, *The Principles of Optics* (McGraw-Hill Book Co., Inc.).

[4] B. L. Crawford, for example, in J. Chem. Phys. **30**, 578 (1940), employs three different magnifications in presenting a single curve.

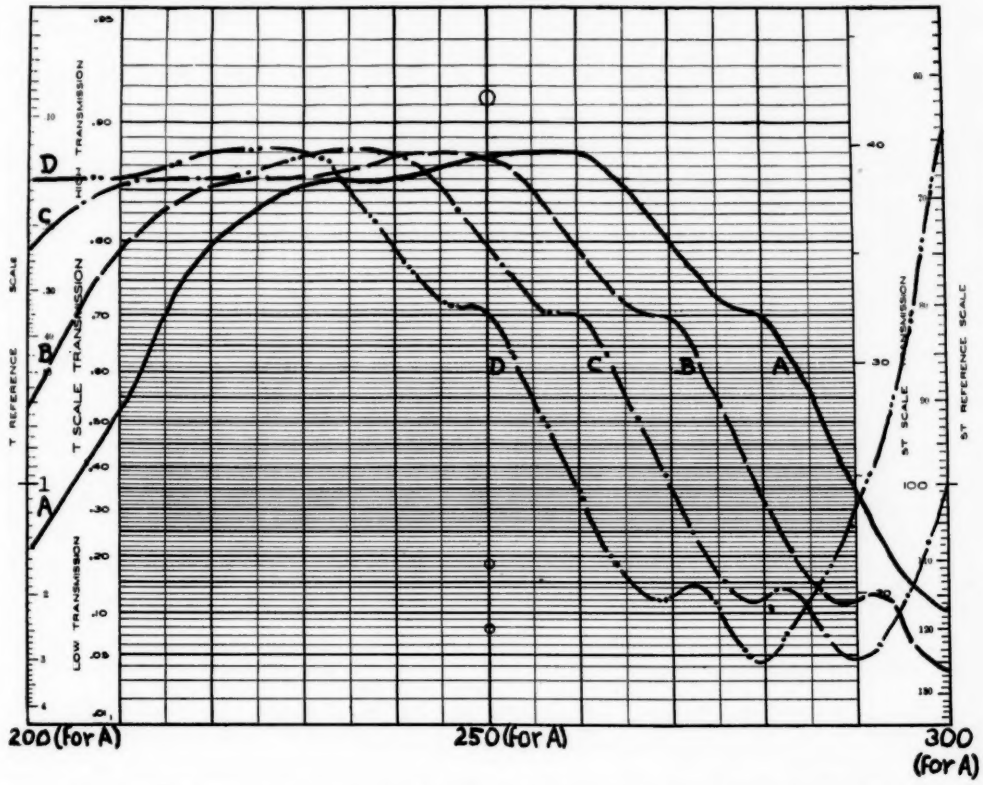

FIG. 2. Demonstration of progressive range-shifts of 1/10 octave. Curves *A*, *B*, *C*, and *D* cover, respectively, the octaves 200–300, 210–310, 220–320, and 230–330 c.r.u., curve *A* being the visual range from 375 to 750 millimicrons.

approximately 8 inches to the visual range is satisfactory for many color problems, much greater spread or magnification is required to reveal visually-significant differences between chromatic samples of certain classes such as scarlets, as has been pointed out by Park[5] and Godlove.[6] Such lateral magnification becomes, of course, increasingly necessary when magnifying ordinate scales are used.

Employing a wave-length or frequency scale, it seems inescapable that the provision of an adequate range of magnifications would entail an inconveniently large number of magnifications. In the case of wave-length, for example, if magnifications of 1 and 5 were provided for use near 12 microns, magnifications of 2 and 10 would be expected to be preferable near 6 microns, magnifications of 4 and 20 near 3 microns, etc. Near 400 millimicrons, magnifications of the order of 100 might be called for.

In the case of a logarithm-of-wave-length scale, however, it is probable that two or at the most three magnifications should suffice throughout a very wide spectral range. Experience gained in orienting studies involving magnifications of 1 and 5 suggests that these alone should be adequate in the great majority of tests.

A LOGARITHM-OF-WAVE-LENGTH SYSTEM OF ESPECIAL CONVENIENCE

A number of different logarithm-of-wave-length systems have been compared, the most attractive of which appears to be one (proposed in large part by Mr. O. W. Pineo[7]) which (a)

[5] R. H. Park, Am. Dyestuff Reporter **29**, 275 (1940).
[6] I. H. Godlove, J. Opt. Soc. Am. **30**, 656 (1940).

[7] Formerly associated with the Calco Chemical Division, American Cyanamid Company.

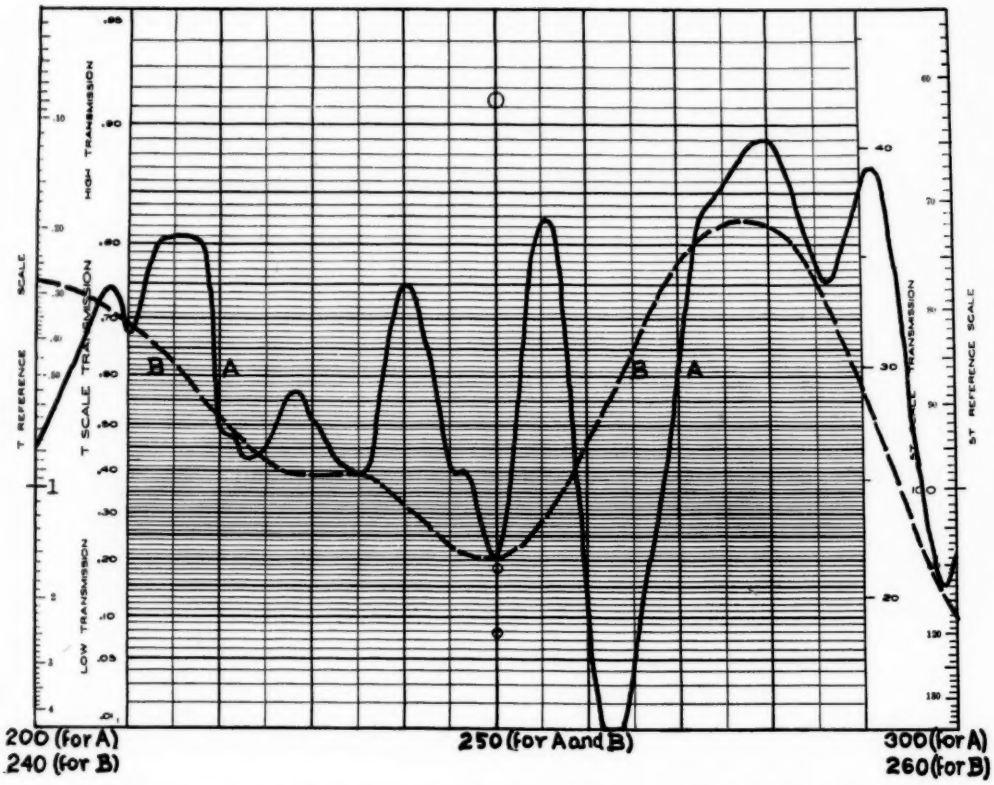

FIG. 3. Demonstration of different lateral magnifications. Curve *B*, magnified five times, corresponds to the 240–260 c.r.u. segment of the (unit-magnification) curve *A*.

emphasizes octave (factor-of-two) relationships, (b) ascribes an even octave to the visual range (375 to 750 millimicrons), (c) provides 100 units for each octave, and (d) requires small but positive logarithm characteristics (i.e., first digit or digits) throughout the range of optical spectrophotometry.

The particular system adopted in the instruments with which the writer is concerned satisfies all these requirements. The name "Octaval" has been used as a tentative designation of the abscissa scale employed, this name being suggestive of the system's utilization of octave relationships. (Webster's *Unabridged Dictionary* includes the word "octaval" as an adjective; under "octave" it includes the meaning of a general 2-to-1 relationship between physical quantities.)

The octaval unit, unlike wave-length and frequency units, is, of course, a pure number. Since, however, a name is required for clarity in discussion, the term "constant resolution unit" (c.r.u.) has been used, this term alluding to the fact that, with a logarithm-of-wave-length system, a fixed slit width implies constant resolution.

The octaval scale is defined such that the following relatively simple correspondence obtains:

Octaval (c.r.u.)	Wave-length	Octaval (c.r.u.)	Wave-length
100	1875 A	600	6 μ
200	375 mμ	700	12 μ
300	750 mμ	800	24 μ
400	1.5 μ	900	48 μ
500	3 μ	1000	96 μ

This arbitrarily-selected correspondence requires the explicit definition:

$$\text{Octaval (c.r.u.)} = 332.19 \log_{10} \lambda(\text{m}\mu) - 655.07$$

which may be regarded as a transformation from:

$$\text{Octaval (c.r.u.)} = 100\left[\log_2 \frac{\lambda(\text{m}\mu)}{375\ \text{m}\mu} + 2\right]$$

where use of log-base-2 again recalls the octave property of the system.

Taking the visual range as 375 to 750 millimicrons is, of course, somewhat arbitrary, but appears to be in general accord with the limits referred to by a number of authorities on color. Certainly the range from 400 to 700 millimicrons is not adequate for a number of color problems, and even for purely analytical work on dyes—notably yellow, green, and blue dyes—it has been found that this range leaves many absorption peaks off-scale.

The ascribing of 100 logarithmic units to each spectral octave makes it immediately possible to adapt the range-shifting and magnification-changing to a decimal system. Thus it has been found very convenient to provide ranges, magnified and unmagnified, starting at each 1/10 octave, so that, in the interval from 375 to approximately 1200 millimicrons (200 to 370 c.r.u.), there are 8 (overlapping) unmagnified ranges, and 16 (overlapping) five-times-magnified ranges. If, on the other hand, one used a wave-length scale of conventional type, one would find it difficult if not impossible to obtain a satisfactory solution to the problem of dividing a range such as 375 to 750 millimicrons or 400 to 700 millimicrons into convenient, overlapping segments. Figures 2 and 3 illustrate the convenience of the 100-units-per-octave system in presenting curves in different ranges and at different magnifications.

Taking the visual range as 200 to 300 logarithmic units (instead of, say 400 to 500) is also arbitrary. However, inspection of the table included above suggests that it is probably as good a choice as any, particularly as it entails the same convenient number (3) of digits to the left of the decimal point for virtually the entire range of spectrophotometry.

APPLICATION

The "octaval" system as here described has been used for some time on several spectrophotometers. An abscissa interval of 19 cm has been used for each octave, because it was found that this is the greatest interval which still leaves room for marginal notations and for binding in reports and folders, when standard $8\frac{1}{2}\times 11$-in. paper is used. It is a fortuitous convenience that Corning didymium filters of melt 512 discussed by Gibson[8] have perhaps their most valuable absorption peak at almost exactly 250 c.r.u., the center of the visual range octave. It is proposed to describe in a later paper the mechanisms mentioned above for shifting range and magnification.

[8] K. S. Gibson, J. Opt. Soc. Am. **31**, 462 (1941).

APRIL, 1942 J. O. S. A. VOLUME 32

A Spectrochemical Method for the Determination of Boron in Synthetic Mixtures of Soil Materials

R. Q. Parks[1]
Ohio Agricultural Experiment Station, Wooster, Ohio
(Received December 22, 1941)

DURING the progress of an investigation at the Ohio Agricultural Experiment Station, concerning the chemical precipitation of boron in soils, it became necessary to devise a rapid and accurate method for the determination of boron in the presence of large quantities of other elements. This report is a summary of studies made in the development of such a method.

[1] Now agent, U. S. Plant, Soil, and Nutrition Laboratory, Ithaca, New York. The author is indebted to Dr. J. D. Sayre of the United States Department of Agriculture, Bureau of Plant Industry, and to Dr. Wallace R. Brode of the Department of Chemistry, Ohio State University, for aid and suggestions during the course of this investigation.

REVIEW OF LITERATURE

Spectrochemical methods of analysis have been used for some time in the fields of metallurgy,

mineralogy, and chemistry, but their applications to biological and agricultural materials has taken place only within the past few years.

McHargue and co-workers,[2,3] have found it possible to determine by various spectrochemical techniques the mineral content of plant tissue, as have Brunstetter and Myers,[4] Wander and Brode,[5] and others. Spectrochemical analysis has also been applied to soils and fertilizers[6] and to soil minerals and rocks.[7,8]

MATERIALS

Solutions of salts containing silicon, aluminum, iron, calcium, magnesium, and phosphorus, and suspensions of electrodialyzed humus and bentonite were mixed, alone and in various combinations, with boric acid. Series of these mixtures were prepared and titrated to *p*H values ranging from 5.0 to 9.0. The spectrographic analysis of the resulting precipitates formed the basis for the present investigation. The results of boron fixation in these systems have been reported elsewhere.[9]

TABLE I. Efficiency of boron-free chemicals as buffers in spectrographic analysis for boron.

Material	Presence (+) and absence (0) of boron lines in spectrograms from samples with boron contents of: 1 p.p.m.	10 p.p.m.	100 p.p.m.
1. Sodium carbonate	0	0	0
2. Sodium oxalate	0	0	0
3. Barium carbonate	0	0	0
4. Lithium carbonate	0	0	0
5. Sodium acetate	0	0	+
6. Sodium bicarbonate	0	0	+
7. Sodium fluoride	0	0	+
8. Sodium bisulfite	0	0	+
9. Barium sulfate	0	0	+
10. Potassium salicylate	0	0	+
11. Bismuth oxide	0	+	+
12. Strontium carbonate	0	+	+
13. Stannous oxalate	0	+	+
14. Calcium carbonate	?	+	+

[2] J. S. McHargue, E. B. Offutt and W. S. Hodgkiss, Proc. Soil Sci. Soc. Am. **4**, 308 (1939).

[3] J. S. McHargue and R. K. Calfee, Ind. Eng. Chem. Analyt. Ed. **4**, 385 (1932).

[4] B. C. Brunstetter and A. T. Myers, J. Opt. Soc. Am. **31**, 163 (1941).

[5] I. W. Wander and Wallace R. Brode, J. Opt. Soc. Am. **31**, 402 (1941).

[6] L. W. Gaddum, L. L. Russoff and L. H. Rogers, J. Agr. Res. **55**, 731 (1937).

[7] A. Lacroix and A. de. Gramont, Bull. Soc. Franc. Min. **44**, 67 (1921).

[8] O. Ivan Lee and Thomas A. Wright, *Sixth Summer Conference on Spectroscopy and Its Applications* (John Wiley, 1939), p. 38.

[9] R. Q. Parks and B. T. Shaw, Proc. Soil Sci. Soc. Am. (in press).

APPARATUS

A Bausch and Lomb medium quartz spectrograph, logarithmic step sector, Eastman 33 spectrographic plates, and an Applied Research Laboratories projection comparator-densitometer[10] were used in this study.

The electrode system found most satisfactory from the standpoint of reproducibility consisted of an upper electrode of $\frac{1}{8}$-inch spectrographic carbon rod with flat ends, and a lower electrode of $\frac{1}{4}$-inch spectrographic carbon rod with a cup-shaped cavity in the end to hold the dry powdered sample. This cavity probably performed the dual function of holding a much larger charge of sample than the flat-ended electrode in common use with the a.c. arc, and of maintaining the sample on the electrode during arcing, to eliminate the complication of variable arcing to the bare electrode.

Unlike the d.c. arc, the 2200-volt a.c. arc caused no contamination from the boron occurring as an impurity in the standard grade spectrographic carbon rod electrodes as long as a charge of sample was maintained between the electrodes, and was therefore selected as the excitation source to be used. The voltage was varied slightly by means of an iron core transformer (Variac) for different samples, to produce a constant flow of 2.1 ± 0.05 amperes.

EXPERIMENTAL

Buffers

The addition of an appropriate buffer salt to the samples before arcing was necessary because of the small amount of sample available, and as a diluting agent to reduce the excitation effects of extraneous elements, since the extraneous elements varied in both number and quantity from sample to sample.

Of a large number of chemicals studied for possible use as buffers, many of those which had satisfactory physical properties were found to have high boron contents, interfering lines, or poor arcing properties.

Fourteen of the more promising of the chemicals found to be boron-free were selected and used as buffers in the preparation of samples containing

[10] Harry W. Dietert and John Schuch, J. Opt. Soc. Am. **31**, 54 (1941).

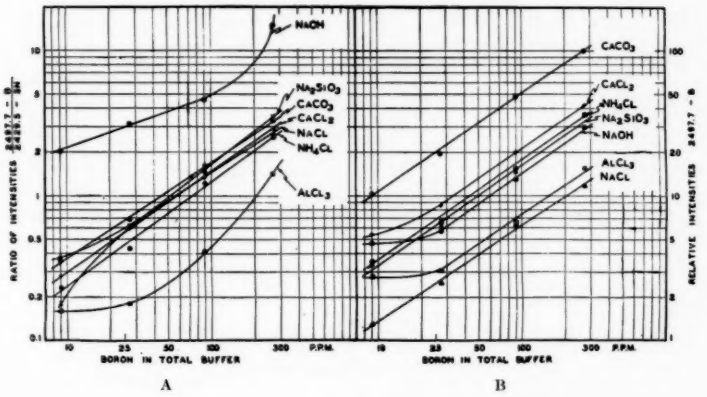

FIG. 1. The effect of extraneous ions on boron: tin intensity ratios and on boron line intensities.

1, 10, and 100 parts per million of boron as boric acid. Arcing was uniform at three 20-second exposures. The data recorded in Table I show that there are marked differences in the ease of detection of traces of boron in different chemicals. The inability to obtain boron lines from even the 100-p.p.m. boron samples of sodium and lithium carbonates, for example, might be attributed to scattering during arcing, and the maintaining of less than a complete charge of the material on the electrode. These particular salts were, however, among the best from the standpoints of steady arcing and remaining on the electrode throughout the arcing period. This is doubtless an evidence of atomic or ionic suppression of the excitation of the boron atoms—a phenomenon to be discussed in greater detail in a later part of this paper.

On the basis of the results recorded in Table I, calcium carbonate was selected as the buffer for use in succeeding phases of this investigation.

Plate Calibration and Internal Standard

All measured line densities were corrected to relative incident light intensities by means of logarithmic step sector plate calibration.[11]

Most procedures of spectrographic analysis require in the sample, in addition to the buffer salt and the element or elements to be measured, the presence of a reference element or internal standard.[12] By using the ratio of relative incident light intensities (from measured line densities) of the variable element and internal standard, instead of the line intensity of the element being measured, correction is made for variations in arcing conditions, length of exposure, and quantity of sample.

Brunstetter and Myers,[13] on the other hand, report the satisfactory determination of boron and other elements in plant tissue without the use of internal standards, buffers, or plate calibration by arcing samples to completion. It was not possible to use such techniques satisfactorily with the systems herein considered.

Some of the internal standards previously suggested for use in boron determinations are Au—2427.9A, Be—3130.4A, Cu—2492.1A, 2480.1A, Pb—2476.4A, Fe—2512.4A and Cu—2494.9A.

The tin lines at 2429.5A and 2495.7A were found to be more satisfactory as internal standards for boron analysis than any other lines of this element, or of lead, cadmium, zinc, calcium, or bismuth.

Extraneous Elements

Of all the obstacles met and now being overcome to place chemical spectroscopy on a firm basis in the various fields of analytical chemistry, the most disconcerting has probably been the effect of extraneous elements in enhancing or suppressing the intensities of lines of other elements being measured. So far as is known no system has as yet been devised which would make possible the prediction of the effect of one

[11] E. K. Jaycox and A. E. Ruehle, Ind. Eng. Chem. **12**, 195 (1940).
[12] O. S. Duffendack, R. A. Wolff and R. P. Smith, Ind. Eng. Chem. Anal. Ed. **7**, 419 (1935).
[13] B. C. Brunstetter, A. T. Myers, H. L. Wilkins and M. A. Hain, *Sixth Summer Conference on Spectroscopy and Its Applications* (John Wiley, 1939), p. 14.

TABLE II. The effect of extraneous ions on boron and tin line intensities.

$CaCO_3$+ 10 percent of	Relative intensities for 27 p.p.m. boron samples 2497.7-B	2429.5-Sn	B/Sn Ratio of intensities	Reduction in intensity 2497.7-B Percent	2429.5-Sn Percent
—	19.3	28.0	0.69	—	—
Na_2SiO_3	6.2	10.0	0.62	68	64
NaCl	2.5	4.1	0.61	87	85
$CaCl_2$	8.5	14.1	0.60	56	50
NH_4Cl	6.6	15.5	0.43	66	45
$AlCl_3$	3.1	17.3	0.18	84	38
NaOH	5.7	1.8	3.17	71	94

element upon the emission spectrum of any other element. Brode, *et al.*,[14,15] in a series of studies on this problem, report data on the effects of bismuth, tin, copper, iron, and other elements upon line densities and intensity ratios of line pairs. It was found that the effect could be negative or positive on either line, and that the effect on two lines of a given element was not necessarily the same. Critical concentration ranges were also noted, above or below which the effect of the extraneous element was constant. Duffendack, *et al.*[16] present data in concurrence with this observation, in showing that the effect of phosphorus upon densities of certain lines became constant above a minimum phosphorus concentration.

In another paper on this problem Brode and Hodge[17] report results of the first recorded investigation in which only anions were extraneous. The suppression of line intensities was correlated with the boiling point of the compound or its decomposition product. It was shown that this suppressing effect may be caused by the lower energy necessary to excite subhalide band spectra in comparison to that required for the lines being considered.

Hemmendinger,[18] in discussing mutual effects of iron and titanium on their intensity variations, suggested that interaction between ions of the elements during arcing was the casual mechanism.

[14] Wallace R. Brode and R. W. Silverthorn, *Sixth Summer Conference on Spectroscopy and Its Applications* (John Wiley, 1939), p. 60.
[15] Wallace R. Brode and Julia L. Appleton, *Seventh Summer Conference on Spectroscopy and Its Applications* (John Wiley, 1940), p. 36.
[16] O. S. Duffendack, K. B. Thompson, W. C. Lee and O. G. Koppius, J. Biol. Chem. **125**, 1 (1938).
[17] Wallace R. Brode and Edwin S. Hodge, J. Opt. Soc. Am. **31**, 58 (1941).
[18] Henry Hemmendinger, J. Opt. Soc. Am. **31**, 150 (1941).

In the light of this work, the possibility of using one set of boron standards for the different series of samples seemed remote. Each system contained different ions, and the precipitates of a given system at different *p*H values contained varying proportions of the ions added in the preparation of that system. Tests were therefore made to determine whether or not the ions present in the precipitates would, after dilution with the buffer salt, have effects on intensities and intensity ratios of the boron and tin lines being used. Seven sets of standards were prepared, each containing 0.02 percent tin and 9, 27, 90, and 270 p.p.m. of boron. One set was prepared with pure $CaCO_3$ as the buffer, the others consisted of 90 percent $CaCO_3$ and 10 percent of the extraneous compound. These extraneous compounds were $AlCl_3$, Na_2SiO_3, $CaCl_2$, NaCl, NaOH, and NH_4Cl. Arcing time was constant at three 30-second exposures. In all samples an excess of material remained in the cup after each 30-second exposure; the excess was removed before adding succeeding charges and completing the exposure.

The resulting working curves (Fig. 1A) show that the ratio of the line intensities of boron and tin was altered markedly by the NaOH and $AlCl_3$, but only slightly in the case of other materials. These latter five working curves are, however, definitely not interchangeable. This constancy of ratios with the addition of extraneous salts may be due to equal increases or

TABLE III. Data and calculations for a typical boron determination Si+Al+B, *p*H 9.0.

Sample	2497.7-B Galvanometer deflection	2497.7-B Relative intensity	2421.5-Sn Galvanometer deflection	2421.5-Sn Relative intensity	B/Sn Ratio of intensities	Boron in precipitate p.p.m.
Standard	40	47.5	86	12.8	3.71	200
Standard	35	54.5	81	15.0	3.63	200
Standard	62	25.5	88	12.2	2.09	66.7
Standard	56	30.3	84	13.8	2.20	66.7
Standard	84	13.8	84	13.8	1.00	16.7
Standard	80	15.5	80	15.5	1.00	16.7
Unknown	64	24.1	83	14.2	1.70	45
Unknown	57	29.5	76	17.2	1.72	46
Unknown	62	25.6	82	14.6	1.75	48
Unknown	63	25.0	81	15.0	1.67	43
Unknown	51	35.0	71	20.0	1.75	48
Unknown	62	25.6	81	15.0	1.71	46

Standard deviation of each of the six determinations is 1.9 p.p.m. boron or 4.1 percent.

decreases in line intensities of both boron and tin lines, or to no effect on either line of the pair. The boron line intensity was strongly reduced in all cases, however. Figure 1B shows the relationship between boron line intensities (omitting the internal standard relationship) and boron content of the several buffers. The lines are of approximately the same slope, linear above 27 p.p.m. boron, and indicate by their decrement below the $CaCO_3$ curve, the suppressing effect on boron line intensity of the respective salts.

It is immediately apparent from a study of Fig. 1 that the presence of extraneous ions also affected the tin line intensities, and not always in the same manner in which the boron line was modified. Na_2SiO_3, NaCl, and $CaCl_2$ caused a suppression approximately equal to that of the boron line. $AlCl_3$ and NH_4Cl reduced the boron line more than the tin line, while NaOH caused a far greater reduction in tin lines than in boron line intensities. Hence, the marked difference in working curves based on the intensity ratios, Fig. 1A. Table II contains the data for all samples containing 27 p.p.m. boron and illustrates the variation in effect on the tin and boron lines.

Attempts to correlate these suppressions with melting points and boiling points of the salts, and excitation potentials of the extraneous ions were fruitless. It is perhaps significant that sodium, with an excitation potential of only 5.1 volts[19] was extraneous in six of the seven instances of greatest suppression.

Separate working curves were therefore constructed for the determination of the boron content of the precipitate at each *p*H value, in each system. The exposure time required to give readable intensities varied with sample composition, from one to four 30-second exposures, with condensing lens and no sector. Typical working curves are reproduced in Fig. 2. The arrows (duplicate determinations) indicate the boron content of the precipitate specific to that particular working curve.

The data from which the second curve was obtained (Si+Al+B, *p*H 9.0), are reported in Table III. The last six exposures recorded were made on the unknown to give an estimate of the

[19] William F. Meggers, J. Opt. Soc. Am. **31**, 39 (1941).

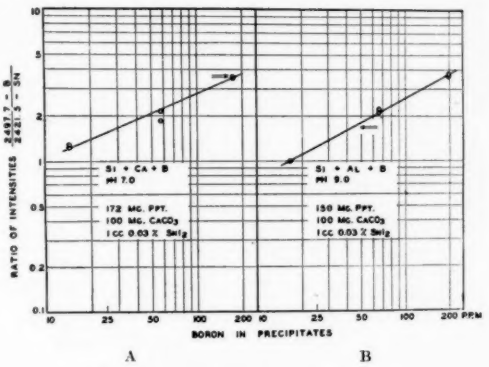

FIG. 2. Typical boron working curves.

reproducibility of the determinations, while the first six exposures in the table were of samples of known boron content, used in preparing the working curve. These data again illustrate the value of the internal standard in compensating for variations in arcing.

SUMMARY OF ANALYTICAL PROCEDURE

In the method of analysis adopted as a result of this study the sample (usually about a 50-mg precipitate) was mixed with 100 mg of calcium carbonate as buffer, and 1 cc 0.03 percent stannous chloride or iodide as internal standard. After drying, the powdered material was completely remixed. Three or four 30-second exposures with a 2200-volt a.c. arc were used for each sample; the electrode cup was refilled between exposures. A vertical separation of 1 mm between the electrodes (filled) was used. Three standards, identical in composition except for known variations in boron content, were prepared and arced in the same manner for each sample. Working curves were prepared by plotting boron contents of the standards against the ratio of intensities of the 2497.7A boron line and the 2429.5A tin line. Photographic line densities were corrected to relative incident light intensities by plate calibration curves made for each plate.

By the use of this method, it was possible to determine the boron contents of the systems studied with standard deviation of from 3 percent to 10 percent for single determinations.

Reflection Factors of Floor Materials

PARRY MOON
Massachusetts Institute of Technology, Cambridge, Massachusetts
(Received December 22, 1941)

IT seems to be universally assumed that floors are black, should be black, and always will be black (or almost black). Tests on carpets show that a reflection factor of 5 percent is high for these materials. Probably nothing can be done about carpets because of the difficulty in cleaning them, but floor tiles and linoleums—which could be much lighter without entailing undue cleaning bills—are usually chosen in the same somber colors because of innate conservatism. A theoretical study of interreflections in rooms[1] shows that a distinct improvement in lighting can be effected by increasing the reflection factor of the floor. The increased multiple reflections improve the level of illumination on the work, and the "quality" of the lighting is improved because of greater diffusion and reduced contrasts. The complaint is often made[2] that with an illumination of 500 lumens per square meter or more, the ceiling of an indirectly lighted room becomes glaring. But calculations seem to indicate that the trouble is in the low brightness of the walls and floor rather than the high brightness of the ceiling;[1] and these calculations show that with high reflection factors, conditions in an indirectly lighted room can be made to approach the highly desirable brightness variations found in nature.[3]

Thus it appears that the reflection factors of floor materials should be considered by the illuminating engineer. One-hundred twenty-nine samples of floor materials were obtained and were measured on the Hardy recording spectrophotometer at the Massachusetts Institute of Technology. The test procedure and method of computation were the same as used in previous work[4] and will not be described here. Representative spectrophotometric curves are shown in

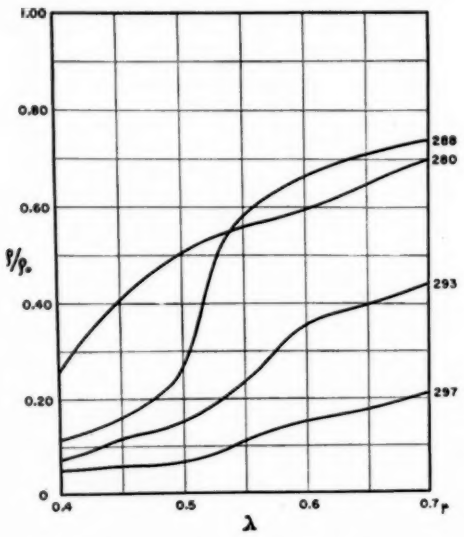

FIG. 1. Spectrophotometric curves for linoleums.

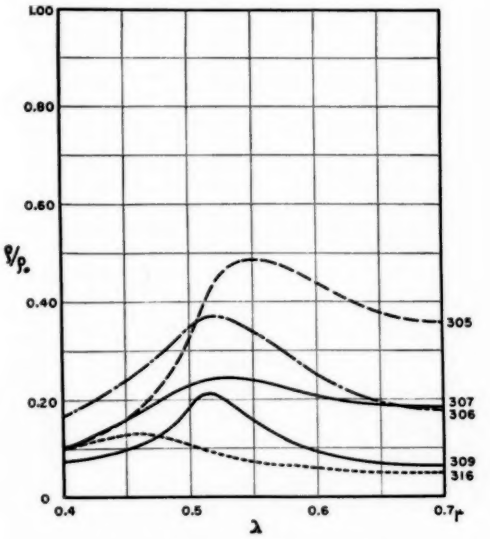

FIG. 2. Linoleums, green and blue.

[1] Parry Moon, "Interreflections in rooms," J. Opt. Soc. Am. **31**, 374 (1941).
[2] Ward Harrison, "What is wrong with our 50 foot-candle installations?" Trans. I.E.S. **32**, 208 (1937).
[3] H. L. Logan, "Specification points of brightness," Trans. I.E.S. **34**, 881 (1939).
[4] Parry Moon, "Optical reflection factors of acoustical materials," J. Opt. Soc. Am. **31**, 317 (1941); "Colors of ceramic tiles," J. Opt. Soc. Am. **31**, 482 (1941); "Wall materials and lighting," J. Opt. Soc. Am. **31**, 723 (1941).

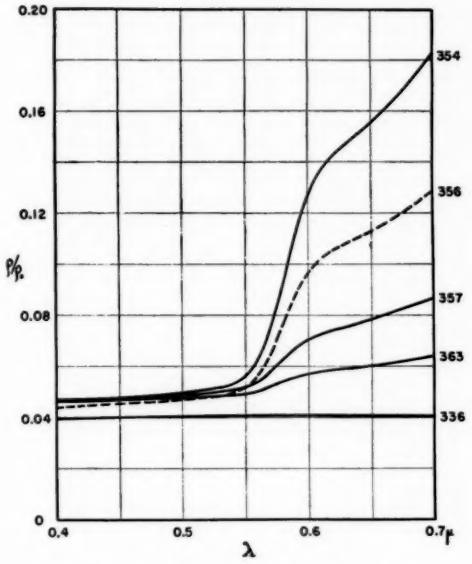

FIG. 3. Asphalt tiles, red and black.

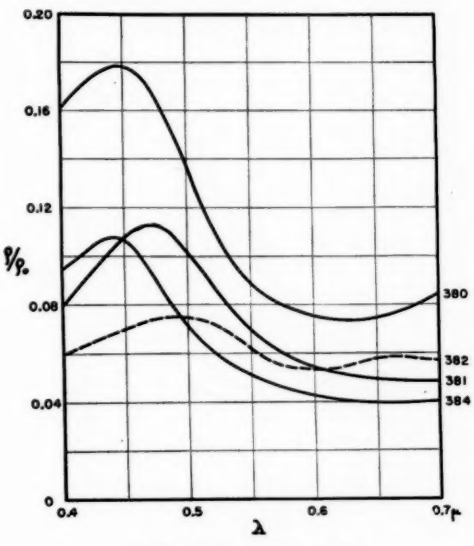

FIG. 4. Asphalt tiles, blue.

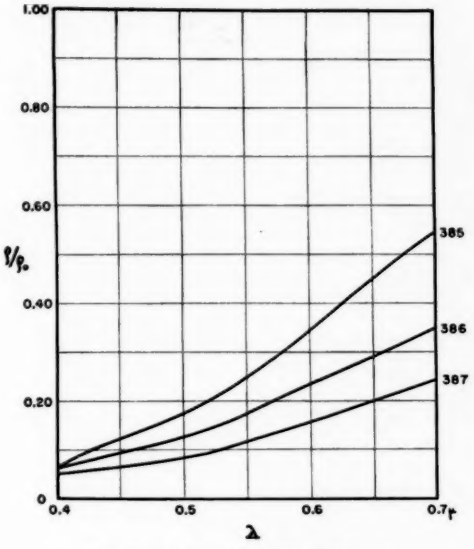

FIG. 5. Oak flooring, stained brown.

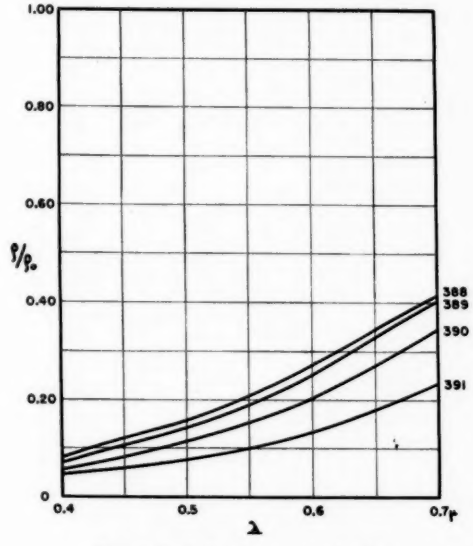

FIG. 6. Cork flooring, natural color.

Figs. 1 to 8. From these curves were computed[5] the reflection factors ρ and the trichromatic coefficients x and y for standard Illuminants A and C. The results are given in Table I.

One interesting result is the similarity of shape of the curves for cork (Fig. 6) and oak (Fig. 5). Various other woods[6] gave spectral curves of the

[5] The author gratefully acknowledges the help of the staff of the Color Measurements Laboratory (M.I.T.), the National Youth Administration, the manufacturers of floor materials, and the computers: Messrs. E. D. Benson, F. Carroll, L. E. Duval, J. M. Fiore, J. Margolskee, J. P. Reilly, D. L. Shapiro, N. A. Teixeira. and W. R. Thurston.

[6] Parry Moon, "Color determination," Trans. I.E.S. **36**, 313 (1941).

TABLE I. Reflection factors and trichromatic coefficients.

No.	Name	Mfgr.	Approx. color	A			C		
				x	y	ρ	x	y	ρ
	Linoleums								
280	No. 23	1	Ivory	0.4723	0.4169	0.563	0.3413	0.3522	0.550
281	No. 24	1	Lt. gray	0.4577	0.4125	0.273	0.3228	0.3324	0.271
282	No. 1123 Sealex	10	Gray	0.4643	0.4220	0.264	0.3356	0.3508	0.258
283	No. 106	26	Gray	0.4641	0.4143	0.146	0.3305	0.3391	0.143
284	No. 1003 Sealex	10	Gray	0.4662	0.4113	0.122	0.3310	0.3352	0.120
285	No. 115	26	Black	0.4450	0.4072	0.0452	0.3068	0.3138	0.0457
286	No. 1005 Sealex	10	Black	0.4450	0.4066	0.0417	0.3068	0.3131	0.0421
287	No. 1113 Sealex	10	Lt. yellow	0.4653	0.4243	0.629	0.3385	0.3594	0.622
288	No. 1110 Sealex	10	Yellow	0.5145	0.4361	0.579	0.4176	0.4244	0.538
289	No. 136	26	Yellow	0.5203	0.4351	0.482	0.4262	0.4289	0.445
290	No. 1126 Sealex	10	Orange	0.6071	0.3634	0.245	0.5244	0.3523	0.190
291	No. 1129 Sealex	10	Orange	0.5784	0.3801	0.222	0.4786	0.3622	0.183
292	No. 135	26	Orange	0.5987	0.3712	0.219	0.5145	0.3656	0.175
293	No. 1130 Sealex	10	Lt. brown	0.5251	0.4117	0.280	0.4121	0.3814	0.254
294	No. 1127 Sealex	10	Red	0.6225	0.3410	0.162	0.5241	0.3214	0.121
295	No. 39	1	Red	0.6130	0.3468	0.144	0.5116	0.3256	0.110
296	No. 100	26	Brown	0.5354	0.4032	0.135	0.4234	0.3712	0.120
297	No. 1000 Sealex	10	Brown	0.5201	0.4114	0.125	0.4019	0.3736	0.115
298	No. 122	26	Red	0.5598	0.3753	0.105	0.4355	0.3365	0.0897
299	No. 1002 Sealex	10	Dk. red	0.5621	0.3746	0.101	0.4352	0.3370	0.0862
300	No. 123	26	Red	0.5893	0.3498	0.101	0.4585	0.3165	0.0822
301	No. 1118 Sealex	10	Chocolate	0.5241	0.4023	0.0980	0.4024	0.3586	0.0889
302	No. 1122 Sealex	10	Dk. red	0.5814	0.3589	0.0953	0.4566	0.3253	0.0792
303	Mastipave 664	26	Dk. brown	0.4842	0.4102	0.0656	0.3513	0.3441	0.0631
304	No. 1004 Sealex	10	Dk. red	0.4835	0.4020	0.0623	0.3461	0.3293	0.0600
305	No. 1124 Sealex	10	Lt. green	0.4724	0.4538	0.434	0.3668	0.4239	0.429
306	No. 44	1	Lt. green	0.4196	0.4417	0.292	0.2967	0.3605	0.305
307	No. 111	26	Green	0.4404	0.4394	0.222	0.3194	0.3639	0.220
308	No. 1119 Sealex	10	Green	0.4395	0.4449	0.169	0.3197	0.3730	0.174
309	No. 1128 Sealex	10	Green	0.3893	0.4653	0.127	0.2750	0.3819	0.139
310	No. 110	26	Dk. green	0.4117	0.4457	0.0751	0.2944	0.3478	0.0750
311	No. 1120 Sealex	10	Dk. green	0.4165	0.4473	0.0731	0.2973	0.3592	0.0757
312	No. 1001 Sealex	10	Dk. green	0.4244	0.4284	0.0683	0.2965	0.3390	0.0709
313	No. 1125 Sealex	10	Blue	0.3331	0.3550	0.0969	0.2136	0.2229	0.113
314	No. 1116 Sealex	10	Dk. blue	0.3877	0.3970	0.0738	0.2544	0.2816	0.0799
315	No. 1114 Sealex	10	Dk. blue	0.3965	0.3841	0.0731	0.2584	0.2652	0.0781
316	No. 29	1	Dk. blue	0.3780	0.3823	0.0687	0.2472	0.2557	0.0744
317	No. 1131 Sealex	10	Dk. blue	0.3975	0.3851	0.0490	0.2596	0.2658	0.0522
318	No. 47	1	Eggplant	0.4819	0.3921	0.0681	0.3369	0.3139	0.0651
	Asphalt tiles								
319	Flexachrome F-4	29	Lt. gray	0.4456	0.4097	0.593	0.3089	0.3198	0.596
320	White 132	17	Gray	0.4751	0.4178	0.310	0.3454	0.3540	0.301
321	Azrock C-6	31	Gray	0.4745	0.4216	0.253	0.3464	0.3604	0.248
322	Flexachrome F-3	29	Gray	0.4440	0.4077	0.245	0.3068	0.3142	0.246
323	No. 266 asphalt tile	1	Gray	0.4674	0.4197	0.221	0.3373	0.3510	0.216
324	Tile-Tex 52	29	Gray	0.4682	0.4189	0.196	0.3384	0.3497	0.192
325	Dove gray 125	17	Gray	0.4731	0.4182	0.164	0.3423	0.3523	0.163
326	Pearl gray, No. 24	15	Gray	0.4527	0.4190	0.150	0.3199	0.3403	0.150
327	Flexachrome F-14	29	Gray	0.4123	0.4037	0.127	0.2781	0.2921	0.132
328	Azrock C-94	31	Gray	0.4631	0.4164	0.117	0.3304	0.3427	0.116
329	Flexachrome F-2	29	Gray	0.4421	0.4057	0.107	0.3041	0.3099	0.108
330	Tile-Tex 46	29	Gray	0.4679	0.4161	0.0850	0.3359	0.3442	0.0832
331	French gray, No. 14	15	Dk. gray	0.4613	0.4156	0.0821	0.3284	0.3383	0.0811
332	Dark gray, No. 6	15	Dk. gray	0.4597	0.4113	0.0582	0.3257	0.3284	0.0572
333	Black, No. 1	15	Black	0.4510	0.4089	0.0492	0.3139	0.3204	0.0492
334	Flexachrome F-1	29	Black	0.4455	0.4066	0.0452	0.3073	0.3131	0.0453
335	Azrock C-1	31	Black	0.4476	0.4079	0.0445	0.3099	0.3164	0.0445
336	Tile-Tex 41	29	Black	0.4475	0.4076	0.0396	0.3100	0.3165	0.0396
337	Flexachrome F-15	29	Cream	0.4796	0.4262	0.595	0.3576	0.3701	0.575
338	Flexachrome F-8	29	Yellow	0.4994	0.4485	0.472	0.4014	0.4405	0.450
339	No. 270 asphalt tile	1	Cream	0.4807	0.4250	0.483	0.3562	0.3729	0.469
340	Azrock C-90	31	Cream	0.4766	0.4214	0.427	0.3496	0.3626	0.414
341	Azrock C-92	31	Tan	0.5016	0.4216	0.342	0.3834	0.3813	0.324
342	Buff, No. 21	15	Buff	0.5330	0.4119	0.187	0.4251	0.3892	0.168
343	No. 247 asphalt tile	1	Brown	0.5305	0.4109	0.165	0.4234	0.3813	0.147
344	Azrock C-11	31	Brown	0.5236	0.4167	0.154	0.4200	0.3952	0.141
345	Flexachrome F-7	29	Red	0.5404	0.3843	0.148	0.4130	0.3390	0.131
346	Tile-Tex 43	29	Brown	0.5413	0.4011	0.144	0.4306	0.3742	0.127
347	Tan, No. 11	15	Brown	0.5358	0.4004	0.117	0.4183	0.3670	0.105
348	Azrock C-9	31	Brown	0.5055	0.4169	0.114	0.3859	0.3726	0.107
349	Azrock C-8	31	Red	0.5509	0.3806	0.114	0.4238	0.3402	0.0997
350	Terra cotta, No. 12	15	Red	0.5513	0.3818	0.112	0.4276	0.3423	0.0972
351	Flexachrome F-6	29	Red	0.5904	0.3510	0.109	0.4622	0.3225	0.0879
352	Rose taupe, No. 22	15	Brown	0.5010	0.4032	0.103	0.3680	0.3443	0.0967
353	Tile-Tex 51	29	Dk. red	0.5486	0.3811	0.0887	0.4202	0.3406	0.0775
354	Toledo red 109	17	Dk. red	0.5391	0.3863	0.0872	0.4143	0.3380	0.0766
355	Flexachrome F-5	29	Dk. brown	0.4992	0.4046	0.0838	0.3675	0.3451	0.0785
356	Tile-Tex 42	29	Dk. red	0.5222	0.3904	0.0718	0.3949	0.3358	0.0648
357	Red, No. 3	15	Dk. red	0.4876	0.4001	0.0598	0.3492	0.3292	0.0569
358	Azrock C-3	31	Dk. red	0.4840	0.4007	0.0589	0.3455	0.3268	0.0563
359	Tile-Tex 45	29	Dk. red	0.4996	0.3976	0.0588	0.3630	0.3332	0.0550
360	Brown, No. 4	15	Dk. brown	0.4752	0.4112	0.0579	0.3408	0.3396	0.0562
361	Azrock C-4	31	Dk. brown	0.4677	0.4120	0.0560	0.3328	0.3356	0.0550
362	Azrock C-5	31	Dk. brown	0.4546	0.4165	0.0534	0.3213	0.3346	0.0533
363	Mahogany, No. 2	15	Dk. red	0.4671	0.4057	0.0520	0.3290	0.3240	0.0508
364	Quarry red, 106	17	Dk. red	0.4740	0.4023	0.0499	0.3346	0.3228	0.0484
365	Azrock C-2	31	Dk. brown	0.4685	0.4039	0.0489	0.3289	0.3230	0.0478
366	No. 257 asphalt tile	1	Green	0.4387	0.4457	0.150	0.3136	0.3844	0.155
367	Flexachrome F-9	29	Green	0.4050	0.4565	0.146	0.2878	0.3820	0.157
368	Azrock C-7	31	Green	0.4482	0.4506	0.134	0.3284	0.3904	0.136

TABLE I.—*Continued.*

No.	Name	Mfgr.	Approx. color	A x	A y	A ρ	C x	C y	C ρ
	Asphalt tiles (*Continued*)								
369	Flexachrome F-10	29	Green	0.3875	0.4406	0.122	0.2680	0.3356	0.132
370	Flexachrome F-11	29	Green	0.3876	0.4430	0.102	0.2674	0.3501	0.123
371	Tile-Tex 50	29	Green	0.4172	0.4539	0.101	0.3010	0.3732	0.105
372	Emerald green, No. 23	15	Green	0.4260	0.4449	0.0899	0.3026	0.3694	0.0942
373	Azrock C-93	31	Dk. green	0.4376	0.4277	0.0741	0.3067	0.3478	0.0759
374	Olive green, No. 5	15	Dk. green	0.4621	0.4214	0.0622	0.3321	0.3481	0.0615
375	Tile-Tex 44	29	Dk. green	0.4364	0.4281	0.0565	0.3080	0.3439	0.0577
376	Ivy green, No. 13	15	Dk. green	0.4507	0.4236	0.0558	0.3208	0.3442	0.0561
377	No. 235 asphalt tile	1	Blue	0.3934	0.4080	0.112	0.2601	0.3012	0.121
378	Light blue, No. 32	15	Blue	0.3991	0.4153	0.112	0.2676	0.3122	0.121
379	Azrock C-91	31	Dk. blue	0.3995	0.3955	0.0877	0.2619	0.2859	0.0941
380	Flexachrome F-13	29	Dk. blue	0.3800	0.3704	0.0861	0.2450	0.2416	0.0929
381	Azrock C-10	31	Dk. blue	0.3806	0.3963	0.0650	0.2516	0.2720	0.0697
382	Dark blue, No. 31	15	Dk. blue	0.4214	0.4064	0.0582	0.2841	0.3057	0.0607
383	Tile-Tex 53	29	Dk. blue	0.3950	0.4031	0.0570	0.2636	0.2864	0.0606
384	Flexachrome F-12	29	Dk. blue	0.3777	0.3676	0.0482	0.2441	0.2353	0.0520
	Wood, cork, and rubber								
385	Bruce block, white oak, light	4	Brown	0.5228	0.4102	0.288	0.4074	0.3790	0.262
386	Bruce block, white oak, medium	4	Dk. brown	0.5158	0.4113	0.198	0.3968	0.3749	0.183
387	Bruce block, white oak, dark	4	Dk. brown	0.5172	0.4076	0.131	0.3951	0.3682	0.121
388	Cork carpet 300	26	Natural	0.5098	0.4103	0.233	0.3837	0.3693	0.216
389	Kencork	17	Natural	0.5142	0.4095	0.216	0.3922	0.3706	0.200
390	Cork tile, light	1	Natural	0.5155	0.4098	0.176	0.3944	0.3733	0.163
391	Cork tile, medium	1	Natural	0.5142	0.4069	0.114	0.3888	0.3660	0.105
392	Cork carpet 310	26	Dk. green	0.4216	0.4431	0.0849	0.3000	0.3649	0.0891
393	Rubber tile 510, quaker gray	1	Gray	0.4644	0.4146	0.318	0.3308	0.3414	0.313
394	Rubber tile 531, white	1	Cream	0.4665	0.4158	0.537	0.3334	0.3450	0.527
395	Rubber tile 538, topaz	1	Buff	0.5271	0.4206	0.280	0.4262	0.3994	0.252
396	Rubber tile 576, robin's egg	1	Bl. green	0.4261	0.4227	0.195	0.2941	0.3302	0.202
	Carpets								
397	No. 1142	3	Tan	0.5028	0.4069	0.119	0.3752	0.3588	0.112
398	No. 3433	3	Red	0.5544	0.3681	0.0750	0.4132	0.3279	0.0652
399	No. 1104	3	Dk. brown	0.5255	0.3956	0.0322	0.3956	0.3549	0.0292
400	No. 3386	3	Dk. red	0.6141	0.3360	0.0271	0.4927	0.3082	0.0207
401	No. 867	3	Dk. red	0.5332	0.3618	0.0148	0.3730	0.2971	0.0131
402	No. 841	3	Dk. red	0.4884	0.3900	0.0116	0.3444	0.3178	0.0110
403	No. 9970	3	Green	0.3911	0.4222	0.0532	0.2640	0.3202	0.0572
404	No. 7717	3	Green	0.4302	0.4295	0.0363	0.3007	0.3503	0.0375
405	No. 9971	3	Dk. green	0.4293	0.4330	0.0186	0.3015	0.3564	0.0193
406	No. 2239	3	Blue	0.4033	0.4089	0.0578	0.2702	0.3033	0.0611
407	No. 2241	3	Blue	0.3766	0.3814	0.0340	0.2442	0.2577	0.0371
408	No. 202	3	Dk. blue	0.3738	0.3806	0.0143	0.2421	0.2568	0.0157

same shape. Another result is the surprisingly low reflection factors of carpets. Black linoleum (No. 285) had a reflection factor of 0.045, black asphalt tiles ranged from 0.049 to 0.040, but a dark-red carpet (No. 402) gave 0.011 and a dark-blue (No. 408) 0.014. A similar result was obtained in the measurement of men's clothing,[7] where blue serge was found to reflect only about one percent, while a medium brown gave only four percent. It is easy to attribute this result to an absence of specular reflection but this explanation does not alter the fact that the materials *appear* to be much better reflectors than they are. No. 402, for instance, is certainly not black, and most trained observers would probably estimate a reflection factor of ten percent.

TABLE II. Effect of floor materials on room lighting.

No.	Description	ρ	Work $\frac{E_{hl}}{L_{o2}}$	Ceiling $\frac{L_2}{L_{o2}}$	Floor $\frac{L_3}{L_{o2}}$	Floor $\frac{L_A}{L_3}$
319	Asphalt tile, lt. gray	0.593	0.94	1.27	0.50	1.5
394	Rubber tile, cream	0.537	0.92	1.24	0.45	1.6
340	Asphalt tile, cream	0.427	0.88	1.18	0.34	2.1
393	Rubber tile, gray	0.318	0.84	1.13	0.25	2.7
282	Linoleum, gray	0.264	0.82	1.10	0.20	3.3
386	Oak flooring, brown	0.198	0.80	1.07	0.15	4.3
372	Asphalt tile, green	0.0899	0.77	1.03	0.065	9.4
332	Asphalt tile, dk. gray	0.0582	0.76	1.02	0.042	14.4

Indirectly lighted room, white ceiling ($\rho_2 = 0.80$), black walls ($\rho_1 = 0$), length and width equal to 5 times the ceiling height.

In small rooms, the reflection factor of the floor has relatively little effect on the lighting of the room,[1] though a dark material may introduce an unpleasantly large contrast. With large rooms having relatively low ceilings, however, the floor becomes an important element in lighting.

Table II shows the effect of using representative floor materials in an office whose length and breadth are five times the ceiling height. The room is indirectly lighted with incandescent lamps, the ceiling is white ($\rho_2 = 0.80$), and the walls are assumed to be almost entirely windows, so their reflection factor can be neglected. Fig. 9 of reference 1 was used in obtaining the calculated values. The fourth column gives the illumi-

[7] Parry Moon and M. S. Cettei, "On the reflection factor of clothing," J. Opt. Soc. Am. **28**, 277 (1938).

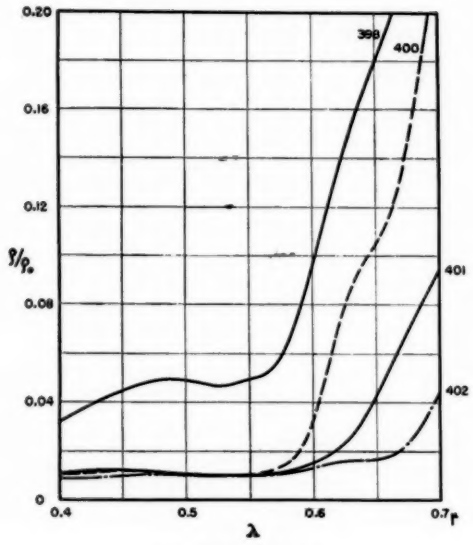

FIG. 7. Carpets, red.

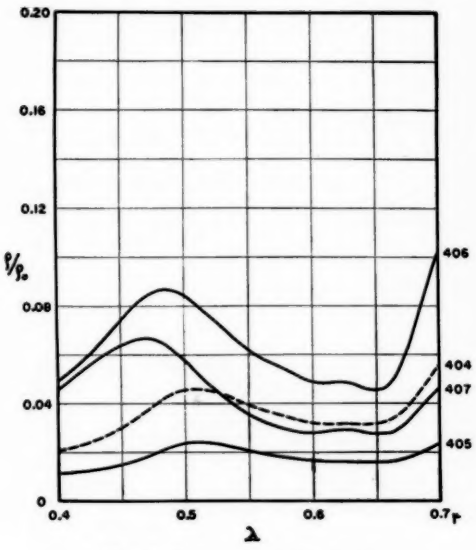

FIG. 8. Carpets, blue and green.

nation of the work, which is assumed to be in a horizontal position on a desk. The data show that if the floor is changed from a dark gray tile to a light gray tile, the lighting system can be reduced about 20 percent, the illumination being the same in both cases.

Column 5 of Table II shows that, for a given lighting system, as the reflection factor of the floor is increased, the luminosity of the ceiling increases. Column 6 gives the luminosity of the floor, while the last column gives the ratio of adapting luminosity to floor luminosity. L_A is the luminosity to which the fovea is adapted when the observer looks at a piece of white paper ($\rho = 0.80$) on the desk. The ceiling of the room is found to be somewhat brighter than the paper, the luminosity ratio (L_2/L_A) being 1.69 for all the materials of Table II. The floor, however, is found to be darker than the paper in all cases, the ratio (L_A/L_3) being 1.5 in the best condition, and 14.4 in the worst. Any of the floor that happens to be in the field of vision of the observer will be unpleasantly dark for floors having reflection factors below approximately 0.30.

The foregoing analysis indicates that in large offices and drafting rooms, some saving can be effected in the lighting system by using floor materials with reasonably high reflection factors. But the principal advantage in the use of such materials is the improved visual conditions resulting from reduced contrasts and the increased cheerfulness in the appearance of the room. The numerical analysis would be more striking with a larger room, such as those sometimes used in windowless factories, or in a room with walls of high reflection factor.

Reflection Factors of Some Materials Used in School Rooms

PARRY MOON
Massachusetts Institute of Technology, Cambridge, Massachusetts
(Received December 22, 1941)

IN a previous paper,[1] results were given for the reflection factors and chromaticities of various materials. The present report gives values obtained in a similar manner on school chalkboards of various kinds, wall and ceiling paints, venetian blinds and window shades. The samples were tested by means of the Hardy spectrophotometer at Massachusetts Institute of Technology.[2] From these curves, the total reflection factors and trichromatic coefficients were obtained by computation. Both standard Illuminant *A* and *C* were used in these calculations to show the effect of changing from incandescent light (Illuminant *A*) to daylight or "daylight" fluorescent lamps (approximated by Illuminant *C*).

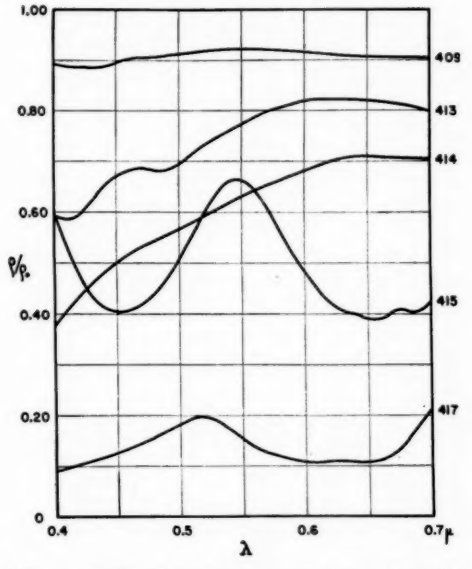

FIG. 1. Spectrophotometric curves for school chalkboards. Curves for white, cream, and green boards are shown. The black boards were almost perfectly nonselective, so their curves are not given.

The general method of test, computation, and check has been described previously[1] and these

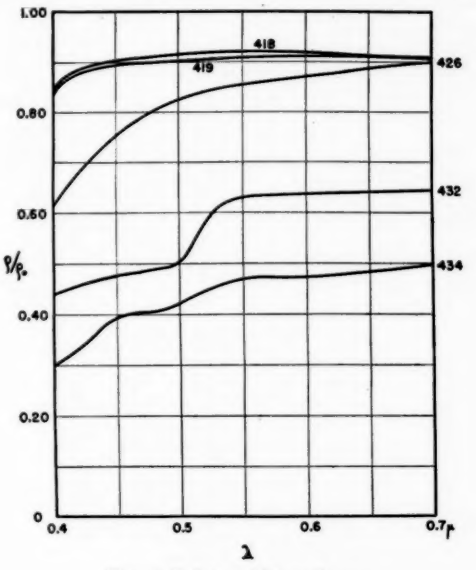

FIG. 2. Paints, white and gray.

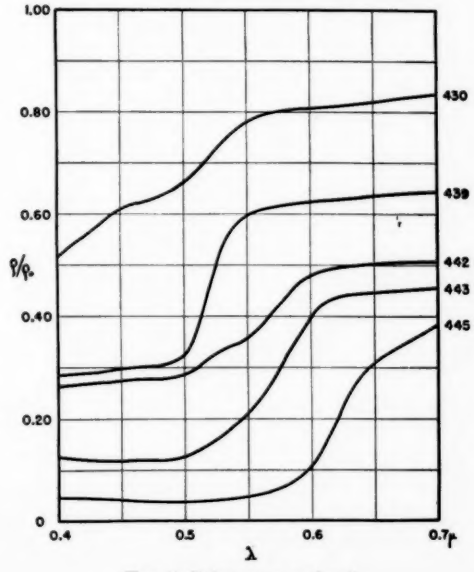

FIG. 3. Paints, tan and red.

[1] Parry Moon, "Optical reflection factors of acoustical materials," J. Opt. Soc. Am. **31**, 317 (1941).

[2] The author gratefully acknowledges the assistance of the manufacturers, the National Youth Administration, the M.I.T. Color Measurements Laboratory, and the computers: Messrs. E. D. Benson, F. Carroll, L. E. Duval, J. M. Fiore, J. Margolskee, J. P. Reilly, D. L. Shapiro, N. A. Teixeira, and W. R. Thurston.

TABLE I. Reflection factors and trichromatic coefficients.

No.	Name	Mfgr.	Approx. color	A x	A y	A ρ	C x	C y	C ρ
	Chalkboards								
409	Vitrolite, white	18	White	0.4478	0.4093	0.906	0.3111	0.3196	0.899
410	Nucite, black	27	Black	0.4463	0.4073	0.0739	0.3085	0.3152	0.0743
411	Vitrolite, black	18	Black	0.4429	0.4050	0.0660	0.3042	0.3089	0.0666
412	Slate	24	Black	0.4424	0.4067	0.0627	0.3046	0.3119	0.0633
413	Vitrolite, cream	18	Cream	0.4620	0.4118	0.768	0.3284	0.3338	0.757
414	Nucite, cream	27	Cream	0.4697	0.4141	0.633	0.3369	0.3426	0.621
415	Vitrolite, green	18	Lt. green	0.4322	0.4428	0.540	0.3120	0.3622	0.554
416	Carrara, jade	27	Lt. green	0.4289	0.4469	0.481	0.3097	0.3659	0.495
417	Nucite, green	27	Green	0.4111	0.4348	0.133	0.2827	0.3478	0.142
	Paints								
418	No. 22141, Save-lite gloss	28	White	0.4482	0.4087	0.901	0.3112	0.3190	0.901
419	No. 22138, Save-lite eggshell	28	White	0.4487	0.4084	0.892	0.3115	0.3186	0.891
420	No. 15185, Flat-tone white	28	White	0.4529	0.4108	0.890	0.3168	0.3257	0.886
421	No. 19177, Save-lite eggshell	28	White	0.4490	0.4093	0.881	0.3120	0.3211	0.881
422	Flat wall No. 4	26	White	0.4540	0.4118	0.873	0.3185	0.3280	0.870
423	No. 22128, Save-lite gloss	28	White	0.4495	0.4093	0.869	0.3125	0.3214	0.868
424	No. 22109, Save-lite gloss	28	White	0.4512	0.4102	0.845	0.3146	0.3241	0.843
425	Flat wall No. 2	26	White	0.4567	0.4130	0.845	0.3222	0.3322	0.839
426	No. 16270, Semi-luster	28	White	0.4566	0.4126	0.844	0.3215	0.3315	0.837
427	Ext. enamel No. 1	26	White	0.4527	0.4142	0.802	0.3186	0.3315	0.800
428	Exterior No. 3	26	Ivory	0.4682	0.4179	0.787	0.3371	0.3491	0.774
429	Semi-luster, ivory white	28	Ivory	0.4784	0.4222	0.772	0.3523	0.3618	0.746
430	Flat-tone, ivory	28	Ivory	0.4666	0.4162	0.767	0.3348	0.3428	0.750
431	Flat-tone, caen stone	28	Ivory	0.4717	0.4154	0.761	0.3402	0.3444	0.741
432	Flat-tone, cream gray	28	Lt. gray	0.4666	0.4173	0.609	0.3350	0.3448	0.598
433	Semi-luster, silver gray	28	Lt. gray	0.4606	0.4150	0.459	0.3272	0.3380	0.453
434	Flat-tone, silver gray	28	Gray	0.4599	0.4162	0.433	0.3273	0.3372	0.428
435	Flat-tone, cream	28	Cream	0.4827	0.4232	0.732	0.3589	0.3657	0.703
436	Semi-luster, cream	28	Cream	0.4775	0.4226	0.695	0.3514	0.3625	0.673
437	Semi-luster, cream gray	28	Cream	0.4720	0.4182	0.641	0.3420	0.3506	0.624
438	Flat-tone, buff	28	Buff	0.5071	0.4237	0.582	0.3957	0.3865	0.540
439	Flat-tone, ivory tan	28	Tan	0.4911	0.4282	0.567	0.3743	0.3814	0.539
440	Semi-luster, buff	28	Buff	0.5100	0.4153	0.549	0.3922	0.3745	0.508
441	Semi-luster, taupe	28	Cream	0.4785	0.4110	0.532	0.3455	0.3427	0.513
442	Flat-tone, rose tan	28	Tan	0.4948	0.4076	0.400	0.3645	0.3456	0.375
443	Flat-tone, terra cotta	28	Tan	0.5431	0.3988	0.285	0.4308	0.3684	0.249
444	Flat-tone, cinnamon brown	28	Brown	0.5222	0.4013	0.126	0.3988	0.3564	0.114
445	Flat-tone, burgundy	28	Dk. red	0.5943	0.3514	0.0922	0.4667	0.3232	0.0742
446	Flat-tone, blossom pink	28	Pink	0.4842	0.4106	0.734	0.3530	0.3433	0.699
447	Semi-luster, peach	28	Pink	0.5102	0.4099	0.680	0.3878	0.3615	0.627
448	Flat-tone, warm beiege	28	Pink	0.4806	0.4161	0.578	0.3512	0.3514	0.556
449	Flat-tone, coral rose	28	Pink	0.5068	0.4066	0.410	0.3797	0.3545	0.379
450	Flat-tone, thistle	28	Dk. pink	0.4982	0.3948	0.242	0.3585	0.3266	0.226
451	Flat-tone, canary yellow	28	Yellow	0.4867	0.4261	0.729	0.3660	0.3756	0.698
452	Semi-luster, canary yellow	28	Yellow	0.4873	0.4269	0.719	0.3669	0.3782	0.690
453	Semi-luster, nile green	28	Lt. green	0.4531	0.4323	0.651	0.3271	0.3650	0.654
454	Flat-tone, lt. green	28	Lt. green	0.4563	0.4337	0.610	0.3334	0.3665	0.607
455	Semi-luster, pale green	28	Lt. green	0.4471	0.4420	0.580	0.3263	0.3796	0.586
456	Flat-tone, pale jade	28	Lt. green	0.4414	0.4355	0.501	0.3157	0.3625	0.510
457	Flat-tone, laurel green	28	Green	0.4407	0.4478	0.464	0.3236	0.3812	0.471
458	Flat-tone, cactus green	28	Green	0.4476	0.4281	0.367	0.3209	0.3503	0.368
459	Semi-luster, mist blue	28	Lt. blue	0.4214	0.4181	0.605	0.2899	0.3222	0.628
460	Flat-tone, light blue	28	Lt. blue	0.4269	0.4177	0.596	0.2946	0.3236	0.614
461	Semi-luster, vogue blue	28	Lt. blue	0.4135	0.4068	0.427	0.2792	0.2999	0.445
462	Flat-tone, delft	28	Blue	0.3625	0.3724	0.104	0.2356	0.2383	0.114
463	Flat-tone, orchid	28	Orchid	0.4695	0.3986	0.640	0.3267	0.3165	0.623
	Venetian Blinds								
464	V-100	8	White	0.4554	0.4114	0.819	0.3194	0.3288	0.814
465	V-121	8	Lt. gray	0.4661	0.4191	0.614	0.3360	0.3485	0.603
466	V-103	8	Gray	0.4705	0.4200	0.369	0.3422	0.3510	0.359
467	V-127	8	Cream	0.4852	0.4228	0.722	0.3628	0.3688	0.691
468	V-119	8	Cream	0.4925	0.4261	0.706	0.3750	0.3821	0.672
469	V-101	8	Cream	0.5035	0.4267	0.628	0.3910	0.3919	0.591
470	V-110	8	Natural	0.5142	0.4214	0.517	0.4022	0.3991	0.481
471	V-102	8	Lt. brown	0.4947	0.4228	0.443	0.3761	0.3740	0.419
472	V-120	8	Lt. brown	0.4975	0.4246	0.439	0.3814	0.3809	0.415
473	V-125	8	Pink	0.5267	0.3988	0.471	0.4025	0.3591	0.425
474	V-123	8	Yellow	0.4900	0.4347	0.737	0.3764	0.4038	0.710
475	V-108	8	Green	0.4491	0.4434	0.267	0.3282	0.3783	0.269
476	V-115	8	Green	0.4374	0.4510	0.245	0.3197	0.3875	0.251
477	V-122	8	Green	0.4139	0.4563	0.229	0.2987	0.3794	0.241
478	VB-124	8	Blue	0.4090	0.4176	0.284	0.2793	0.3153	0.300

details will not be repeated here. Most of the window shades were slightly translucent and were tested with a backing of black velvet, corresponding approximately to the conditions in a lighted room at night. Most of the paints had been sprayed on pieces of white paper. In each test, two identical samples were placed on top of each other and were backed by a block of magnesium carbonate. In neither the window shades nor the paints was the translucency high, so the kind of backing would effect the transmission factor by only a few percent at most.

Typical spectrophotometric curves are shown in Figs. 1 to 9. Trichromatic coefficients and

TABLE I.—*Continued.*

No.	Name	Mfgr.	Approx. color	A x	A y	A ρ	C x	C y	C ρ
	Window Shades								
479	Tontine No. 500, snow	11	White	0.4425	0.4068	0.758	0.3046	0.3129	0.763
480	Niagara, eggshell white	8	White	0.4550	0.4136	0.754	0.3207	0.3324	0.749
481	Tontine No. 500B	11	White	0.4453	0.4087	0.731	0.3080	0.3178	0.735
482	Niagara, parchment	8	Ivory	0.4890	0.4245	0.657	0.3687	0.3764	0.629
483	Tontine No. 517, pearl	11	Lt. gray	0.4679	0.4215	0.578	0.3391	0.3515	0.566
484	Fabrikoid, SR-992-8, plain silver	11	Silver	0.4478	0.4090	0.500	0.3107	0.3194	0.501
485	Fabrikoid 900, plain silver	11	Silver	0.4436	0.4075	0.490	0.3062	0.3139	0.492
486	Fabrikoid, SR-992-8, grain, silver	11	Silver	0.4476	0.4086	0.430	0.3104	0.3184	0.430
487	Tontine No. 508, afterglow	11	Gray	0.4776	0.4251	0.416	0.3534	0.3644	0.402
488	Tontine No. 573, pongee	11	Gray	0.4811	0.4229	0.413	0.3568	0.3636	0.397
489	Fabrikoid 900, skiver, silver	11	Silver	0.4440	0.4076	0.397	0.3064	0.3144	0.399
490	Tontine No. 574, dusk	11	Gray	0.4797	0.4233	0.200	0.3550	0.3612	0.192
491	Niagara, chamois	8	Buff	0.4998	0.4279	0.635	0.3877	0.3916	0.599
492	Niagara, persian gold	8	Buff	0.4996	0.4283	0.635	0.3872	0.3918	0.599
493	Tontine No. 512, dawn	11	Buff	0.4795	0.4269	0.599	0.3570	0.3693	0.578
494	Niagara, aureole	8	Buff	0.5082	0.4236	0.559	0.3965	0.3903	0.521
495	Tontine No. 506, sunset	11	Brown	0.4948	0.4258	0.459	0.3773	0.3796	0.435
496	Fabrikoid, SR-324-4, plain gold	11	Gold	0.4900	0.4255	0.449	0.3710	0.3813	0.429
497	Fabrikoid, SR-324-4, grain, gold	11	Gold	0.5005	0.4258	0.440	0.3864	0.3913	0.415
498	Niagara, strained honey	8	Tan	0.4957	0.4248	0.418	0.3789	0.3799	0.395
499	Niagara, beige	8	Tan	0.4862	0.4238	0.359	0.3644	0.3708	0.345
500	Niagara, circassian brown	8	Lt. brown	0.5057	0.4126	0.350	0.3836	0.3642	0.325
501	Tontine No. 578, russet	11	Brown	0.4997	0.4195	0.324	0.3794	0.3722	0.306
502	Niagara, java	8	Brown	0.5088	0.4120	0.269	0.3871	0.3676	0.251
503	Tontine No. 575, autumn	11	Brown	0.5049	0.4142	0.145	0.3837	0.3656	0.135
504	Tontine No. 510, sunrise	11	Lt. pink	0.4683	0.4177	0.691	0.3375	0.3449	0.675
505	Tontine No. 534, sunrose	11	Pink	0.5013	0.4125	0.587	0.3772	0.3581	0.548
506	Niagara, peachskin	8	Pink	0.4905	0.4201	0.557	0.3677	0.3671	0.528
507	Tontine No. 509, mid-day	11	Yellow	0.5035	0.4290	0.624	0.3932	0.3935	0.584
508	Tontine No. 504, chrysanthemum	11	Yellow	0.5126	0.4411	0.609	0.4204	0.4281	0.565
509	Tontine No. 515, apple green	11	Lt. green	0.4678	0.4480	0.551	0.3568	0.4015	0.542
510	Tontine No. 536, springleaf	11	Green	0.4058	0.4508	0.368	0.2874	0.3754	0.392
511	Tontine No. 525, moss	11	Green	0.3887	0.4592	0.246	0.2730	0.3812	0.270
512	Niagara, hunter green	8	Green	0.3996	0.4511	0.151	0.2814	0.3690	0.162
513	Naiagara, canton jade	8	Green	0.3818	0.4262	0.0929	0.2585	0.3236	0.102
514	Tontine No. 553, meadow	11	Dk. green	0.4184	0.4438	0.0923	0.2961	0.3665	0.0972
515	Tontine No. 555, forest	11	Dk. green	0.3810	0.4334	0.0846	0.2592	0.3335	0.0927
516	Niagara, evergreen	8	Dk. green	0.4141	0.4150	0.0662	0.2824	0.3132	0.0690
517	Tontine No. 551, laurel	11	Dk. green	0.4149	0.4217	0.0621	0.2844	0.3271	0.0656
518	Tontine No. 523, robins egg	11	Blue	0.4308	0.4310	0.262	0.3042	0.3472	0.269
519	Tontine No. 520, larkspur	11	Blue	0.3645	0.3561	0.179	0.2313	0.2263	0.199

reflection factors were computed from the curves and are given in Table I. Glass chalkboards of various colors were tested, also a slate board. Sample No. 416 is not a chalkboard but is a piece

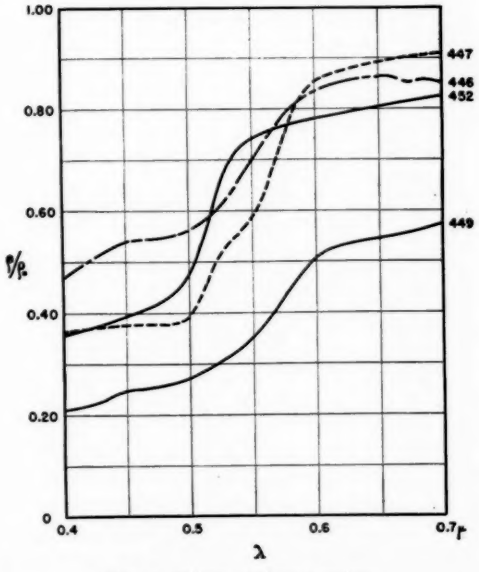

FIG. 4. Paints, pink and yellow.

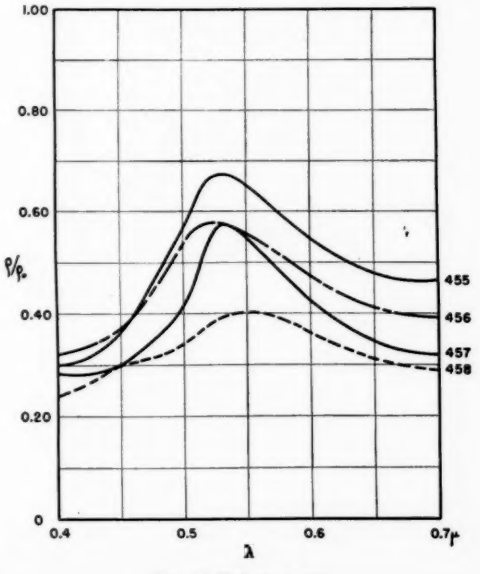

FIG. 5. Paints, green.

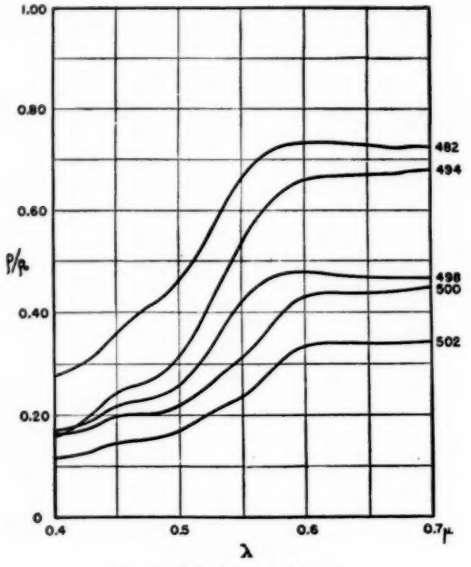

FIG. 6. Window shades, tan.

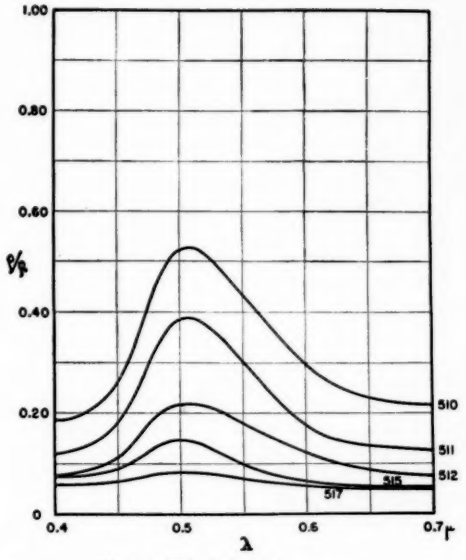

FIG. 8. Window shades, green.

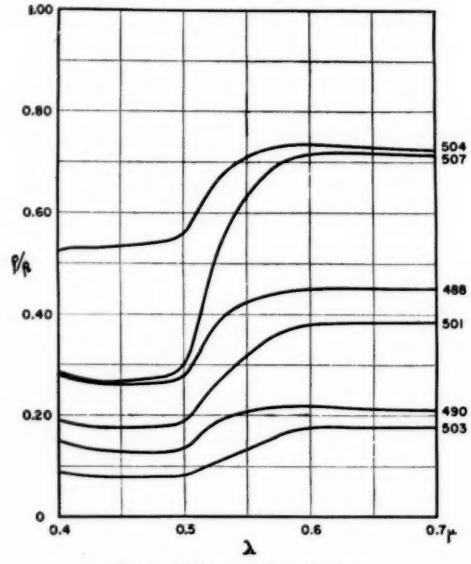

FIG. 7. Other window shades.

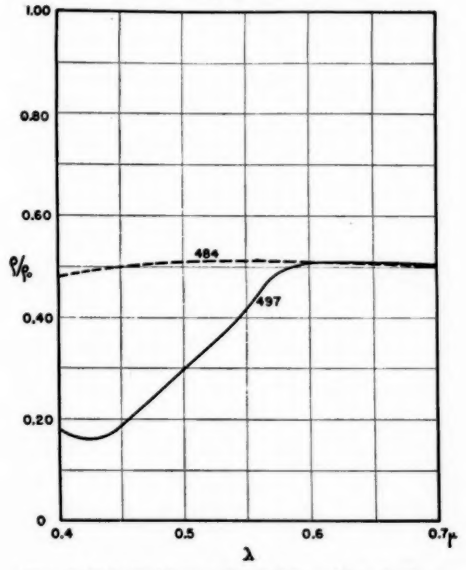

FIG. 9. Fabrikoid, metallic finish, gold and silver.

of light-green polished glass. It is included in the table merely for comparison with the green glass chalkboards.

The venetian-blind slats were of wood and all were painted in the manufacturer's standard colors except No. 470, which was coated with a clear varnish. The manufacturers of window shade cloths supplied a variety of attractive colors as well as a number of dark greens, most of which had such low reflection factors that they are not included in the table. Fabrikoid with metallic gold and silver finishes is not ordinarily used for window shades but is included because of its general interest.